

POLITECNICO DI TORINO

Facoltà di Ingegneria
Corso di Laurea in Ingegneria Energetica e Nucleare

Tesi di Laurea Magistrale

Uncertainty Quantification in steady-state multi-physics simulations of the Molten Salt Fast Reactor



Relatore:
Sandra Dulla

Candidato:
Mario Santanoceto

Dicembre 2019

To my family

Contents

| | |
|---|-----------|
| Abstract | 4 |
| Introduction | 5 |
| 1 Generation IV Reactors: the Molten Salt Reactor | 7 |
| 1.1 The Molten Salt Reactor | 9 |
| 1.1.1 History | 10 |
| 1.1.2 The Molten Salt Fast Reactor | 10 |
| 2 Uncertainty Quantification and Sensitivity Analysis | 14 |
| 2.1 Polynomial Chaos Expansion | 16 |
| 2.2 Sensitivity Analysis | 19 |
| 2.2.1 Sobol’s sensitivity indices | 20 |
| 3 Computational Tools For Uncertainty Quantification and Model Evaluations | 22 |
| 3.1 The thermal fluid-dynamic code: DGFlows | 22 |
| 3.2 The neutron transport code: PHANTOM-S _N | 23 |
| 3.3 The global polynomial chaos code: OpenGPC | 23 |
| 3.4 Scripts for the external coupling | 24 |
| 4 Steady-state Simulations of the CNRS Benchmark | 26 |
| 4.1 Preliminary approach to the benchmark | 27 |
| 4.2 Temperature field with single stochastic input and output | 29 |
| 4.3 Single-physics case: thermal fluid-dynamics only problem | 31 |
| 4.3.1 Normally distributed heat transfer coefficient | 31 |
| 4.3.2 Uniformly distributed heat transfer coefficient | 31 |
| 4.4 Single-physics case: neutronics-only problem | 35 |
| 4.4.1 Relevant input determination: mean value approach | 35 |
| 4.4.2 Relevant input determination: class approach | 36 |
| 4.4.3 Results comparison between <i>class approach</i> and <i>mean value approach</i> | 39 |
| 4.5 Multi-physics case: coupled neutronics and thermal fluid-dynamics problem. | 42 |
| 4.5.1 Monte Carlo Sampling | 42 |
| 4.5.2 Results: maximum temperature | 44 |
| 4.5.3 Results: effective multiplication factor | 47 |
| 4.6 Summary | 49 |
| 5 Steady-state Simulations of the Molten Salt Fast Reactor | 50 |
| 5.1 Preliminary approach to the problem | 52 |
| 5.2 Single-physics case: neutronics-only problem | 55 |
| 5.3 Multi-physics case: coupled neutronics and thermal fluid-dynamics problem | 57 |

| | | |
|----------|---|-----------|
| 5.3.1 | Strategy for the computational time reduction | 57 |
| 5.3.2 | Results: single-value temperatures | 62 |
| 5.3.3 | Results: temperature field | 64 |
| 5.3.4 | Results: effective multiplication factor | 67 |
| 5.4 | Summary | 71 |
| 6 | Conclusions | 73 |
| | References | 77 |
| | Acknowledgments | 80 |
| | Appendices | 81 |
| A | Details on communication scripts | 81 |
| B | Boussinesq approximation | 84 |

Abstract

Since the birth of first nuclear power plants in mid-1950, the nuclear sector has seen substantial developments from a number of viewpoints. Especially the concept of safety, along with the sustainability and economic, has become crucial in their design, which in turn has requested more and more efforts for its completion. Gen-II reactors are concepts developed and built until the end of 1990 and they were supposed to operate for about 40 years, but at present, their technology is outdated in all respects. In addition, the climate changes have pointed out the vital role of the nuclear, but at the same time, new challenges that the nuclear industry had to face requested radical changes in the reactors plants design. The Molten Salt Reactor (MSR) is one of the six revolutionary concepts proposed by the Generation IV International Forum.

Its improvements with respects to previous systems, especially from the safety point of view, makes it extremely attractive, but being an immature technology it needs intense research. Meanwhile, Uncertainty Quantification (UQ) gained increasing importance in last decades thanks to a change in the design procedure from a conservative approach to the so-called Best Estimate Plus Uncertainty (BEPU) methodology.

Monte Carlo (MC) methods have been widely used for this purpose thanks to their flexibility of application. On the other hand, the general high number of model evaluations to retrieve statistical information makes their computational cost prohibitive while applied to complex, multi-physics problems, included the MSR. Thus, novel techniques, such as Polynomial Chaos Expansion (PCE), have attracted interest. PCE belongs to non-intrusive spectral projections methods and it is able to derive statistical information of a response with a restricted number of model evaluations and without needing a modification of the model underlying equations. In this thesis, Smolyak sparse grids and Gauss quadrature rules are adopted to build the PCE approximation.

PCE are applied to the MSR, considering at the beginning a simplified version, the CNRS benchmark, which contains all relevant physical features, and then the actual preliminary design, the Molten Salt Fast Reactor (MSFR). Global parameters, such as the maximum temperature and the effective multiplication factor, are chosen as responses. In the CNRS benchmark, after a reduction of the parameter space with single-physics evaluations, the coupled problem is tackled and results are compared with a 10^3 samples MC reference, showing excellent agreement. Afterwards, the same analysis is performed on the MSFR preliminary design, taking advantage of results obtained in the previous analyses. Using the same criteria for the parameter ranking and selection, the analysis is extended to the whole temperature field, but, at the same time, it focuses on the maximum, minimum and average temperature. PCE method showed its effectiveness even in such a complex application with high dimensionality, being able to determine the main statistical information with a limited number of simulations.

Introduction

The nuclear industry is experiencing profound changes, with the design of a new generation of reactors: they will prove to be potentially game-changing in the fight for climate changes, providing carbon-free electricity, minimizing the safety-related risks, along with the production and management of radioactive wastes. In particular, the Molten Salt Reactor (MSR) presents unique features and advantages, first of all the presence of liquid fuel, but, despite other kind of new generation reactors, it requires strongest efforts because of its revolutionary design. The assessment of such aspects needs more powerful means, especially computational ones, to optimize the configuration. Further complications come from imprecise salt thermal and neutronics properties since its composition is not known *a priori*.

At the same time, computational tools have been developed to assist the feasibility, design and optimization processes. Codes and simulations have gained a crucial role in these studies. Verification, validation, uncertainty and sensitivity analysis are essential tools to make sure the results of simulations are comparable with real experiments. Among them, Uncertainty Quantification (UQ) and Sensitivity Analysis (SA) are the main topic of the thesis, as they are highly relevant in the analysis and design of complex systems, since uncertain input parameters interact and influence outputs generally in a non-linear and unpredictable way. Monte Carlo methods have been widely used thanks to their reliability and possibility of application in many situations. Unfortunately, they are computationally expensive, as they require a high number of model evaluations to retrieve accurate enough information on the responses. To overcome this issue, novel UQ techniques are able to considerably reduce the computational burden, especially for complex, multi-physics problems. Among them, Polynomial Chaos Expansion (PCE) seems to have convincing properties, being able to fetch accurate statistics with a limited number of model evaluations and having the possibility to be applied on top of existing models without any modification of underlying equations.

The objective of this thesis is to apply PCE to complex and relevant systems which need careful and deep analysis, such as the MSR. This reactor design not only presents a deep correlation between neutronics and thermal fluid-dynamics, but it also introduces high inputs dimensionality, which is one of the weaknesses of the PCE technique. In addition, this work underlines the improvement this method offers with respect to conventional methods, and especially MC.

The PCE meta-model is applied to a simplified system, the CNRS benchmark, as a test case. Deep coupling between thermal fluid-dynamic and neutronics, precursors movement and fast spectrum are the main features shared with the actual system. Here, physical phenomena involved are studied with in-house developed codes, while inputs are defined, together with a strategy for parameter space reduction. Afterwards, exploiting the experience and the results obtained with the test case, attention is focused on a specific variant of the MSR, the Molten Salt Fast Reactor (MSFR), developed inside the Horizon2020 European project. Differently from the CNRS benchmark, MSFR introduces turbulence models, complex geometry and different variety of materials, making the computational problem even more challenging.

Chapter 1 is devoted to the description of the MSR, with particular attention on the fast spectrum one (MSFR). Chapter 2 is focused on the theoretical foundations of the Uncertainty Quantification and Sensitivity Analysis methodologies. Within it, PCE method is described in details, highlighting key passages, as well as Sensitivity indices, fundamental for the parameter ranking. Computational tools, namely the neutronics and thermal fluid-dynamic codes, along with the PCE code implementation and *ad hoc* designed scripts that allow codes interaction, are discussed in Chapter 3. Chapter 4 shows the results related to the CNRS benchmark, quantifying the discrepancies between the PCE approximation and the MC reference. Chapter 5 presents the results of PCE application to the MSFR, showing similarities and differences with respect to the previous case. Finally, in Chapter 6 some conclusions are drawn.

Chapter 1

Generation IV Reactors: the Molten Salt Reactor

The nuclear industry has been making great strides from several points of view. In particular, safety and sustainability have played a more and more crucial role in the design procedure. Currently generation II and III (Gen-II and Gen-III) reactors operate worldwide, almost exclusively for electric energy production, representing the 10.4% of the whole amount [1]. Gen-II reactors especially are concepts developed and built until the end of 1990 and they were supposed to operate for about 40 years [16], but at present their technology is outdated in all respects. In addition, the climate changes have pointed out the vital role of the nuclear, but at the same time the new challenges for nuclear industry requested radical changes in the design. In this context, the Generation IV International Forum (GIF) was founded in 2000 by the USA DoE (Department of Energy): it proposed a roadmap that will culminate with the construction of the the so-called generation IV reactors. This reactors concepts present unique features able to fulfill precise goals. The Gen-IV goals are (reported from [14]):

- *Sustainability.* Generation IV nuclear energy systems will provide sustainable energy generation that meets clean air objectives and provides long-term availability of systems and effective fuel utilization for worldwide energy production. They will minimize and manage their nuclear waste and notably reduce the long-term stewardship burden, thereby improving protection for the public health and the environment.
- *Economics.* Generation IV nuclear energy systems will have a clear life-cycle cost advantage over other energy sources. They will have a level of financial risk comparable to other energy projects.
- *Safety and Reliability.* Generation IV nuclear energy systems operations will excel in safety and reliability. They will have a very low likelihood and degree of reactor core damage and will eliminate the need for off-site emergency response.
- *Proliferation resistance and physical protection.* Generation IV nuclear energy systems will increase the assurance that they are very unattractive and the least desirable route for diversion or theft of weapons-usable materials, and provide increased physical protection against acts of terrorism.

Based on these requirements, a large number of new concepts have been considered. The GIF has selected six of these designs, focusing only on the most promising ones, whose schematic plant is reported in Figure 1.1.

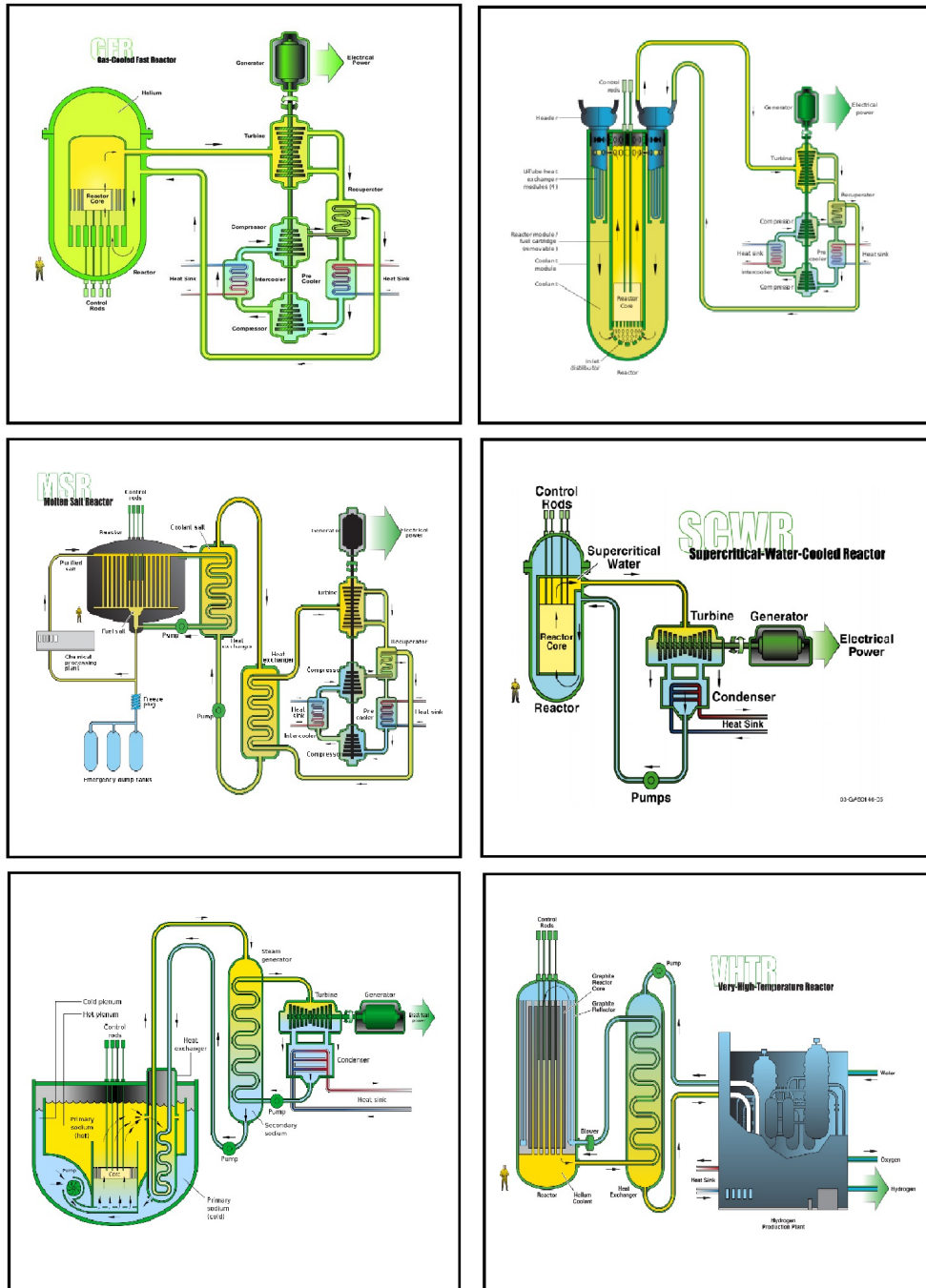


Figure 1.1: Schematic plants of the six reactor concepts selected by GIF. Top left: Gas-cooled Fast Reactor. Top right: Lead-cooled Fast Reactor. Center left: Molten Salt Reactor. Center right: Supercritical Water-cooled Reactor. Bottom left: Sodium-cooled Fast Reactor. Bottom right: Very High Temperature Reactor.

1.1 The Molten Salt Reactor

The Molten Salt Fast Reactor (MSFR) is one of the six new concept reactors proposed by the Generation IV International Forum. The molten salt coolant and/or liquid nuclear fuel represents the main design feature and guarantees many intrinsic advantages, especially from the safety point of view [2]. More in detail, its advantages are listed below.

- *High operating temperature.* Differently from Light Water Reactors, the liquid fuel allows high operating temperature without salt evaporation. Thus, the thermodynamic efficiency increases and a Brayton cycle can be activated. In some configurations, it can be exploited for the hydrogen production, which, however, requires even higher temperatures [22].
- *Low pressure.* Despite high nominal temperature (above 1000 K in many designs), the primary system pressure is nearly atmospheric. It implies that from the safety point of view, if the system is subjected to a loss of coolant accident due to a break in the vessel, the phenomenon violence is more moderated and it do not involve a liquid-to-vapor phase change (with flashing), as in Pressurized Water Reactors. In addition, the vessel thickness can be reduced, saving materials and reducing manufacturing costs.
- *High energy density.* Thanks to the absence of the vast majority of in-vessel components, the energy density is very high and it allows the construction of small and compact reactors, even in case of high thermal power (i.e. order of GW_{th}). For some designs, it can exceed 300 W cm^{-3} [24].
- *Enhanced salt thermodynamic properties.* In particular the heat capacity is higher than liquid metals. Consequently, heat exchangers, pumps and other components can be reduced in dimensions, making them more compact and thus more economic, further reducing the primary circuit size and cost. In addition, this property guarantees an intrinsic protection against unexpected power production, since the fuel salt can accumulate energy with a contained increase in temperature.
- *Strongly negative feedback coefficients.* Feedback coefficients quantify the reactivity variation with respect to some key quantities (e.g. the coolant/moderator temperature, the fuel temperature) . In order to dampen unexpected insertion of positive reactivity they need to be negative and the more negative they are the less the reactor is sensitive to reactivity and/or temperature transients.
- *Irrelevance of core melting accidents.* Transients leading to core melting are of primary importance in the accident analysis especially for water cooled reactors, since they can lead to considerable releases of radioactive substances. As the primary feature of the MSR is the presence of liquid fuel, the core meltdown is not only possible, but necessary to operate the plant. This implies that the safety assessment on MSFR has to identify new relevant accidental sequences and initiating events.
- *Retention of radioactive products in the salt.* Analogous to the fuel pellet, the fuel salt has the double role of producing necessary heat and avoid the dispersion of fission products. The fuel salt composition has to be such that fission products are soluble, thus being effectively segregated in the salt [35].
- *Strong reduction of radioactive wastes.* In fast neutron spectrum configurations, minor actinides are subjected to fertilization or fission. Other fission products responsible of long term radioactivity can be separated online. The remaining radioactive species can decay within a very short time (300 years against $\sim 10^5$ years) [21].

On the other hand, this reactor requires strong efforts in R&D, both from the experimental and numerical point of view. The following aspects are especially important.

- *Early stage of development.* With respect to other Gen IV reactors, MSRs need much more R&D because of their radical diversities with exiting and other gen IV reactors. Europe, China, Japan, USA and others are developing their own reactor design aiming to build experimental facilities at least by 2025 [5].
- *Complicated chemical processes.* MSRs require sophisticated chemical plants able to produce the fuel and extract the fission products. In addition, the fuel salt composition itself is not known and the experience about this kind of composites is very scarce.
- *Material issues.* High temperature and high neutron flux resistant structural materials available at the moment are not sufficiently performing and thus research needs to focus on improving existing or new alloys [25].

1.1.1 History

The MSR concept was born well before the creation of GIF. This technology has seen its first practical application (as thermal reactor) with the Aircraft Reactor Experiment (ARE) in 1950s, in which the high energy density of MSR was intended to be used to power a bombardier making it capable of withstanding a much higher number of flight hours, compared to conventional-fueled ones.

In the 1960s, the Oakridge National Laboratory designed and built the first reactor for civil-based application, commonly known as the Molten Salt Reactor Experiment (MSRE). Its configuration is known as single fluid graphite moderated (it was still a thermal reactor). It was a breeder reactor, potentially able to convert ^{233}Th to ^{233}U . It became critical in 1965 and it provided crucial results in this field, from the fuel salt chemistry, the neutronic behavior, materials compatibility and so on. Despite the project showed encouraging results, it was closed due to lack of funds in the early 1970s [15, 21].

1.1.2 The Molten Salt Fast Reactor

Recently, the molten salt reactor concept has emerged again. At the moment, several countries have been developing different MSR concepts, both independently or as international projects. In particular, Canada is trying to combine the MSR with the Small Modular Reactor (SMR) concept, accelerating the design, licensing and construction processing; China is allocating conspicuous resources and funds to build pilot and demonstrator reactors between 2020 and 2035. The concept chosen in this work is the one proposed by the Centre National de la Recherche Scientifique (CNRS) developed in the EVOL (Evaluation and Viability Of Liquid fuel fast reactor system) project and subsequent SAMOFAR (SAfety of MOlten salt FAst Reactors) and SAMOSAFER, supported by the European Union in the Horizon 2020 framework. This reactor concept is known as the Molten Salt Fast Reactor (MSFR) and its preliminary design is currently under examination to ensure it fulfills criteria established by GIF.

Core description The core consists of a cylindrical-like cavity surrounded by a toroidal blanket in which the fertile material (with a composition $\text{ThF}_4\text{-LiF}$ 78-22 mol%) is contained. Pumps and heat exchangers, organized in 16 sectors, are located behind it, thus being shielded by the blanket itself and other protecting materials. Figure 1.2 shows the MSFR preliminary design, developed in the context of EVOL European project. The vessel and blanket geometry, as well as the one of upper and lower reflectors, are designed to minimize pressure losses, following the fluid

streamlines. The reactor is foreseen to produce 3 GW_{th} in nominal conditions (approximately 1.3 GW_e), ensuring a maximum fuel temperature around $760 \text{ }^\circ\text{C}$ and a temperature increase inside the core of $100 \text{ }^\circ\text{C}$ [23]. The average temperature is expected to be around $700 \text{ }^\circ\text{C}$. The system pressure is nearly atmospheric in the vast majority of the core, except near the pumps. However, even there its magnitude is of the order of few bars.

The main component of the reactor core is the fuel salt. It consists of 18 m^3 liquid salt containing fissile isotopes which also acts as a coolant. At this stage of development, two possible fuel compositions are available, according to [3]. The former is $\text{LiF-ThF}_4\text{-}^{233}\text{U}$ (77.5-20-2.5 mol%), using fresh nuclear fuel, while the latter is $\text{LiF-ThF}_4\text{-UF}_4\text{-(Pu/MA)F}_3$ (77.5-6.6-12.3-3.6 mol%), operating the reactor to consume minor/major actinides. These compositions are chosen as best compromise to optimize the neutronic balance, enhance thermodynamic properties, while containing corrosion and other composition-related issues. In addition, the salt composition has to ensure a fast neutron spectrum, required for the fission of minor actinides, since they need high energy neutrons, and a sufficiently high breeding ratio (1.1 for this configuration). Moreover, this composition allows strongly negative feedback coefficients (around -5 pcm/K [12], for 18 m^3 of fuel salt), fundamental feature to guarantee safe transient operations. Finally, the precursors movement, due to the fuel salt circulation, has repercussions on the neutronics behavior, especially in transient scenarios.

Thermodynamic properties are generally estimated through several methods (as done in [7]). Despite the thermal conductivity is lower with respect to other liquid metals under the same conditions, it is an intrinsic protection against high temperatures. On the other hand, the thermal heat capacity (i.e. product between density and specific heat capacity) is above $1 \text{ MJ/m}^3\text{K}$, ensuring slower temperature transients.

In addition to the precursors' movement, the fuel salt is subjected to inner power generation, density feedback and Doppler effects, as well as turbulence and other phenomena. Thus, specific computational tools are needed for the analysis of both steady-state and transients simulations on this kind of reactor. Considering, these properties and all the phenomena previously mentioned, [6, 19] performed steady-state and transient analysis on the MSFR with 2D and 3D geometries, with existing tools (e.g. OpenFOAM).

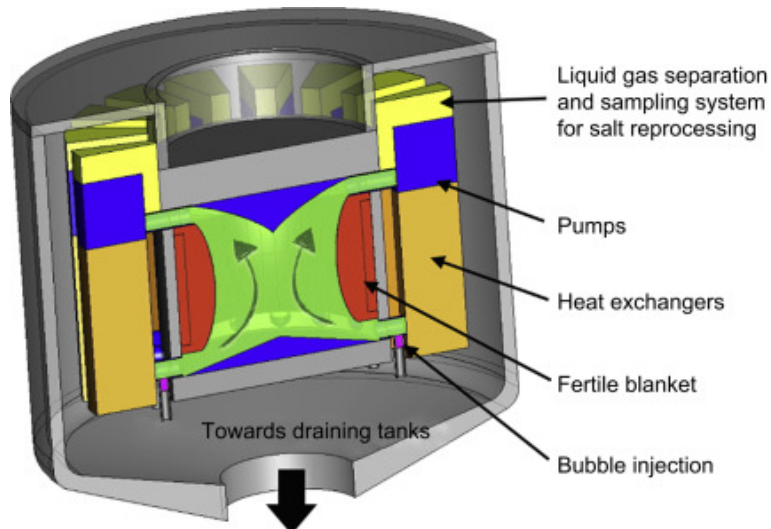


Figure 1.2: *Molten Salt Fast Reactor (MSFR) preliminary design [2]. Main components along with the fuel salt circuit (innermost green part with arrows) are shown. The secondary loop is not represented.*

Main Fuel Salt Loop Components Excluding the core, the fuel salt circuit includes several other components to operate continuously. The main ones are listed below.

- *Reflectors.* They are located at the top and bottom of the vessel nad they are vital to reduce the neutron leakage. Because of the power distribution and the fuel motion, the upper plate is subjected to the highest temperatures, which set stricter constraints for materials. Their shape has been established in order to minimize negative effects on the flow. The choice of material is not definitive, but nickel alloys seem to be good candidates thanks to their resistance to high temperatures (above 700 °C) and corrosion.
- *Blanket.* Thorium, chemically bounded with fluorine, is mainly contained in the blanket, which is placed as near as possible to the region with highest flux, to maximize transmutations and increase the breeding ratio, i.e. ratio between the quantity of fuel produced by fertilization and the quantity burned. The blanket has to be cooled, because of energy release by fissions of ^{233}U or by captures in Th. The composition was chosen to minimize this effect since it is detrimental both for materials and for the reactor breeding capabilities.
- *Heat exchangers.* One per sector, it has to be able to extract one sixteenth of the total power (187MW_{th}). They need to be compact and minimize pressure drops. Until now, despite some requested features are known, the component choice is not unique and may present a further complication for the design process.
- *Pumps.* Analogously to the heat exchanger, there is one per sector and it has the function of increasing the fluid velocity allowing the fluid motion. It is placed before the heat exchanger because increasing salt speed improves the energy transfer between the primary and secondary circuit, despite the pump has to face higher temperatures.
- *Bubbling system.* It has the function of purifying the fuel, contaminated by fission products and particle-sized debris removed by the components and vessel walls. By the removal of the fission products there is a double advantage. First, the inventory of radioactive material is lowered, which has a positive effect in case of accident. Secondly, the initial excess of reactivity can be reduced since especially ^{135}Xe is periodically separated.

For more detailed information see [2, 3].

Plant Schematics and Safety Systems The primary system described in Chapters 1.1.2 has to be completed, allowing the conversion of the thermal power. Then, as done for any kind of nuclear power plant, a number of safety systems must be included, even if this plant showed very good responses in case of sharp increase of reactivity and power [3]. Figure 1.3 shows secondary and tertiary loops, along with the Emergency Draining Tank (EDT), the main safety system, and the protection barriers. Differently from other solid fuelled reactors, the excess of initial reactivity is much lower because a continuous refuelling is possible. In Figure 1.3, in fact, a storage area is connected with the primary system to introduce additional fissile material when needed, to maintain criticality.

The EDT is located below the reactor vessel, thanks to the emergency draining shaft. In case of abnormal transients in which the power production tends to increase without control, a valve is opened (or a plug melts above a threshold temperature) and the salt can be drained in a sub-critical volume, where it is cooled and stored for an adequate time. However, the geometry of such a system is still under examination, as well as the number and location of Draining Shafts. In fact, it is important to underline that sometimes system safety and reliability design are in

competition. In this case, increasing the pipes number enhances safety because the probability that a high fraction of pipes is not able to vehicle the salt decreases. On the other hand, at the same time, the probability of a spurious opening of a valve during normal operations rises, becoming a problem from the production point of view.

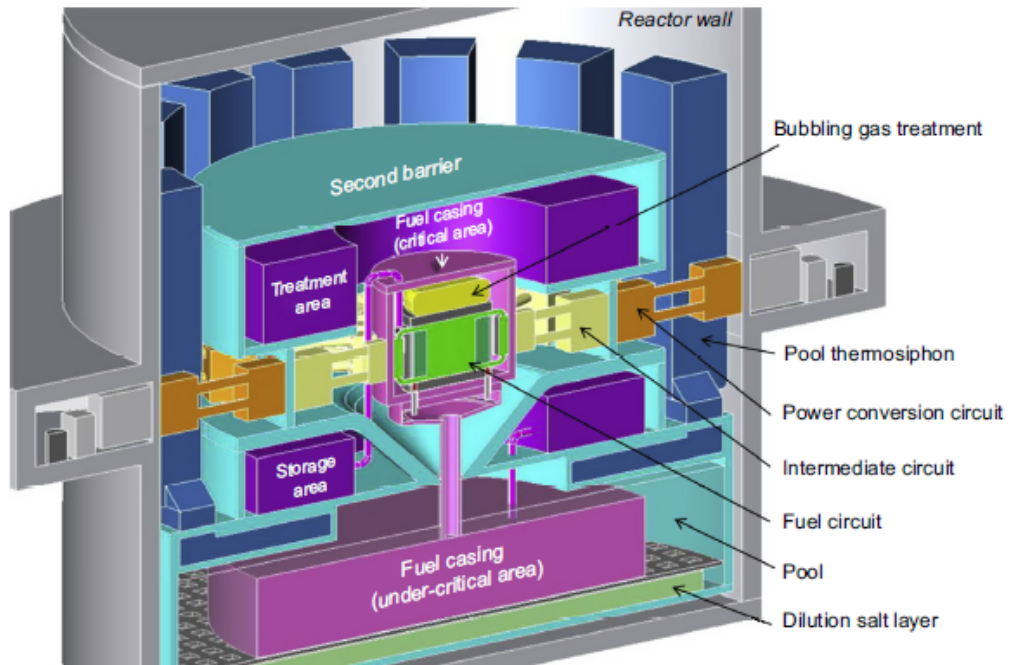


Figure 1.3: MSFR power plant scheme, including conversion components and safety systems [2].

Chapter 2

Uncertainty Quantification and Sensitivity Analysis

Uncertainty quantification (UQ) was developed to infer statistical information of the output(s) assuming a variability on data, models and tools. It gained increasing importance in last decades thanks to a change in the design procedure from a conservative approach to the so-called Best Estimate Plus Uncertainty methodology [40], which focuses on the evaluation of the variability of the results in the most precise and complete way. Recently, regulations were modified according to this change of perspective, especially in the nuclear sector [11].

UQ of computer simulations is highly relevant in the analysis and design of complex systems, since uncertain input parameters interact and influence outputs generally in a non-linear and unpredictable way.

Several sources of uncertainties prevent computer simulations outputs to be known exactly. These can be associated to:

- *Model errors.* They come from the simplification and the assumptions made to develop the equations, which are eventually solved. In some cases, they may come from a poor understanding of the physical phenomena involved, because they can be still matter of research, whereas in others these errors are introduced with closures/state equations.
- *Numerical errors.* As mentioned in the previous point, (integro-differential) equations are the basis of the mathematical models of interest and seldom an analytic solution is available, which is even rarer for complex and engineering-relevant applications. Thus they need to be discretized in their independent variable space (e.g. space, time, energy). The real world, continuous by nature, is treated as discontinuous, since the solution can be computed in a high but still finite number of points in the parameter space. The algorithm for the solution has to ensure convergence (i.e. the numerical solution tends to the exact one if the grid spacing tends to zero [13]). By difference, this error is associated to the discrepancy between the exact solution and the one in presence of a computational grid. The round-off error and the iteration error belongs to the same category along with the discretization error. The first is related to the impossibility to represent numbers with infinite digits, and the second appears only in case an iterative procedure is needed. If only a finite number of iterations is possible (reaching a target tolerance), a residual error is left. For each of these errors an uncertainty can be associated and the total uncertainty due to numerical errors (U_{NUM}) can be computed, according to [30], simply as

$$U_{NUM} = U_{DE} + U_{IT} + U_{RO} \quad (2.1)$$

where U_{DE} , U_{IT} and U_{RO} are the uncertainties on the discretization, the iterations and on the round-off errors respectively.

- *Data errors*. Inside the model some variables are assumed to be known (e.g. material properties, geometry, empirical/semi-empirical constants etc). Unfortunately, they may be not evaluated exactly, since they can derive from experimental campaigns or they are subjected to manufacturing processes or because they are not fixed, as in the case of a new design phase.

The uncertainties can be also classified as

- *Aleatory*. These are uncertainties related to the intrinsic random variability of the quantity or phenomenon [4]. They are represented by using a probability density function, along with a mean value and a variance. Background noise, particles interactions, wind velocity and similar belong to this category. Material properties and other quantities known by experiments, can be treated as aleatory if enough data are available [4, 30].
- *Epistemic*. These are uncertainties related to lack or partial knowledge about the system, physical phenomena and so on. Differently from aleatory uncertainties, these can be reduced by producing a more complete set of experimental data or different model adoption [30]. They cannot be represented via statistical information since available data are not numerous enough. For this reason, they are usually defined within one or more intervals, but no other clue can be deduced.

Despite numerical errors are generally classified as numerical uncertainties, someone interprets them differently [26]. Numerical errors are, in fact, acknowledged errors, which give a precise and quantified effect. It is not due to imperfections in data or model, but simply to feasibility issues, related to the calculation time and power. They are responsible of an imprecise evaluation of the response, but, since they can be determined exactly, they are more properly defined as errors rather than uncertainties.

Verification and Validation (V&V) studies have the purpose to check the correctness of the model. The former verifies the appropriate implementation and programming of the equations with their solvers, highlighting possible bugs and mistakes, whereas the latter ensures that the model possesses a satisfactory range of accuracy consistent with its the intended application [34]. Generally, in the validation study, the model results (with their uncertainties) are compared with experimental data or with already validated correlations/models.

Verification quantifies numerical errors. The quantification of each term mentioned in the list of numerical error can be challenging. The most relevant contribution is in general the discretization one, which can be also controllable. There are two kind of methodologies to evaluate it: higher-order estimators, such as the Richardson extrapolation, or residual-based estimators [30], as well as alternative and more advanced methodologies [9, 36].

Propagation of uncertainty due to data errors can be assessed in multiple ways. First, there is a main distinction of approaches between aleatory and epistemic. This thesis focuses only on aleatory variables related to data. Historically, uncertainties quantification on aleatory variables was carried out using collocations methods, such as Monte Carlo (MC) methods or Latin Hypercube Sampling (LHS), which consist of random generation of a sufficiently high number of inputs (that can reach order of millions), with proper mean value, standard deviation and with the correct distribution, followed by the evaluation of the responses for each combination of inputs, through a proper model. The outputs are finally manipulated to build the probability density functions (pdf) and/or cumulative density functions (cdf). Nowadays, accurate simulations are commonly computationally expensive, making, in fact, these methodologies unfeasible in many situations [37]. Recently, novel methodologies have been applied to mitigate

the computational burden such as stochastic collocation [33], response surface approximation methods or spectral methods.

Spectral expansions have gained interest in this perspective. Different methods belong to this category: Karhunen-Loève Expansion, known as Proper Orthogonal Decomposition (POD), as well as Polynomial Chaos Expansion (PCE).

Proper Orthogonal Decomposition is also classified as Reduced Order Model (ROM) techniques. It is basically an eigenvalue problem, which tries to reduce the problem complexity by decreasing its dimensionality (i.e. the parameters space). However, this operation needs to preserve the features of the full scale model, minimizing the error introduced by the parameters reduction.

Polynomial Chaos Expansion is the method for Uncertainty Quantification chosen in this work and it is introduced in detail in the following.

2.1 Polynomial Chaos Expansion

Advanced simulations have seen a progressively increasing computational time. Parametric studies or, like in this case, UQ require to perform multiple simulations. These two factors have given birth to alternative methods, which generally tend to minimize the number model evaluations.

Polynomial Chaos Expansion is a technique based on the approximation of the response with a polynomial up to an appropriate order. If performed properly, the expression obtained in this way contains the response statistical information as function of the stochastic inputs. Then, the pdf is evaluated by random sampling on the polynomial rather than on the model itself, taking just few second for million samples. PCE was developed by Wiener [39], with the application of Hermite polynomials only, and later generalized (generalized Polynomial Chaos, gPC) to many distributions, using different kind of polynomial [41].

The polynomial is a sum of products between a basis and a coefficient. The basis functions are defined depending on the statistical nature of inputs (i.e. their distribution) and the polynomial order, whereas the coefficients need to be computed by performing some evaluations, thus retrieving information on the model. Carefully taking the evaluation points, the expansion coefficients can be computed very efficiently, requiring a number of model evaluations sometimes order of magnitudes lower than MC methods. On the other hand, the main issue related to this method is the "curse of dimensionality": in case of high number of inputs, the number of coefficients drastically increases, requiring a higher number of model evaluations, making PCE performances comparable to MC methods in some cases. In addition, it is impossible to know a priori the correct polynomial order capable to reconstruct the response with sufficient fidelity.

Theory Define the probability space $\Gamma = (\Theta, \Sigma, \mathbb{P})$, where Θ is the sample space and such that $\theta \in \Theta$, being θ the random event, Σ is the σ -algebra (collection Σ of subsets of Θ), and \mathbb{P} is the value of probability in the interval $[0, 1]$. Random inputs $\xi(\theta)$ belongs to Υ , which is the support of their probability density function (pdf) $p(\xi)$. The present work focuses only on independent random variables. Thus, any joint pdf is $p_{\bar{\xi}}(\bar{\xi}) = \prod_{i=1}^N p_{i_{\xi_i}}(\xi_i)$, where N is the number of stochastic inputs and $\xi = (\xi_1, \xi_2 \dots \xi_N)$. The response is defined such that

$$R(\theta) : \Theta \rightarrow \mathbb{R} \quad \text{and} \quad \langle R_1, R_2 \rangle = \int_{\Gamma} R_1(\bar{\xi}) R_2(\bar{\xi}) p_{\bar{\xi}}(\bar{\xi}) d\bar{\xi} \quad , \quad (2.2)$$

where $L_2(\Theta, \mathbb{P})$ space is the second order random variable in which the inner product is defined and it is finite. As mentioned, the response can be expressed in the form

$$R(\bar{\xi}) = \sum_{i=0}^{\infty} a_i \Psi_i(\bar{\xi}) \approx \sum_{i=0}^{\mathcal{P}} a_i \Psi_i(\bar{\xi}) \quad , \quad (2.3)$$

where a_i is the i -th coefficient and Ψ_i is the i -th basis. For practical reasons the sum has to be truncated up to \mathcal{P} terms.

Full basis set definition. PCE involves the definition of multi-dimensional basis vectors. The i -th basis is built by tensorization of one dimensional polynomials, according to

$$\Psi_i(\bar{\xi}) = \prod_{j=1}^N \psi_{j,\gamma_{i,j}}(\xi_j) \quad , \quad (2.4)$$

where $\bar{\gamma}_i = (\gamma_{i,1}, \gamma_{i,2}, \dots, \gamma_{i,N})$ is the multi-index in which each component is the polynomial order of the j -th random variable ξ_j . $\psi_{j,\gamma_{i,j}}$ is the polynomial type referred to the random variable ξ_j of order $\gamma_{i,j}$ and it can belong to different families (e.g. Hermite, Legendre, Laguerre) depending on the probability density function of the random variable.

Taking the i -th basis and omitting the i subscript for clarity, the multi-index set is defined as

$$\lambda(o) = \left\{ \bar{\gamma} : \sum_{j=1}^N \gamma_j = o \right\} \quad (2.5)$$

and it expresses the set of indices such that their sum over the number of input variables is equal to the generic order o . The set of polynomial basis is computed using the multi-index set

$$\Gamma(o) = \left\{ \bigcup_{\bar{\gamma} \in \lambda(o)} \prod_{j=1}^N \psi_{j,\gamma_j}(\xi_j) \right\} \quad . \quad (2.6)$$

Defining the maximum polynomial order O , the total set of multi indices is the union of each set for o in the range $[0, 1 \dots O]$

$$\mathcal{L}(O) = \bigcup_{o \in [0, 1 \dots O]} \lambda(o) = \left\{ \bar{\gamma} : \sum_{j=1}^N \gamma_j \leq O \right\} \quad . \quad (2.7)$$

Analogously the set of basis is defined

$$\Gamma(O) = \bigcup_{o \in [0, 1 \dots O]} \Gamma(o) = \left\{ \bigcup_{\bar{\gamma} \in \mathcal{L}(O)} \prod_{j=1}^N \psi_{j,\gamma_j}(\xi_j) \right\} \quad . \quad (2.8)$$

The number of terms of the polynomial can be found through the formula

$$\mathcal{P} + 1 = \frac{(N + O)!}{N!O!} \quad , \quad (2.9)$$

which is also equal to the number of coefficients to be calculated. Finally, the response can be expressed as Eq. (2.3)

$$R(\bar{\xi}) \approx \sum_{i=0}^{\mathcal{P}} a_i \Psi_i(\bar{\xi}) \quad , \quad (2.10)$$

with $\Psi_i(\bar{\xi}) \in \Gamma(O) \forall i$.

Non-intrusive spectral projections. If the response approximation is obtained by a projection on a basis $\Psi = (\Psi_0, \Psi_1, \dots, \Psi_N)$, the approach is called Non Intrusive Spectral Projections (NISP). Then, if the basis is also orthogonal, it is valid

$$\langle \Psi_i, \Psi_j \rangle = \int_{\Gamma} \Psi_i(\bar{\xi}) \Psi_j(\bar{\xi}) p_{\bar{\xi}}(\bar{\xi}) d\bar{\xi} = \lambda_i^2 \delta_{i,j} \quad (2.11)$$

where λ_i^2 is a (positive) constant and $\delta_{i,j}$ is the Kronecker delta.

Thanks to this property, the response mean value can be expressed as

$$\mu_R = \int R(\bar{\xi}) p_{\bar{\xi}}(\bar{\xi}) d\bar{\xi} = a_0 \quad . \quad (2.12)$$

Independently from the polynomial type, $\Psi_0(\bar{\xi}) = 1$ and thus the integral in Eq. (2.12) is the projection of the response on the 0-th order polynomial, equal to a_0 because of the orthogonality. On the other hand, the variance is computed as

$$\sigma_R^2 = \int (R(\bar{\xi}) - \mu_R)^2 p_{\bar{\xi}}(\bar{\xi}) d\bar{\xi} = \sum_{i=1}^{\infty} a_i^2 \lambda_i^2 \approx \sum_{i=1}^P a_i^2 \lambda_i^2 \quad . \quad (2.13)$$

It is important to notice that, differently from MC methods, the mean value and the variance are not related to the number of evaluations needed to build the pdf, since they are calculated directly from expansion coefficients.

The advantage of using orthogonal polynomials reflects on the coefficients calculation. In fact, they can be computed by the ratio

$$a_i = \frac{\langle R, \Psi_i \rangle}{\langle \Psi_i, \Psi_i \rangle} = \frac{1}{\lambda_i^2} \langle R, \Psi_i \rangle \quad , \quad (2.14)$$

where

$$\begin{aligned} \langle R, \Psi_i \rangle &= \int_{\Gamma} R(\bar{\xi}) \Psi_i(\bar{\xi}) p_{\bar{\xi}}(\bar{\xi}) d\bar{\xi} = \\ &= \int_{\Gamma} R(\xi_1, \xi_2, \dots, \xi_N) \prod_{j=1}^N \psi_{j,\gamma_j}(\xi_j) p_{\xi_1}(\xi_1) p_{\xi_2}(\xi_2) \dots p_{\xi_N}(\xi_N) d\xi_1 d\xi_2 \dots d\xi_N \quad . \quad (2.15) \end{aligned}$$

The problem is therefore shifted to the efficient calculation of the integral in Eq. (2.15). As the name "Non-Intrusive" suggests, this property allows applying this method without any alteration of the original model. The polynomial chaos meta-model is directly superposed on top of the already implemented code for the response evaluation.

The evaluation of the integral can be performed through stochastic or deterministic approaches. The former consists in the evaluation using MC methods or using some enhanced implementations, such as the Latin Hypercube Sampling or Quasi Monte Carlo; the latter applies quadrature formulae, which consist in the decomposition of the integral in a sum of the product between a function and a weight, which depend on the input variables. MC methods-based models have a convergence $\propto 1/\sqrt{N}$, where N is the number of model evaluations. To perform the integral more efficiently, the second approach is generally chosen.

For a single variable we have

$$I^{(1)} f = \int_a^b f(\xi_j) p_{\xi_j}(\xi_j) d\xi_j \approx Q_{lev}^{(1)} f = \sum_{i=1}^{n_{lev}} f\left(\xi_{j,lev}^{(i)}\right) w_{lev}^{(i)} \quad . \quad (2.16)$$

Superscript (1) indicates that the quadrature rule is applied on a single variable. For N random variables we have

$$I^{(N)} f = \int_{a_1}^{b_1} \int_{a_2}^{b_2} \dots \int_{a_N}^{b_N} f(\bar{\xi}) p_{\bar{\xi}}(\bar{\xi}) d\xi_1 d\xi_2 \dots d\xi_N \approx Q_{lev}^{(N)} f = \sum_{i=1}^{n_{lev_1}} \sum_{i=1}^{n_{lev_2}} \dots \sum_{i=1}^{n_{lev_N}} f\left(\xi_{1,lev_1}^{(i_1)}, \xi_{1,lev_2}^{(i_2)}, \dots, \xi_{1,lev_N}^{(i_N)}\right) w_{lev_1}^{(i_1)} w_{lev_2}^{(i_2)} \dots w_{lev_N}^{(i_N)} \quad . \quad (2.17)$$

There are two big families of quadrature formulae: Gauss and Nested quadrature. The advantage of Gauss formulae is that they ensure exact integral solution for high polynomial order, up to order $2n_{lev} - 1$, where n_{lev} is the number of quadrature points relative to the quadrature level lev . Values of weights and abscissas depend on the kind of polynomial used for the variable representation. On the other hand, they are not efficient in the construction of nested grids.

Nested quadrature rules have faster convergence with respect to quadrature rules, along with natural predisposition to nested configurations and adaptivity. As disadvantage, they involve a number of nodes increasing proportionally to 2^{lev} , where lev is the level of the quadrature (i.e. they double at each level). For further information, see [20]. The number of model evaluations can grow exponentially if high quadrature levels are requested for a proper integral evaluation. In this work, the problem is tackled by combining the Gauss formulae with Smolyak sparse grids.

Smolyak sparse grids Solving multi-dimensional integral with a full-grid quadrature rule can involve a large number of points in the parameter space. A strong tool to overcome the issue is the construction of sparse grids, briefly treated in this Chapter. Before introducing them, it is important to define a special notation for sparse grids, which is

$$\Delta_{lev}^{(1)} f = Q_{lev}^{(1)} f - Q_{lev-1}^{(1)} f \quad \text{with} \quad Q_0^{(1)} f = 0 \quad . \quad (2.18)$$

The superscript (1) indicates that the quadrature rule is applied on a single variable. $\Delta_{lev}^{(1)} f$ is a quadrature rule itself, having the same abscissas of Q_{lev} and weights equal to the difference between the grid of level lev and the one of $lev - 1$. From 2.18, it derives $Q_{lev}^{(1)} f = \sum_{l=1}^{lev} \Delta_l^{(1)} f$, which extended to N variables it is written as

$$Q_{lev}^{(N)} f = \sum_{l_1=1}^{lev_1} \sum_{l_2=1}^{lev_2} \dots \sum_{l_N=1}^{lev_N} \left(\Delta_{l_1}^{(1)} \otimes \Delta_{l_2}^{(1)} \otimes \dots \otimes \Delta_{l_N}^{(1)} \right) f \quad . \quad (2.19)$$

The level multi-index set \bar{l} can be defined in multiple ways: the one proposed in this work is the Smolyak grid construction. Assuming the quadrature level is the same in each direction ($lev_j = lev$), it is defined as

$$\mathcal{I}^{Smolyak}(lev) = \left\{ \bar{l} : \sum_{j=1}^N l_j \leq lev + N - 1 \right\} \quad . \quad (2.20)$$

2.2 Sensitivity Analysis

Sensitivity analysis has the scope of pointing out how the statistical information of the responses are decomposed and distributed, according to the uncertainty of inputs. The uncertainty quantification and the sensitivity analysis are performed together, with the second applied after the

first. Once the statistic features of the response(s) are determined by the uncertainty quantification study, the sensitivity study tries to relate the statistical information to the inputs in a quantitative way, estimating which of them are responsible to the strongest contributions.

Sensitivity analysis can be local or global. Local sensitivity analysis is attractive since it is easy to implement and it needs low computational efforts, involving the computation of derivatives. On the other hand, its implementation involves ad hoc alterations of the responses-computing code (i.e. it is intrusive). In addition, since it is local, it gives information on the studied point, being impossible to find any other global information. This is particularly evident in case of functions of unknown linearity, which is the most frequent case, preventing the analyst to infer any kind of information from local to global. Vice versa, with global sensitivity analysis all inputs are varied at the same time over the whole interval.

Sensitivity analysis tools can be distinguished in derivatives and sigma-normalized derivatives, regression coefficients, variance-based measures, scatter plots and other. In this work, the analysis is performed using variance-based methods since they have intrinsic advantages [31]:

- they do not depend on the model for the response calculation;
- they are compatible with global sensitivity analysis, allowing a study over the whole parameter space;
- they can treat groups of inputs, discovering inter-dependencies among them.

Being able to split the variance of the response in contribution of each input (and combinations of them) is vital to identify which uncertain parameters are the most critical and which other have negligible effects. Among the methods adopted to perform global sensitivity analysis, Sobol's sensitivity indices are the most widely used.

2.2.1 Sobol's sensitivity indices

Assuming to have a set of independent and uniformly distributed input \mathbf{X} in the interval $[0, 1] \forall X_i$, they combine to give the response Y through the general function f , such that $Y = f(\mathbf{X})$. $f(\mathbf{X})$ can be any kind of mathematical model (e.g. it can be the response reconstruction obtained with PCE meta-model). According to [32], the response Y can be written as

$$Y = f_0 + \sum_{i=1}^d f_i(X_i) + \sum_{i<j}^d f_{ij}(X_i, X_j) + \dots + f_{1,2,\dots,d}(X_1, X_2, \dots, X_d) \quad , \quad (2.21)$$

being valid

$$\int_0^1 f_{i_1, i_2, \dots, i_s}(X_{i_1}, X_{i_2}, \dots, X_{i_s}) dx_{i_w} = 0 \quad , \quad (2.22)$$

where $1 \leq i_1 < i_2 < \dots < i_s \leq k$, $i_w \in \{i_1, i_2, \dots, i_s\}$ and k is the dimensionality. Consistently, coefficients f in Eq. (2.21) are defined as

$$f_0 = E(Y), \quad (2.23)$$

$$f_i = E_{\mathbf{X}_{\sim i}}(Y|X_i) - f_0, \quad (2.24)$$

$$f_{ij} = E_{\mathbf{X}_{\sim ij}}(Y|X_i, X_j) - f_i - f_j - f_0 \quad (2.25)$$

and so on. We define

$$V_i = V(f_i(X_i)), \quad (2.26)$$

$$V_{ij} = V(f_{ij}(X_i, X_j)) \quad (2.27)$$

and analogously for higher orders. V_i is the fraction of variance relative to the input X_i , averaging other inputs contributions. Higher orders include contributions related to the combinations of two or more inputs. Substituting the previous expressions, the variance of Y can be decomposed as

$$V(Y) = \sum_{i=1}^d V_i + \sum_{i<j}^d V_{ij} + \dots + V_{1,2,\dots,d} \quad . \quad (2.28)$$

Normalizing the terms with respect to the total variance, sensitivity indices are defined as

$$S_i = \frac{V_i}{V(Y)} \quad , \quad (2.29)$$

which is called *first order sensitivity index*. As mentioned previously, it measures the influence on the variance of each input singularly. However, despite inputs are by definition statistically independent, the response variance can have non negligible contributions related to the combination of variables effects. A common procedure is to define a total sensitivity index for each input, rather than showing all higher order sensitivity indices. It contains all the contributions to the variance related to the input X_i due to interactions of any order. Mathematically it is defined as

$$S_{tot,i} = \frac{E_{\mathbf{X}_{\sim i}}(V_{X_i}(Y|\mathbf{X}_{\sim i}))}{V(Y)} = 1 - \frac{V_{\mathbf{X}_{\sim i}}(E_{X_i}(Y|\mathbf{X}_{\sim i}))}{V(Y)} \quad . \quad (2.30)$$

Differently from the other sensitivity indices, summing all the total sensitivity indices the result is ≥ 1 , since higher order contributions are accounted more than once. In case $\sum_{i=1}^d S_{tot,i} = 1$, the model is purely additive, so it is valid

$$f(x + y) = x + y \quad (2.31)$$

and the response variance is not affected by combinations of inputs variance (i.e. only first order terms give relevant contributions).

Chapter 3

Computational Tools For Uncertainty Quantification and Model Evaluations

To perform the uncertainty quantification on the MSFR, a purposely developed, multi-physics code and a global polynomial chaos code are considered. The former is able to model the MSFR behavior in transient scenarios, while the latter is superposed on top of the previous to build the PCE approximation. The multi-physics solver is separated into two codes, a thermal fluid-dynamic and a neutronics one.

3.1 The thermal fluid-dynamic code: DGFlows

The `DGFlows` code is a solver for compressible Navier-Stokes equations in case of low Mach number. It was developed, along with the neutronics code, at TU Delft in the frame of the SAMOFAR project [38]. It solves simultaneously the set of mass, momentum and energy conservation equations, which is

$$\frac{\partial \rho}{\partial t} + \nabla \cdot (\mathbf{u}\rho) = 0 \quad , \quad (3.1)$$

$$\frac{\partial \rho \mathbf{u}}{\partial t} + \nabla \cdot (\mathbf{u}\rho \mathbf{u}) = -\nabla p + \nabla \tau + \mathbf{S}_u \quad , \quad (3.2)$$

$$\frac{\partial \rho h}{\partial t} + \nabla \cdot (\mathbf{u}\rho h) = -\nabla \cdot \mathbf{q} + S_h \quad . \quad (3.3)$$

where ρ is the density, \mathbf{u} is the velocity vector, p is the pressure, τ is the shear stress tensor, \mathbf{q} is the heat flux, while \mathbf{S}_u and S_h are sources of momentum and energy respectively. For further info on the formulation see [38]. S_h is particularly important since it contains the energy source deriving from fissions, highlighting a first coupling with the neutronics. Turbulence is modeled using Reynolds Averaged Navier-Stokes (RANS). The most common, two equations models, $k-\epsilon$ or $k-\omega$, are implemented, together with proper boundary conditions, as discussed in [38]. The Discontinuous Galerkin (DG) finite element method is adopted for the spatial discretization. It assumes discontinuous approximate solution and it works on a trial space of functions that are only piecewise continuous [10], which allows local conservation, high-order accuracy, and high geometric flexibility [38]. Backward differentiation formulae are used for time discretization, allowing the simulation of transients or pseudo-transients to compute the steady state solution [38].

3.2 The neutron transport code: PHANTOM-S_N

The PHANTOM-S_N neutronics code solves the Boltzmann transport equation, with multiple energy groups. It is based on the discrete ordinates method to express the flux angular dependency. The model equation is

$$\frac{1}{v} \frac{\partial \varphi_g}{\partial t} + \Omega \cdot \nabla \varphi_g + \Sigma_t \varphi_g = \sum_{g'} \int_{4\pi} \Sigma_{s,g' \rightarrow g}(\Omega' \cdot \Omega) \varphi_{g'} d\Omega' + \frac{(1-\beta)\chi_g^p}{4\pi} \sum_g (\nu \Sigma_f \Phi)_g + \frac{\chi_g^d}{4\pi} \sum_i \lambda_i C_i \quad , \quad (3.4)$$

where φ is the angular flux, Φ is the scalar flux, Ω is the angular direction, Σ_t is the macroscopic total cross section, Σ_s is the macroscopic scattering cross section, Σ_f is the macroscopic fission cross section, β is the total delayed neutron precursors fraction, χ is the fission spectrum, and C_i is the i -th concentration of neutron precursors. For what concerns subscripts and superscripts, g indicates the g -th energy group ($g = 1, 2, \dots, G$), d stands for delayed, p for prompt.

At the same time, it treats the equations for precursors, which contain transport term to take into account their motion, which is a key feature in the MSFR:

$$\frac{\partial C_i}{\partial t} + \nabla(\mathbf{u}C_i) + \lambda_i C_i = \nabla \cdot (D_e \nabla C_i) + \beta_i \sum_g (\nu \Sigma_f \Phi)_g \quad i = 1, 2, \dots, N_{fam} \quad . \quad (3.5)$$

where β_i is the i -th family delayed neutron fraction and $D_e = D + \nu_t / Sc_t$ (D is the molecular diffusion coefficient, ν_t is the eddy viscosity and $Sc_t = 0.85$ is the turbulent Schmidt number).

The coupling between neutronics and thermal fluid-dynamic is obtained by iterating these codes, which use the same mesh, following the scheme in Figure 3.1. DGFloWS takes the power distribution generated by fissions reactions as input, it computes the flow and temperature field and gives back these information to PHANTOM-S_N. With the new temperature field, PHANTOM-S_N introduces the density feedback, interpolating cross sections values from libraries, and the Doppler effect. Then, it computes the updated neutron distribution taking into account the salt motion through the flow and eddy diffusivity fields. Criticality eigenvalue problem is solve to compute the steady state solution. More details on the calculation of the solution and on the interaction between codes is found in [38].

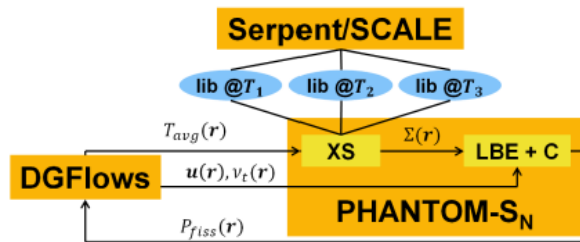


Figure 3.1: Representation of the coupling scheme between the thermal fluid-dynamic and the neutronics code. DGFloWS (thermal fluid-dynamics) and PHANTOM-S_N (neutronics) exchange data at each iteration.

3.3 The global polynomial chaos code: OpenGPC

OpenGPC is a code developed by Z. Perko at TU Delft. It is based on a set of MATLAB® functions in which formulae from Chapter 2.1 are implemented. It can build the PCE approximation of a

high number of responses, which is not limited a priori. The code uses Smolyak sparse grids to reduce the number of model evaluations to perform efficient non-intrusive spectral projection. Inputs pdfs can belong to different families (e.g. normal, uniform), whose polynomial classes (e.g. Hermite, Legendre) are associated according to [41]. The main code inputs are the set of mean values, standard deviations (or half width of variation in case of uniform distributions), the maximum polynomial order and the maximum quadrature level. `OpenGPC` automatically builds the set of quadrature points, according to this information. The output consists of the set of the expansion coefficients and basis functions for each response, as well as the list of quadrature points with their respective list of computed responses. The calculation of expansion coefficients follows its definition in Eq. (2.14). Very often responses are not immediately evaluated. In order to speedup the process, the PCE code is able to check progressively whether the i -th simulation ended with success, taking the set of outcomes. Moreover, `OpenGPC` is able to communicate with external environments for the evaluation of responses in two ways. The former involves an additional MATLAB® function, in which user-defined commands can be inserted; the latter involves Python scripts, able to submit calculations to an externally-implemented code, and waiting for the outcomes to be available. The second option is taken into account and the actions that these scripts perform are explained in the next Chapter 3.4.

In addition, sensitivity analysis, performed via sensitivity indices, is available with additional built-in functions, together with a random sampler. Thanks to this, the PCE approximation is exploited to rapidly evaluate the responses and build its probability density function inside the MATLAB® environment.

This code was successfully used to perform UQ and sensitivity analysis on complex systems in case of high number of inputs [28].

For further information on the code and its applications see [27, 28].

3.4 Scripts for the external coupling

Excluding the analysis on the results and the setup of simulations, the main task I had to perform was to write some scripts for the communication between codes for the model evaluations and the PCE code. Since we tried to couple these particular codes for the first time, the scripts needed strong efforts to be designed. As mentioned in Chapter 2.1, using NISP technique the approximation of the response's statistical information can be retrieved by projecting the response itself on a proper basis, not involving any modification of the original set of equations. Nevertheless, the PCE model needs to take the responses to compute the integral thanks to the cubature rules. `OpenGPC` allows the communication with external codes, e.g. `PHANTOM-SN` and/or `DGFloWS` in our case, but it needs some additional pieces. Their role is to take the set of abscissas (generated by the PCE code) as inputs, giving the set of responses as output.

Thanks to the collaboration with TU Delft, calculations are performed on its High Performance Cluster (HPC). Simplifying its structure, the HPC is composed by a number of nodes. Organized hierarchically, the *master node* allows the access to any node (*slave node*). Each slave node has access to its processors (generally up to 48), giving the possibility to run parallel calculations, customizing the number of required processors. The *master node* is equipped with the `qsub` command which sends the submission in queue, waiting for the requested resources to be available. In addition, it disposes the `qstat` command, to check the status of already running simulations.

Following the implementation of PCE code, the communication is made by designing three Python scripts. They use some status to identify the simulation progression. The most relevant are: *Being posted*, set when the i -th set of abscissas is sent to the external environment; *Submitted*, set when the simulation is sent to the cluster queuing system; *Fetches*, set when the

output files are read and their content stored properly; and finally *Read*, set when the results are read by the PCE code. Qualitatively presented, they are:

- *PrepareSubmission*. It receives, via .json file, the MATLAB® structure containing the total set of abscissas, together with their names. It generates folders and re-organizes the structure, activating an additional Python script (*SubmitCalculation*) to actually set up the simulation. Studying the MSFR, each simulation requires lots of resources, which can run out of memory the processors, stopping all processes. For this reason, the script was equipped with an active control on the number of running simulations, pausing their submission process if it recognizes there is an excess of submissions.
- *SubmitCalculation*. It is called by the *PrepareSubmission* script. It receives the *i*-th vector of perturbed inputs along with their names. Thanks to this information, it recognizes which parameters are perturbed, setting nominal values for the others. Then, it modifies the inputs files with the proper values, sending the calculation to the cluster. The HPC performs it, generating the outputs files when the process ends. It changes the status from *Being posted* to *Submitted*.
- *RequestStatusUpdate*. Once the submission procedure is over, MATLAB® periodically checks if and which simulations ended. This script communicate with the cluster asking if the submission, identified with a unique jobID, is still running. If not, it checks if the output files were generated and, if present, it takes the results. Then, it updates the MATLAB® structure until each calculation is completed. It changes the status from *Submitted* to *Fetches*.

The PCE code can be run directly from the master node and, thanks to the *qsub* and *qstat* functions, it can retrieve information from the model, computing the expansion coefficient. Unfortunately, being calculations sometimes expensive it is preferably to start a PCE model on a slave node to guarantee good performances of the submission processes for the whole community that uses the HPC. However, slave nodes are not equipped with *qsub* and *qstat* functions. To overcome the problem, it is necessary to return temporarily to the master node and submit/check the submissions. This complication requires two additional scripts (*SubmissionAux* and *StatusAux*). For a detailed description of the Python scripts and the submission/check process, see Appendix A.

Chapter 4

Steady-state Simulations of the CNRS Benchmark

As mentioned in Chapter 1.1.2, several analyses have already been performed on the actual geometry of the MSFR. However, novel, *ad hoc* codes were developed, as the ones presented in Chapter 3, but the verification and validation is a delicate task in absence of experimental data. A numerical benchmark was proposed at CNRS/LPSC/Grenoble, commonly known as the CNRS benchmark. It contains the main features of the MSFR, such as the precursors motion, strong coupling between thermal hydraulics and neutronics, as well as fast neutron spectrum. The problem was purified by other key features of the MSFR (e.g. turbulence, 3D geometry) which are relevant complications, but not fundamental to understand the overall behavior.

The domain, reported in Figure 4.1, is a $2\text{ m} \times 2\text{ m}$ cavity with adiabatic walls on which the no-slip boundary condition is imposed. However, the upper wall (lid) can move with a velocity u_{lid} , analogously to the well-known CFD benchmark (i.e. the lid driven cavity [13]). The salt, whose composition is $LiF - BeF_2 - UF_4$, is at initial temperature of 900 K and it is cooled via an artificial heat sink $S = \gamma(T - T_{ext})$, where γ is the volumetric heat transfer coefficient, uniform on the domain, and T_{ext} is the heat sink temperature, constant at 900 K. Buoyancy is modeled with the Boussinesq approximation. Thermodynamic properties are uniform in the domain and temperature independent. The energy dependency is discretized with 6 groups and neutron precursors are grouped in 8 families. The neutronics solution for the steady-state problem is an eigenvalue calculation normalized the reactor power. A 50×50 uniform grid is chosen for the spacial discretization, ensuring mesh independent results with second order discretization for the velocity and first for other quantities (i.e. pressure and temperature). From [17, 38], S_2 discretization, equivalent to the diffusion model, is appropriate for the angular variable.

For more detailed information and quantitative data about composition and other material-related data see [17].

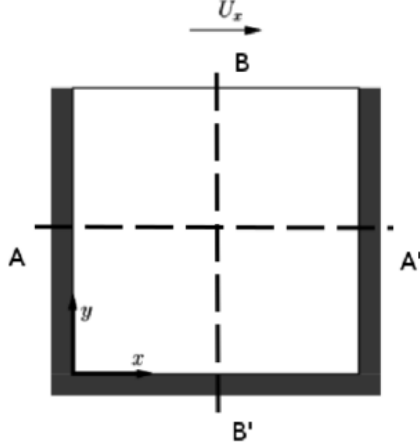


Figure 4.1: *Computational domain of the numerical benchmark proposed at CNRS/LPSC/Grenoble, the CNRS benchmark. Image from [17].*

4.1 Preliminary approach to the benchmark

The PCE method is applied, as a test case, on the CNRS benchmark to perform uncertainty quantification on multi-physics problem with several stochastic inputs and outputs. Then, results are analyzed to check their correctness and evaluate if this method is appropriate for a study on the actual MSFR design.

Before facing the complete problem, simplified versions are studied. Constraints are gradually removed to finally face a more realistic problem. Conceptually following [17], four progressively more complicated steps are examined:

- Temperature field with single stochastic input and output.
- Single-physics case: thermal fluid-dynamics only problem.
- Single-physics case: neutronics only problem.
- Multi-physics case: coupled neutronics and thermal-fluid-dynamics problem.

According to this procedure, inputs are distinguished in thermal fluid-dynamics and neutronics. For clarity, they are summarized in Table 4.1.

Table 4.1: *Complete set of input parameters for both thermal fluid-dynamics and neutronics for the CNRS benchmark. Symbols are introduced with their respective meanings.*

| Thermal fluid-dynamics | | Neutronics | |
|------------------------|--------------------------------------|----------------|--|
| <i>Symbol</i> | <i>Meaning</i> | <i>Symbol</i> | <i>Meaning</i> |
| u_{lid} | Lid velocity | $\Sigma_{f,g}$ | g-th energy group fission macroscopic cross section (6 groups) |
| β_{exp} | Thermal expansion coefficient | β_i | i-th family delayed neutron fraction (8 families) |
| ν | Kinematic viscosity | λ_i | i-th family decay constant (8 families) |
| γ | Volumetric heat transfer coefficient | $\chi_{p,g}$ | g-th energy group prompt neutron emission (6 groups) |
| P | Reactor power | ν_g | g-th energy group fission neutron yield (6 groups) |
| | | $S_{ij,0}$ | 0-th order scattering matrix (6 x 6 matrix) |

Due to the high problem dimensionality, performing a PCE on the whole set of inputs without any basis or grid adaptivity is computational expensive. However, some inputs are

supposed to have reduced effects on the response(s). Single-physics cases are studied to perform a parameter ranking, excluding irrelevant inputs from further tests (especially for the coupled problem).

Statistical properties of stochastic inputs have to be defined in a complete and consistent way. Mean value, variance and statistical distribution are key information to completely describe a random phenomenon. Inputs can be distinguished between material properties and controllable parameters. They have very different statistical properties.

- *Material properties.* According to Chapter 2, material properties can be represented as aleatory variables with normal distribution, assuming a sufficiently high number of measurements. The mean value of the normal distribution is assumed to be coincident with the nominal value of that property used in the non-stochastic calculations. Its variance depends on the accuracy of each experiment. For this benchmark, the same variance is associated to each input to understand which has the most relevant impact on the response. It is equal to 5% of the mean value.
- *Controllable parameters.* The other kind of input is related to controllable parameters (e.g. volumetric heat transfer coefficient, reactor power etc). Analogously to material properties, their mean value is coincident with the nominal value, but their distribution and variance depend on the way they vary and on the precision/accuracy of control systems. Since this is a test case and it will remain only theoretical, the features of control systems are not available. Formally, they have to be treated as epistemic variables because we have no information on the statistics, which involves different techniques with respect to aleatory variables, beyond the scope of the thesis. Uniform distributions are selected to approximate the distribution of controllable parameters, with a half interval of variation usually of 20% with respect to the mean value.

The maximum temperature (T_{max}), along with the minimum temperature, and the effective multiplication factor (k_{eff}) are defined as responses to study the thermal fluid-dynamic and the neutronics behavior, respectively. Before starting with the uncertainty/sensitivity analysis it is important to define the nominal values for the responses assuming non-stochastic inputs, by running the codes in nominal conditions. Referring to Table 4.2, the maximum temperature in the single-physics case is the one obtained by computing steady-state solution, solving at the same time the conservation equations (i.e. mass, momentum and energy). The heat source derives from separate static neutronics study, which led to a double-cosine power distribution. The effective multiplication factor in the single-physics case is computed assuming that the flow field is known. The flow field comes from the solution of the coupled problem with nominal thermal fluid-dynamics parameters. Since the k_{eff} in the neutronics-only case is basically computed starting from the coupled solution, both values of the effective multiplication factor for the single physics and coupled problem are the same.

Table 4.2: *Reference values in nominal condition for non stochastic case. They refers to the relevant responses: the maximum temperature T_{max} for the thermal fluid-dynamic and effective multiplication factor k_{eff} for the neutronics.*

| | Single physics | Coupled problem |
|---------------|----------------|-----------------|
| T_{max} [K] | 1344 | 1333 |
| k_{eff} [-] | 0.99295 | 0.99295 |

4.2 Temperature field with single stochastic input and output

The main purpose of the case under examination is to study the communication between the OpenGPC and DGFlows through specifically designed scripts, described in Chapter 3.4. Thus, being more a test case, it is not important which input is chosen. At first, the only uncertain variable is the thermal expansion coefficient β_{exp} . It appears because of the introduction of the Boussinesq approximation. For further information see Appendix B.

The thermal expansion coefficient is a material property and thus its distribution is assumed to be normal, with a mean value of $\beta_{exp,0} = 2 \times 10^{-4} \text{ K}^{-1}$ and a percentage relative standard deviation (RSD) of 5%. The input properties are summarized in Table 4.3.

The thermal-hydraulic problem consists of solving the mass, momentum and energy equations simultaneously, providing the correct temperature and flow field relative to the input configuration. The power generation is fixed (single physics problem) and it is set as input; the heat source derives from separate static neutronics study and its distribution is simply a double cosine (i.e. power distributes following the cosine function on the x and y axis). The power peak appears in the center of the domain. Since this is a single-physics problem (thermal fluid-dynamic only), the analyzed response is the maximum temperature. Before commenting the results, it is important to ensure that the polynomial expansion order and quadrature grid level are sufficiently high, as done in Figure 4.2 to correctly represent the dependence between the input and the output. Actually, the quadrature grid level lev is correlated to the maximum polynomial order. As mentioned in Chapter 2.1, the exact integration of a polynomial is limited to order $2n_{lev} - 1$. To avoid imprecise integral evaluations the grid level is set equal to the polynomial order for each case.

Figure 4.2(a) compares the pdfs, obtained with 10^5 samples and represented with 100 bins, on the third order and fifth order polynomial approximation. They are almost superposed, excluding statistical oscillations. Considering that a higher order (and thus higher level) implies an higher number of model evaluations, third order polynomial is chosen as a good compromise. Focusing on the third order polynomial, since the response (T_{max}) is almost linear with respect to β_{exp} , the pdf shape is nearly normal (with mean value equal to 1343 K, almost equal to the one in nominal conditions, and variance equal to 4.77 K^2), following the distribution of its only input. However, small deviations appear at tails, due to slight non-linearity for values higher than 15 %, as showed in the normal probability plot in Figure 4.2(b).

In addition, it emerged that increasing the thermal expansion coefficient, related to the buoyancy, decreases the maximum temperature. For this problem, buoyancy induces a motion of fluid in the cavity from the bottom to the top, forming two big vortexes symmetric with respect to the y-axis (B-B' line in Figure 4.1). Increasing β_{exp} enhanced this kind of motion. Since the power production is assumed to be double cosine-like, the maximum temperature is in proximity of the cavity center. However, the vortexes induced by the natural circulation increase the mixing in the central region thus reducing the peak temperature.

As a final remark, the effect the expansion coefficient has on the response is not very relevant, being lower than 1 %.

Table 4.3: *Input parameter of temperature field test case. Being a material property, its distribution is assumed to be gaussian with mean value coincident with the nominal one.*

| Symbol | Unit | Distribution | Mean value | RSD |
|---------------|----------|--------------|----------------------|-----|
| β_{exp} | K^{-1} | Normal | 2.0×10^{-4} | 5% |

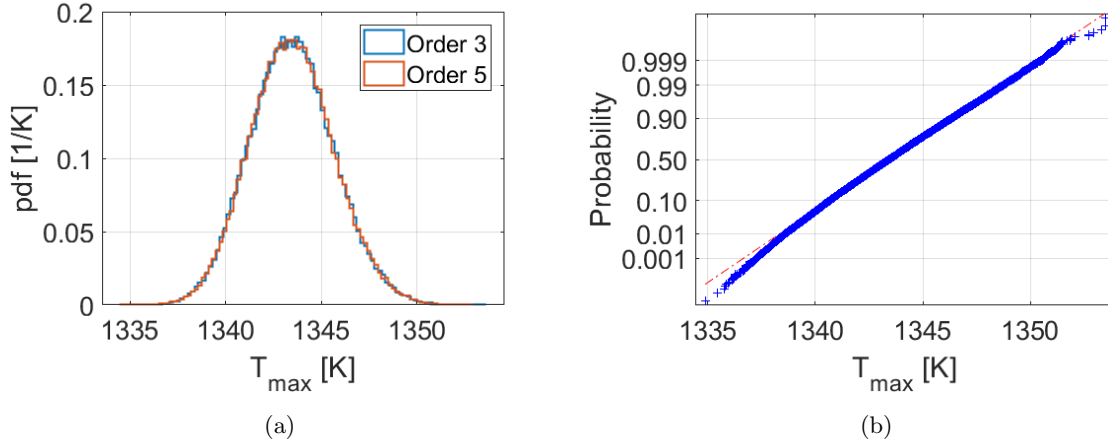


Figure 4.2: (a) *Pdf representation using different orders polynomials. It is obtained by random sampling (10^5 samples) on the polynomial representation of the response. Order 3 polynomial is able to correctly capture the response statistical information.* (b) *Normal probability plot on the order 3 polynomial: blue crosses are the related to the sampling whereas the dashed line is the reference gaussian. The samples distribute normally in the range [1340 K; 1350 K], but they show discrepancies at tails.*

Table 4.4: *Summary of input parameters for multiple input and multiple output single physics case. Simulations are run with different γ distribution, using uniform and normal. From now on, for uniform distributions relative standard deviations should be intended as the half interval of variation.*

| Symbol | Units | Distribution | Mean value | RSD |
|---------------|-----------------|--------------|----------------------|-----|
| u_{lid} | ms^{-1} | Uniform | 0.5 | 15% |
| ν | $cm^{-2}s^{-1}$ | Normal | 0.025 | 5% |
| β_{exp} | K^{-1} | Normal | 2.0×10^{-4} | 5% |
| γ | Wm^2K^{-1} | Normal | 1.0×10^6 | 5% |

4.3 Single-physics case: thermal fluid-dynamics only problem

The distinction between the present case and the one mentioned in Chapter 4.2 is mainly due to important changes in the set of scripts needed to let the PCE meta-model and the thermal fluid-dynamics solver communicate.

Table 4.4 lists input parameters for this case, according to their definition in Chapter 4.1. The maximum and minimum temperature inside the domain are the responses elaborated by the PCE meta model. Since the external temperature is fixed to 900 K and thus it is the lower limit to the cavity temperature, a change in these input parameters does not provoke any evident variation in the minimum temperature, so the analysis on this output is considered irrelevant.

Material properties such as the kinematic viscosity and the thermal expansion coefficient have a distributions set to normal, since they derive from measurements, whereas the lid velocity, an adjustable quantity, has an uniform distribution. In this first case, the heat transfer coefficient distribution is set as normal (assumed to be a material property); being related to the heat sink action, function generally dispatched by heat exchangers and thus controllable, it should be set to uniform. Normally and uniformly distributed γ are analyzed separately.

4.3.1 Normally distributed heat transfer coefficient

Keeping the fission power fixed, a steady-state solution is sought for the flow and temperature fields. Single-input PCE calculations are performed to isolate parameters with the greatest influence on the maximum temperature and to identify the appropriate polynomial order to correctly represent it, as it is not known a priori. These results are reported in Figure 4.5. Third order polynomials appear to be sufficient, being the response almost linear with respect to each input, excluding γ , which shows a modest non-linearity.

Some inputs perturb the response more strongly. γ has by far the most substantial effects. Despite the influence is almost identical, the β_{exp} has slightly more impact than the ν . On the other hand, the lid velocity does not seem able to provoke any variation on the maximum temperature.

Extending the analysis to two input PCE, γ and β_{exp} are chosen since they are responsible for the biggest variations on the response. Third-order polynomials and 17 model evaluations only are sufficient to properly represent the response. Due to the problem simplicity, the maximum temperature is almost linearly dependent on both inputs, but for strong variations of γ (beyond 20%), some deviation from linearity appears, which can be seen in Figure 4.4(b). The probability density function is obtained in the multi-input case by random sampling the inputs and computing the response through the polynomial obtained via PCE, as shown in Figure 4.4(a). The pdf follows a gaussian with mean value 1344 K and variance of 319 K². Since the inputs have a gaussian distribution and the maximum temperature is almost linear with respect to the inputs themselves, the pdf shape is preserved: as shown from the normal probability plot in figure 4.4(b), if the left tail shows deviation from the normal distribution in a limited part, the right one presents more widespread discrepancy.

4.3.2 Uniformly distributed heat transfer coefficient

To be consistent with the whole discussion, the previous analysis had to be carried out again. In fact, γ distribution should be uniform. However, this variation has relevant consequences, in particular on the pdf shape: γ is the parameter which has the strongest influence, as showed in Figure 4.3. In addition, in this second evaluation, all parameters are varied at the same time, since β_{exp} and ν especially have a similar influence on the response. The mean value is 1347 K and the variance is 1740 K². Due to a change in the distribution, the variance became 5 times

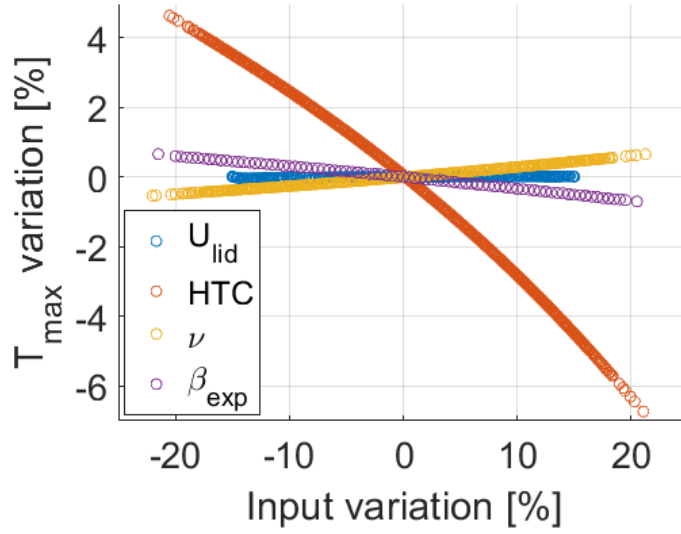


Figure 4.3: *Polynomial visualization of T_{max} for single input variation and the thermal fluid-dynamic case only. γ provokes strongest effects on the response, whereas β_{exp} and ν have similar effects. On the other hand, the lid velocity has almost no contribution.*

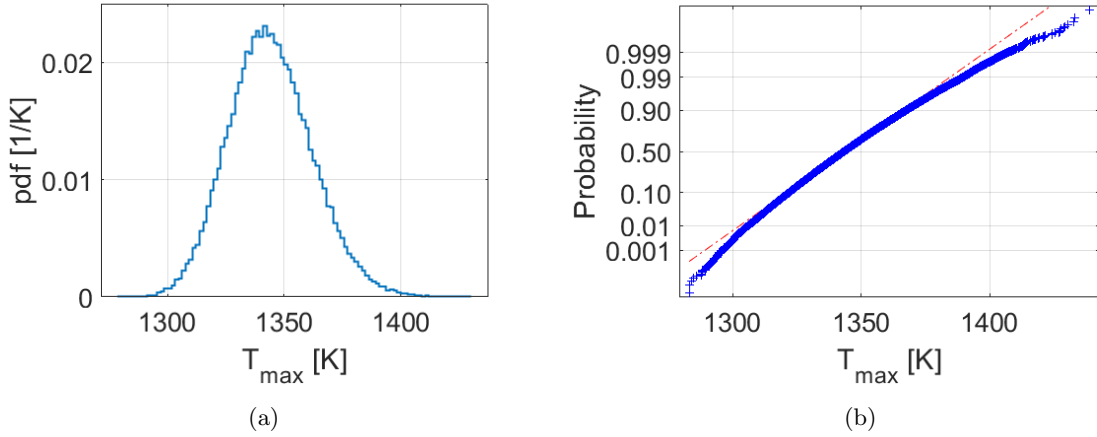


Figure 4.4: (a) *Maximum temperature pdf in the multiple inputs case by random sampling (10^5 samples) on the polynomial approximation of the response.* (b) *Samples (blue crosses) compared to the gaussian (dashed line) in the normal probability plot. The pdf is lightly asymmetric. The pdf follows a gaussian with mean value 1344 K and variance of $319 K^2$. the left tail shows deviation from the normal distribution in a limited part, whereas the right one presents more widespread discrepancy.*

Table 4.5: *Sensitivity indices for the thermal fluid-dynamic only case with uniform γ on the maximum temperature. No substantial differences between the first and the total indices imply a negligible influence of higher order interactions. γ has the only relevant contribution.*

| | u_{lid} | ν | β_{exp} | γ |
|-------------|-----------------------|-----------------------|-----------------------|-----------------------|
| S_i | 3.05×10^{-5} | 1.97×10^{-3} | 2.66×10^{-3} | 9.95×10^{-1} |
| $S_{tot,i}$ | 5.96×10^{-5} | 2.03×10^{-3} | 2.67×10^{-3} | 9.95×10^{-1} |

higher. Figure 4.5 reports the pdf for uniformly distributed γ . To properly explain the main features of the pdf, it is better to analyze the sensitivity indices, reported in Table 4.5.

It emerges γ is responsible of the 99.5% of the response variance. In fact, the shape of the pdf is nearer to a uniform distribution rather than a gaussian. Secondly, as stressed by the sensitivity indices, the contribution of the kinematic viscosity and the thermal expansion coefficient is comparable and one cannot be preferred over the other.

The total sensitivity indices are almost equal to the first order ones, showing no relevant higher order dependencies and, in addition, $\sum_i S_{tot,i} = 1.000$. Finally, it is interesting to see the pdf is not exactly uniform but it has some deviations due to a slight non-linearity in γ . Focusing on the sensitivity indices, the only relevant terms in the PCE approximations are γ -only ones, since it is possible to exclude any kind of second or higher order interactions. Therefore, the response can be approximated as

$$T_{max} = C_0 + C_1 P_1(f(\gamma)) + C_2 P_2(f(\gamma)) + C_3 P_3(f(\gamma)) \quad (4.1)$$

where P_1 , P_2 , P_3 are the Legendre polynomials of order 1, 2 and 3 and C_i , with $i \in (0, 1, 2, 3)$, are their respective coefficients. $f(\gamma)$ takes into account the normalization (i.e. the argument of the Legendre polynomials has to be in the range $[-1, 1]$). C_2 is approximately one order of magnitude lower than C_1 which makes the term proportional to γ^2 non-negligible.

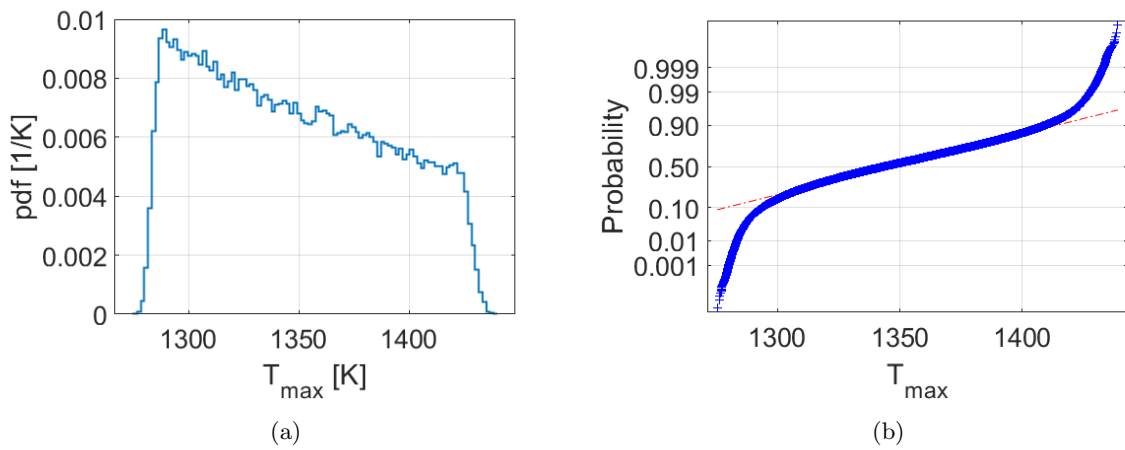


Figure 4.5: (a) *Maximum temperature pdf in the multiple inputs with uniform γ . Obtained by random sampling (10^5 samples) on the third order polynomial approximation of the response. The variance became 5 times higher than the normally distributed γ case.* (b) *Normal probability plot on the third order polynomial approximation. It shows evident deviations from the normal distribution especially at tails.*

4.4 Single-physics case: neutronics-only problem

The second part of the study on the benchmark regards the neutronics behavior. Analogously to what described in Chapter 4.3, the distribution of the neutron population is analyzed separately. The flow field is set as the one obtained from the multi-physics coupling with nominal values both for thermal-hydraulic parameters ($\gamma = 1 \times 10^6 \text{ W}/(\text{m}^2\text{K})$, $\nu = 2.5 \times 10^{-2} \text{ cm}^2/\text{s}$ and $\beta = 2.0 \times 10^{-4} \text{ K}^{-1}$), which remain fixed for the whole neutronics-only analysis, and neutronics ones.

As showed in Table 4.1, now there are 70 stochastic inputs (including all elements of the 0-th order scattering matrix) and a way to discriminate the relevant-only parameters is needed. In fact, increasing the number of inputs largely increases the number of model evaluations (e.g. assuming third polynomial order and 7 quadrature points for the level 3 quadrature, considering 70 inputs and a full grid, the total number of model evaluation is $7^{70} = 1.44 \times 10^{59}$).

Every input should be considered a material property, thus having a normal distribution, with mean value equal to the nominal value and 5% variance. Nominal values are reported in Table 4.6.

Two approaches are analyzed to treat the high dimensionality: the "mean value approach" and the "class approach". The *mean value approach* consists of the definition of a class (e.g. Σ_f class, β class), computing a representative value and performing the PCE analysis on this single value. Starting from it, the value of g-th energy group/family is retrieved by rigid (linear) translation, maintaining proportions among the class members and the representative value. The *class approach* consists of the definition of classes, analogously to the previous one, but all inputs belonging to that class are studied at the same time. Obviously, both approaches have pros and cons. The former defines a single input for each class, ensuring that, if the class has a relevant contribution to the response, the stochastic variable is only one. On the other hand, it introduces correlation among the members of the class, thus modifying the statistics. The latter is computationally heavier, since 6 or 8 inputs are involved at a time. In addition, at the end of the analysis, more than one input can be relevant, reducing the effectiveness of the input parameters limitation. Nevertheless, it has the big advantage to avoid correlations among inputs.

The response is the effective multiplication factor k_{eff} , since it is a key design parameter, while providing global information on the neutron population. In case of systems near to criticality, like this one, a change in the input can imply a change from subcritical to supercritical condition. An important step of the analysis is the comparison between two approaches to find if the correlation adds major variation to the response pdf.

4.4.1 Relevant input determination: mean value approach

In this first and simplified case, only Σ_f class and β class are assumed to be relevant. The representative value for the beta class can be the total delayed neutron fraction, which is also a relevant physical parameter, defined as

$$\beta_{tot} = \sum_{i=1}^{N_f} \beta_i \quad ,$$

where N_f is the number of precursors' families (in this case 8). On the contrary, the mean fission cross section is not chosen with a solid physical definition, but rather as the averaged value over the energy groups.

$$\Sigma_{f,mean} = \frac{\sum_{g=1}^{N_g} \Sigma_{f,g}}{N_g} ,$$

where N_g is the number of groups (equal to 6 in this case). In addition, this definition does not preserve the physics. The average cross section, for the g -th energy group, is defined such that the number of interactions is preserved. In order to do it, the cross section need to be weighted on the flux in the g -th group.

As mentioned in Chapter 4.4, this is based on the assumption that the statistics is not substantially modified, since in both cases it introduces a correlation. For the two quantities, starting from one-value input, it is necessary to reconstruct the subdivision for each group/family. As an additional assumption, the proportions for each group/family is constant, while changing the representative value. This step is performed before starting simulations, as a preliminary evaluation. Table 4.7, provides a proper summary of inputs.

As usual, a preliminary single output study is performed to individually investigate the dependency with the response. Analogously to the previous case, 3^{rd} order polynomials are sufficient to properly represent the effective multiplication factor. Results show that k_{eff} seems to be insensitive to β_{tot} and almost linear with respect $\Sigma_{f,mean}$. In fact, the mean macroscopic fission cross section has direct and relevant effects on the neutron population since it directly affects the neutron balance. Vice versa, the delayed neutron fraction has a contribution only on a small fraction of neutrons (less than 1%). In molten salt reactor the effect of β_{tot} on the multiplication factor is non-zero, even if it is very low. This is conceptually different from other kind of reactors, since the precursors contribute on the k_{eff} only in transient scenarios. In fact, molten salt reactors foresee the fuel movement and precursors can decay in regions with lower importance. Analogously to the thermal fluid-dynamic case, the probability density function along with its normal probability plot is reported in Figure 4.6. According to Figure 4.6(b), the shape is still gaussian, maintaining the input distribution features; the response is linear in the worst case and it can be interpreted as a superposition of effects between two gaussian inputs. In second place, the mean value is below 1 (subcritical reactor) but there is a non negligible probability to have a supercritical configuration. The standard deviation is ± 2980 pcm, which is generally too high, but it is tolerable in this case since the study is finalized to a parameter ranking.

4.4.2 Relevant input determination: class approach

Following the approach introduced in Chapter 4.4, six classes are identified. They are: the fission yield (ν) class (6 members) , fission cross section (Σ_f) class (6 members), scattering cross section (Σ_s) class (6 members), prompt neutron emission (χ) class (6 members), delayed neutron fraction (β) class (8 members) and the delayed decay constant (λ) class (8 members). Each parameter is normally distributed with a relative standard deviation of 5%, allowing a parameter ranking with same inputs variability.

A comment has to be made about the scattering cross section (linked to the scattering matrix). Actually, provided data from the molten salt system under consideration contain scattering matrices up to order 3 (i.e. there 4 matrices are defined, from order 0 to order 3). Each element (i, j) of the order 0 matrix represents the probability a neutron scatters from the energy group i to the group j. In fact, it can be shown that only scattering moments of order zero give the value of the macroscopic scattering cross section. Summing the elements on i-th row, one can obtain the macroscopic cross section relative to the i-th energy group. Table 4.8 represents the 0-th order scattering matrix with nominal values.

Table 4.6: *List of neutronics input parameters with mean values. The 0-th order scattering matrix is not included.*

| Symbol | Value | Symbol | Value | Symbol | Value | Symbol | Value |
|------------------------------------|--------------------------|--------------|--------------------------|--------------------------------|--------------------------|--------------------------------|--------------------------|
| $\Sigma_{f,1}$ [cm ⁻¹] | 1.11309×10^{-3} | ν_4 [-] | 2.4313 | β_1 [-] | 2.33102×10^{-4} | λ_2 [s ⁻¹] | 2.82917×10^{-2} |
| $\Sigma_{f,2}$ [cm ⁻¹] | 1.08682×10^{-3} | ν_5 [-] | 2.4333 | β_2 [-] | 1.03262×10^{-3} | λ_3 [s ⁻¹] | 4.25244×10^{-2} |
| $\Sigma_{f,3}$ [cm ⁻¹] | 1.52219×10^{-3} | ν_6 [-] | 2.4333 | β_3 [-] | 6.81878×10^{-4} | λ_4 [s ⁻¹] | 1.33042×10^{-1} |
| $\Sigma_{f,4}$ [cm ⁻¹] | 2.58190×10^{-3} | χ_1 [-] | 3.53812×10^{-1} | β_4 [-] | 1.37726×10^{-3} | λ_5 [s ⁻¹] | 2.92467×10^{-1} |
| $\Sigma_{f,5}$ [cm ⁻¹] | 5.36326×10^{-3} | χ_2 [-] | 5.23642×10^{-1} | β_5 [-] | 2.14493×10^{-3} | λ_6 [s ⁻¹] | 6.66488×10^{-1} |
| $\Sigma_{f,6}$ [cm ⁻¹] | 1.44917×10^{-2} | χ_3 [-] | 1.21033×10^{-1} | β_6 [-] | 6.40917×10^{-4} | λ_7 [s ⁻¹] | 1.63478 |
| ν_1 [-] | 2.8552 | χ_4 [-] | 1.35457×10^{-3} | β_7 [-] | 6.05805×10^{-4} | λ_8 [s ⁻¹] | 3.55460 |
| ν_2 [-] | 2.5453 | χ_5 [-] | 1.51226×10^{-4} | β_8 [-] | 1.66016×10^{-4} | | |
| ν_3 [-] | 2.4333 | χ_6 [-] | 7.37236×10^{-6} | λ_1 [s ⁻¹] | 1.24667×10^{-2} | | |

Table 4.7: *List of inputs for the neutronics-only case using the mean value approach.*

| Symbol | Meaning | Units | Distribution | Mean value | RSD |
|-------------------|--|------------------|--------------|-----------------------|-----|
| β_{tot} | Total precursors fraction | — | Normal | 6.88×10^{-3} | 5% |
| $\Sigma_{f,mean}$ | Mean macroscopic fission cross section | cm ⁻¹ | Normal | 4.36×10^{-3} | 5% |

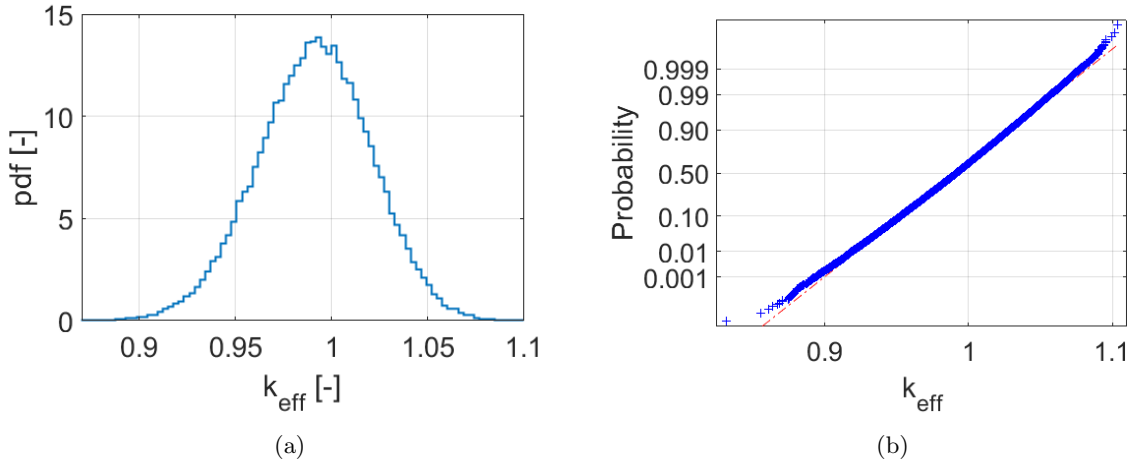


Figure 4.6: (a) *Effective multiplication factor pdf in the multiple inputs case by random sampling (10^5 samples) on the polynomial approximation of the response.* (b) *Samples (blue crosses) compared to the gaussian (dashed line) in the normal probability plot. The shape is almost perfectly superposed with the gaussian reference.*

Observing Table 4.8, one cannot exclude the scattering contribution to the effective multiplication factor, since its value (as mentioned before, summing the elements on the i -th row) is two orders of magnitude higher than the macroscopic fission cross section.

It is important to notice that elements of the main diagonal, related to the self scattering, have probabilities at least one order of magnitude higher than the other, whereas the up-scattering is assumed to be impossible, i.e. the probability of jumping from a lower energy group to a higher energy one is taken exactly equal to zero. For this reason, only the main diagonal terms are considered relevant and so subjected to the uncertainty/sensitivity analysis. For this reason, 6 members are associated to the scattering cross section class.

Classes composed by 6 members needed 97 evaluations to build the PCE approximation, while the ones with 8 needed 161. The standard deviation that each class introduced on the k_{eff} , reported in Table 4.10, is used to determine which of them has a relevant contribution.

Standard deviation of ν and Σ_f classes is comparable, but more importantly, it is at least one order of magnitude higher than other classes. Being these values so different, they are neglected, while ν and Σ_f classes are kept for further studies.

However, inside the Σ_f and ν classes only a fraction of energy groups may give a relevant contribution to the k_{eff} variance. This aspect is addressed with sensitivity indices, reported in Table 4.11. Both the fission cross section and the fission yield have a primary role in the quantity of neutrons generated in each energy group, as they appear in the transport equation always as the product $(\nu \Sigma_f)_g$. In fact, sensitivity indices are approximately the same for both quantities.

Groups 1 and 2 introduce a small perturbation in the response (below 2%). Taking Σ_f class as a reference, it is important to notice the contribution of the 6th group is smaller than the 5th, despite the 6th group ($E_n < 0.75$ keV) has a much higher fission cross section. In fact, since the average flux in this group is higher (Table 4.9), fissions are more abundant at higher energies (order keV) because this reactor lacks of moderator and the overall spectrum is harder. Vice versa, for high neutron energies (group 1, 2 MeV–20 MeV) the contribution is negligible since the neutron population is scarce.

The difference between the first order sensitivity indices and the total sensitivity indices quantifies the contribution of second or higher order interactions.

High energy groups can be excluded from the analysis since they produce a small variation compared to more thermal ones. However, this choice is not unique and some options are provided.

- Groups 5 and 6 contain the 70 % of the variance and they represent the minimum amount of inputs.
- Groups 4, 5 and 6 contain 85 % of variance, reducing the approximation related to the parameter space limitation.
- Groups 3, 4, 5 and 6 contain 98 % of variance. In addition, groups 3 and 4 contribute to the variance almost in the same way, thus there are no particular reasons to include only one. On the other hand, the number of inputs is higher.

The first choice is the most attractive one since it minimizes the parameter space, while considering at the same time a good fraction of the response variance, for both ν and Σ_f class.

Finally, having started from 70 inputs, ν_5 , ν_6 , $\Sigma_{f,5}$ and $\Sigma_{f,6}$ is the whole set of relevant neutronics parameters, which constitutes a big improvement for what concerns the performances of the PCE code, in terms of number of requested model evaluations.

4.4.3 Results comparison between *class approach* and *mean value approach*

Once analyzed the results of both approaches, a comparison is performed to ensure they give correct results. The *mean value approach* is definitely superior with respect to the *class approach* since, having to analyze only one input ($\Sigma_{f,mean}$) it needed just 4 model evaluations. On the other hand, the Σ_f class analysis by itself required about 100 simulations. The comparison involves only the Σ_f class since during the *mean value approach* a reduced set of inputs was analyzed.

The pdfs obtained with 10^5 samples on third order polynomials approximations are reported in Figure 4.7. Despite the mean value is nearly the same (0.99270 for *class approach* against 0.09909 for *mean value approach*), the variance is substantially different. It is 8.89×10^{-4} for the *mean value approach* while only 1.96×10^{-4} , approximately 5 times lower. Evidently, despite the *mean value approach* gives an advantage from the computational point of view, it deforms the statistical behavior, becoming useless. Thus, the *class approach* was proved to be a reliable tool for the parametr space reduction and is adopted when needed.

Table 4.8: *Nominal values of the 0-th order scattering matrix. The up scattering is assumed to be impossible. Values in $[\text{cm}^{-1}]$.*

| Group j → i ↓ | 1 | 2 | 3 | 4 | 5 | 6 |
|------------------|--------------------------|--------------------------|--------------------------|--------------------------|--------------------------|---------------------------|
| 1 | 1.08476×10^{-1} | 5.23316×10^{-2} | 4.01805×10^{-3} | 1.09869×10^{-4} | 2.5329×10^{-5} | 3.78334×10^{-6} |
| 2 | 0 | 1.83666×10^{-1} | 3.19138×10^{-2} | 2.34218×10^{-5} | 2.25259×10^{-6} | 2.00405×10^{-7} |
| 3 | 0 | 0 | 2.98293×10^{-1} | 1.63470×10^{-2} | 1.70575×10^{-5} | 1.24625×10^{-6} |
| 4 | 0 | 0 | 0 | 2.17472×10^{-1} | 1.90243×10^{-2} | 1.68580×10^{-8} |
| 5 | 0 | 0 | 0 | 0 | 2.27173×10^{-1} | 1.05885×10^{-2} |
| 6 | 0 | 0 | 0 | 0 | 0 | 2.378261×10^{-1} |

Table 4.9: *Space-averaged neutron flux in the domain for the CNRS benchmark test case for each energy group.*

| | Group 1 | Group 2 | Group 3 | Group 4 | Group 5 | Group 6 |
|---|---------|---------|---------|---------|---------|---------|
| $\Phi [\text{cm}^{-2}\text{s}^{-1}] \times 10^{16}$ | 1.22 | 4.92 | 9.19 | 5.94 | 4.74 | 1.43 |

Table 4.10: *Standard deviation comparison between input classes in the neutronics-only case. Σ_f and ν have a variance at least two orders of magnitude higher with respect to other classes.*

| | ν class | Σ_f class | Σ_s class | χ class | β class | λ class |
|----------|-----------------------|-----------------------|-----------------------|-----------------------|------------------------|------------------------|
| Variance | 5.57×10^{-4} | 1.95×10^{-4} | 4.37×10^{-6} | 9.86×10^{-8} | 3.57×10^{-10} | 9.80×10^{-12} |

Table 4.11: *Sobol indices for k_{eff} response in the neutronics-only case with the class approach (Σ_f class and ν class). Classes variances are equal to 1.95×10^{-4} and 5.57×10^{-4} respectively.*

| | Group 1 | Group 2 | Group 3 | Group 4 | Group 5 | Group 6 |
|------------------|-----------------------|-----------------------|-----------------------|-----------------------|-----------------------|-----------------------|
| $S_{i,\Sigma}$ | 1.97×10^{-3} | 2.16×10^{-2} | 1.29×10^{-1} | 1.53×10^{-1} | 4.20×10^{-1} | 2.75×10^{-1} |
| $S_{i,\nu}$ | 1.64×10^{-3} | 2.02×10^{-2} | 1.27×10^{-1} | 1.52×10^{-1} | 4.19×10^{-1} | 2.80×10^{-1} |
| $S_{tot,\Sigma}$ | 1.97×10^{-3} | 2.16×10^{-2} | 1.29×10^{-1} | 1.53×10^{-1} | 4.20×10^{-1} | 2.75×10^{-1} |
| $S_{tot,\nu}$ | 1.64×10^{-3} | 2.02×10^{-2} | 1.27×10^{-1} | 1.52×10^{-1} | 4.19×10^{-1} | 2.80×10^{-1} |

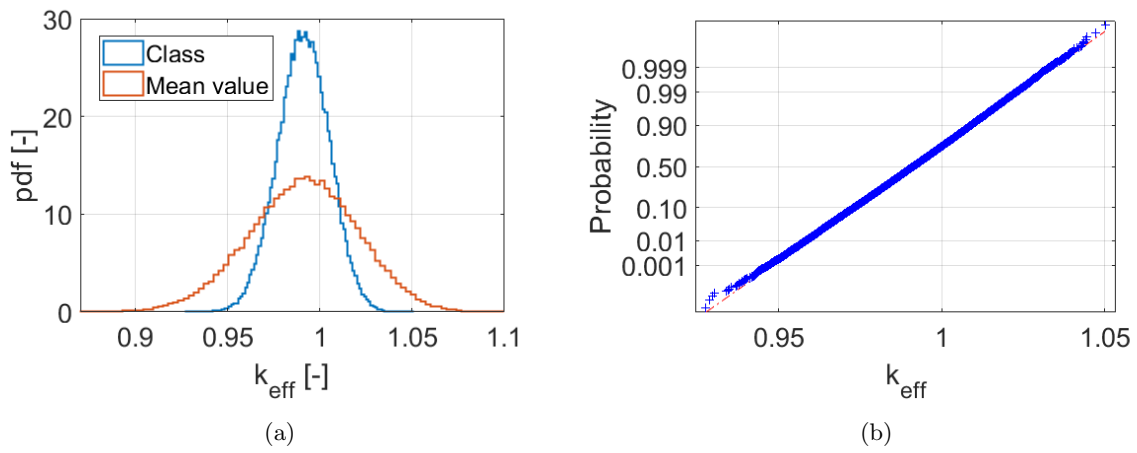


Figure 4.7: (a) Pdf comparison between the pdf obtained through sampling of the class approach and mean value approach polynomials, considering fission cross sections only. Despite the mean value is similar, the variance is substantially different since the statistics is deformed with the "mean value approach". (b) Normal probability plot on the "class approach" order 3 polynomial: blue crosses are the related to the sampling whereas the dashed line is the reference gaussian

4.5 Multi-physics case: coupled neutronics and thermal fluid-dynamics problem.

Differently from Chapters 4.2, 4.3 and 4.4, the coupling between neutronics and thermal-fluid-dynamics triggers feedback effects. Feedback generally affects macroscopic cross sections, which can vary by varying either the atomic density or the microscopic cross section. The neutronic code allows including the density feedback and Doppler effects. The former corrects the macroscopic cross section by changing the density of the atomic species, which is altered because of temperature differences. The latter is related to the broadening of the resonance capture cross section when the nuclei kinetic energy increases (i.e. when temperature increases). In the following analysis only density feedback effects are considered. However, Doppler effects are mostly relevant in transients to study the reactor dynamic and thus they are supposed to have very little influence on the outcome of steady-state simulations.

Another difficulty derives from a more complex interaction between the codes themselves and with the cluster. For further information on this topic see in the Appendix A.

For this part, it is possible to take advantage of previous analysis to identify relevant inputs. In particular, inputs whose effect is below 1% of response variation are considered negligible. This leads to the exclusion of all thermal fluid-dynamics parameters, except for the volumetric heat transfer coefficient γ . On the other hand, for the neutronics part, following the results reported in Chapter 4.4.2, the fission cross sections of groups 5 and 6 are chosen along with ν for groups 5 and 6. The whole set of input parameters is reported in Table 4.12. Finally, the power produced (P) is added as input: it is introduced only in the coupled case as it is related to the neutronics part, but, since previous analysis focused only on the effective multiplication factor and it used the power as normalization factor, its variation would have had no effects on the solution. As it is not a material property, but more a controllable variable, its distribution is set to uniform.

Even in this case, the maximum temperature and the effective multiplication factor are the considered responses (along with the minimum temperature, which is however irrelevant, as explained in Chapter 4.3).

4.5.1 Monte Carlo Sampling

Despite the pdf obtained by sampling on the PCE approximation showed a reasonable behavior, they need to be compared with a reliable reference. MC sampling is generally the best way to approach this comparison, thanks to its capability of retrieving the statistical information of any system, provided a sufficient number of experiments.

In this case, 10^3 samples are assumed sufficient to have a preliminary, yet meaningful statistics. Inputs are generated according to Table 4.12.

Figure 4.8 shows the results of the MC sampling on the maximum temperature, while Figure 4.9 on the effective multiplication factor.

Figure 4.8(a) confirms that 10^3 are a good amount samples. In fact, according to the central limit theorem, the mean value of a random phenomenon is a random number itself, with a mean value equal to the mean value of the phenomenon and a variance equal to the variance of the phenomenon divided by the number of experiments. After few tens of samples, the relative standard deviation respects the $1/\sqrt{N}$ behavior, where N is the number of experiments. The mean value is (1338 ± 2) K, with a probability of 68 %, whereas the standard deviation of the phenomenon is 3.71×10^3 K².

Analogous comments for the k_{eff} . The mean value is 0.99297 [–] within an interval of ± 72 pcm, with a probability of 68 %. The standard deviation of the phenomenon is 5.28×10^{-4} [–].

Table 4.12: *Input parameters for coupled problem. The mean value corresponds to their value in nominal conditions. The reactor power is added on to of the relevant only parameters.*

| Symbol | Unit | Mean value | Standard deviation | Distribution |
|----------------|-------------------------------|------------------------|--------------------|--------------|
| γ | $\text{Wm}^{-1}\text{K}^{-1}$ | 1.0×10^6 | 20% | Uniform |
| P | W | 1.0×10^9 | 20% | Uniform |
| $\Sigma_{f,5}$ | cm^{-1} | 5.363×10^{-3} | 5% | Normal |
| $\Sigma_{f,5}$ | cm^{-1} | 1.449×10^{-2} | 5% | Normal |
| ν_5 | — | 2.4333 | 5% | Normal |
| ν_6 | — | 2.4333 | 5% | Normal |

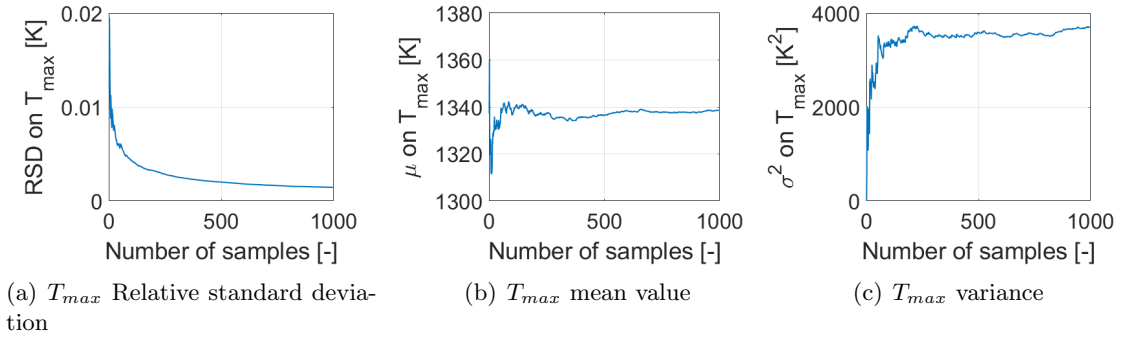


Figure 4.8: (a) T_{max} relative standard deviation. According to the central limit theorem, the variance on the sample average decreases inversely proportionally to the square root of the number of samples (b) T_{max} mean value. Despite the low number of experiments, the mean value has not big oscillations after 700 samples. (c) T_{max} variance. After 900 samples it is stable around 3700 K^2 .

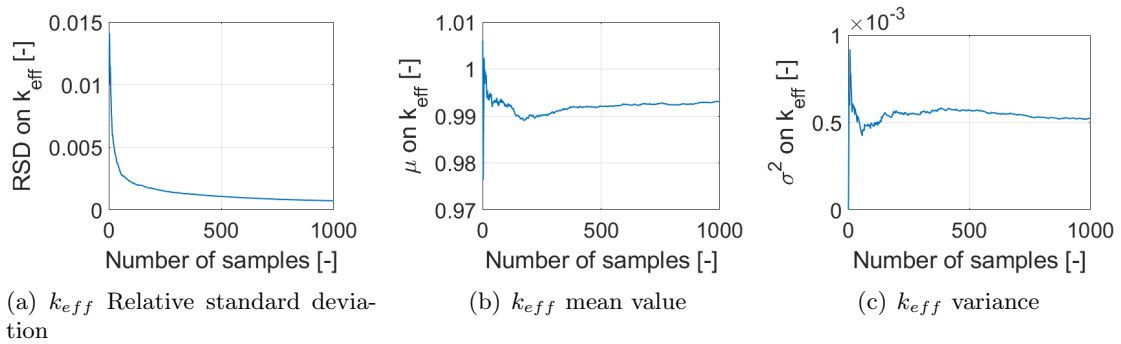


Figure 4.9: (a) k_{eff} relative standard deviation. According to the central limit theorem, the variance on the sample average decreases inversely proportionally to the square root of the number of samples (b) k_{eff} mean value. Despite the low number of experiments, the mean value has not big oscillations after 500 samples. (c) k_{eff} variance. After 700 samples it is stable around $5.5 \times 10^{-4} [-]$.

It is worth to notice that each simulation needed on average more than one hour, leading to a total computational time of approximately 1500 h.

4.5.2 Results: maximum temperature

In order to check the correctness of the PCE approximation on the maximum temperature, a comparison between the polynomial of order 3 with 10^5 samples and the polynomial of order 4 with 10^6 samples is performed in Figure 4.10. In spite of the large number of samples for the PCE approximations, the number of bins is limited to 15 because of the representation in the same figure of the responses obtained with MC sampling. As evident, between order 3 and 4 PCE no relevant discrepancies appear, confirming third order polynomials are enough to represent the correct response behavior. The main difference stands in the number of model evaluations: 97 in case of order 3, 533 for order 4. Consequently, the polynomial of order 3 is taken as best compromise.

A second comparison is made among the PCE evaluations (both of orders 3 and 4) and the MC reference. Parameters used for the comparison are the mean values, the variances and the maximum error on the probability density function. The last one is computed by taking the random inputs generated by the MC code and plugging them to evaluate the response with the PCE approximation. Each value (1000 in total) is compared with the MC-evaluated value, showing the maximum one. These numbers are reported in Table 4.13.

Table 4.13: *Comparison among the PCE evaluations (both of orders 3 and 4) and the MC reference. The two PCE approximations are able to represent the statistical information with excellent accuracy. The error on the variance is higher for the order 4 PCE due to a general low amount of model evaluations for the MC reference.*

| | e_μ [%] | e_{σ^2} [%] | $\max e_{pdf}$ [%] |
|-------------|-------------|--------------------|--------------------|
| PCE order 3 | 0.17 | 1.00 | 0.21 |
| PCE order 4 | 0.16 | 1.09 | 0.21 |

For both order 3 and 4 PCE approximations, the agreement with reference MC sampling is excellent. The error on mean value is around 10^{-3} and as expected, it is lower for the order 4 PCE. In addition, they have the same maximum error on the pdf, suggesting no evident improvement if the polynomial order increases, and thus confirming quantitatively what explained in Figure 4.10. On the other hand, the error on the variance is lower for the order 3 PCE, probably due to a not sufficient number of MC evaluations. As last remark, for orders 3 and 4 the mean values (1337 K) are within the 68% probability range with respect to the MC average, corresponding to the interval [1336 K; 1340 K].

Figure 4.10(b) reports the normality test, performed on the data set obtained with 3rd order polynomial and 10^5 samples. Despite in the range [1270 K; 1470 K] the curve is almost gaussian, it shows substantial discrepancies at the tails. The reason of it can reside in the input distribution and in the relation between the inputs and the response. The reason of the pdf asymmetry is related to non-linearity of the response, in particular with respect to γ .

Sensitivity indices. Sensitivity indices are shown in Table 4.14. First order γ and P interactions are the only relevant contributions. However, differently from the single physics case, the influence of higher order terms is evident especially for $\Sigma_{f,i}$ and ν_i . They increase their contribution to the variance of three orders of magnitude. In fact, they are neglected in any case since their sensitivity indices are 4 orders of magnitude lower than those related to P or γ .

In fact, the former is responsible of the 45% of the maximum temperature variance, whereas the latter of 55%. Neutronics related parameters seem to have negligible influence on the maximum temperature because the oscillations in the power shape they create are at least one order of magnitude lower with respect to the power intensity. This aspect is vital to confirm the correctness of the whole analysis. The parameter ranking performed on single physics problems, assuming the feedback effects give secondary contributions on the responses, i.e. the maximum temperature in this case. In fact, γ and P have a direct effect on the maximum temperature since they explicitly appears in the energy balance.

In addition, $\sum_i S_{tot,i} = 1.044$, which underlines second order iterations between P and γ may be relevant. Assuming these interactions are negligible, the response can be expressed in an analogous form of Eq. (4.1), including terms for the power.

Table 4.15 reports the polynomial chaos expansion coefficients up to the 3rd order. The sign of the first order coefficient for γ is correct since the maximum temperature decreases if γ increases. Despite the first order coefficients for both quantities are of the same order of magnitude, the second and third orders are much higher for γ , stating that the effect of non-linearity is definitely relevant. Unfortunately, due to the introduction of the reactor power as input, the comparison with the single physics case is not performed. In fact, the power is a parameter introduced only in the coupled problem and it is responsible of more than a half of the maximum temperature variance.

Table 4.14: *Sensitivity indices in the coupled case for maximum temperature response. P and γ give the only relevant contribution to the response variance.*

| | P | γ | $\Sigma_{f,5}$ | $\Sigma_{f,6}$ | ν_5 | ν_6 |
|-------------|-----------------------|-----------------------|-----------------------|-----------------------|-----------------------|-----------------------|
| S_i | 5.50×10^{-1} | 4.45×10^{-1} | 1.91×10^{-8} | 2.59×10^{-8} | 1.84×10^{-8} | 2.21×10^{-8} |
| $S_{tot,i}$ | 5.55×10^{-1} | 4.50×10^{-1} | 2.49×10^{-5} | 2.49×10^{-5} | 2.49×10^{-5} | 2.49×10^{-5} |

Table 4.15: *PCE coefficients for the power and γ . Despite the first order coefficient has the same order of magnitude, the second and the third ones show relevant effects of non-linearity for γ .*

| | Order 0 | Order 1 | Order 2 | Order 3 |
|----------|---------|---------|---------|---------|
| γ | 1337 | -69.7 | 8.39 | 0.875 |
| P | 1337 | 77.8 | 0.734 | 0.0383 |

Feedback effects. The effect of feedback on the pdf can be seen by comparing the pdf obtained in the single physics, thermal fluid-dynamics only, with the pdf obtained with the coupled problem excluding the power as stochastic input. Figure 4.11 compares these two pdfs.

The overall shape is similar, but it is moved to lower temperatures. The difference in the mean value is surely related to the coupling: in fact, an increase in temperature provokes a reduction of the salt density and thus a reduction in the cross section, including the fission one. The region of maximum temperature is subjected to the strongest reduction of the cross sections. The global effect is a decrease in the maximum temperature, which is evident from Figure 4.11. The comments on the shape are analogous to the one mentioned in section 4.3. The decrease to zero is even sharper since the contribution of γ on the variance, and thus on the pdf shape, is stronger. The variance, on the other hand, is nearly the same (1.64×10^3 for coupled versus 1.75×10^3 for single physics, which is approximately 6% difference), since,

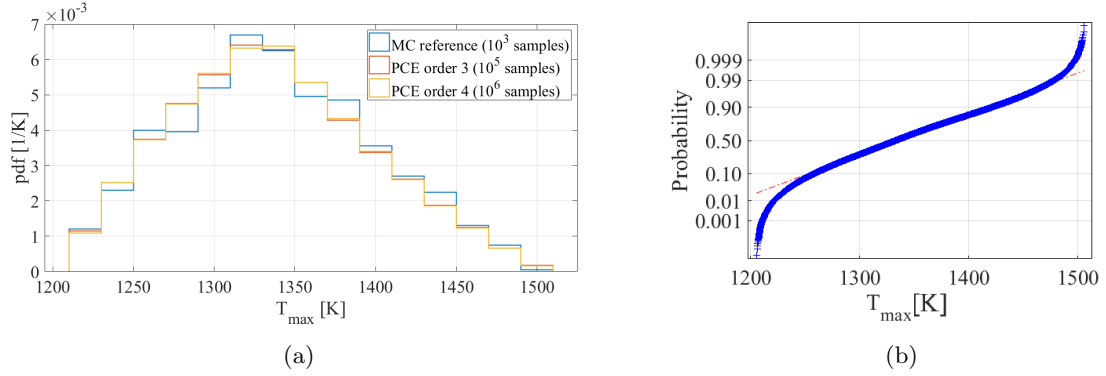


Figure 4.10: (a) Pdf representation of T_{max} using different polynomials orders and number of samples compared with the reference MC sampling. (b) Normal probability plot on the 3rd order polynomial curve. Blue crosses are the related to the sampling whereas the dashed line is the reference Gaussian. The samples distribute normally in the range [1270 K; 1470 K], but they show strong deviations at tails.

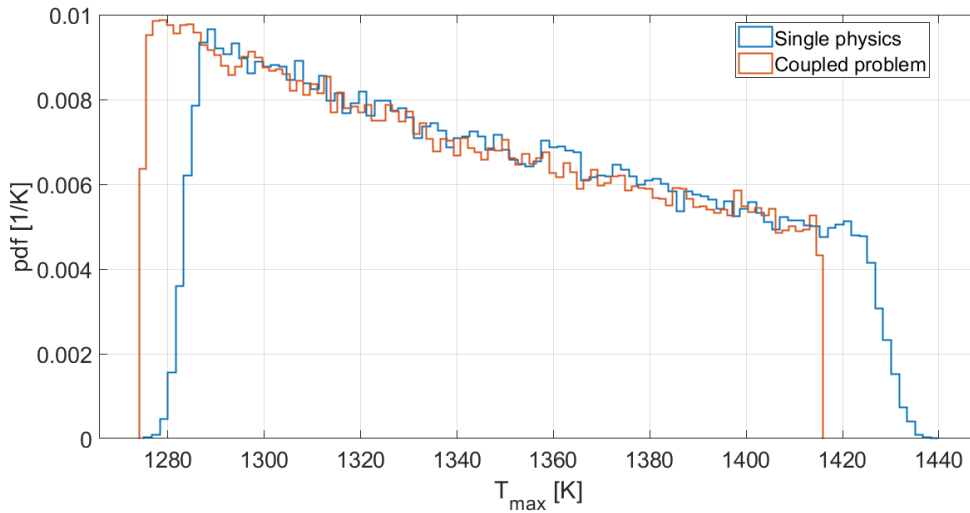


Figure 4.11: T_{max} pdf comparison with uniform heat transfer coefficient in the single physics (thermal fluid-dynamic only) and in the coupled problem. The differences between the two curves are mainly due to density feedback effects.

as sensitivity indices show, it can be attributed almost only to γ contribution. However, this decrease may indicate an attenuation of γ contribution on the maximum temperature, thanks to the presence of density feedback. Thus, the overall variance share may be different, but no dramatic variations appear due to the introduction of feedback effects.

4.5.3 Results: effective multiplication factor

Figure 4.12 shows the effective multiplication factor pdf, for both the single physics and coupled case, as well as the normal probability plot.

Analogously to what commented for the maximum temperature, the difference between order 3 and 4 is negligible with respect to the saving in term of computational cost, as highlighted qualitatively in Figure 4.12(a). Quantitatively, order 3 and 4 PCE are compared with the MC sampling in Table 4.16, using the same quantities of Chapter 4.5.2.

Again, errors on the mean value, variance and maximum error on the pdf are below 1%. The mean values for order 3 and 4 PCE (0.99253 for both approximations) are within the range $[\mu_{MC} - \sigma_{MC}; \mu_{MC} + \sigma_{MC}]$, where μ_{MC} is the mean value evaluated via MC sampling (0.99297) and σ_{MC} is its standard deviation (72 pcm).

Figure 4.12(b) shows the response is gaussian and it confirms the linear behavior appeared in previous cases. It is evident after analyzing multiple cases that the neutronic model is linear with respect to the macroscopic fission cross sections and the neutron fission yields, whereas the fluid-dynamic one may introduce a non-linearity. In this case, despite the coupling, the result is still linear due to the irrelevance of the fluid-dynamics in the computation of k_{eff} . Since the macroscopic fission cross section and the neutron fission yield for the energy groups 5 and 6 vary in the same way (same mean value, variance and distribution) of the neutronics-only case, the pdf obtained is almost the same, excluding variation due to secondary effects related the power and heat transfer coefficient and the statistics oscillations. In addition, as evident from Figure 4.13 the curve obtained with the coupled problem is almost superposed to the single physics one. In fact, recalling Chapter 4.4, the flow field obtained from the nominal steady-state coupled problem is also the one used as input for the neutronics-only calculations ($\gamma = 1.0 \times 10^6 \text{ W}/(\text{m}^2\text{K})$, $\nu = 2.5 \times 10^{-2} \text{ cm}^2/\text{s}$ and $\beta_{exp} = 2.0 \times 10^{-4} \text{ K}^{-1}$). Despite the reactor power and γ are added as input parameters in the coupled case, they do not change dramatically the k_{eff} , because they act indirectly. In fact, they influence the value of k_{eff} by changing the flow field or via density effects, both much weaker mechanisms than a variation in the $\Sigma_{f,g}$ or ν_g which causes a linear variation in the effective multiplication factor. This aspect is evident by analyzing sensitivity indices in Table 4.17. Sensitivity indices for the heat transfer coefficient and the power are in fact two order of magnitude lower than neutronics inputs.

These results are fundamental to ensure the correctness of the entire procedure. The choice of relevant parameters was carried out in single physics problems, assuming this parameter ranking to be valid also for the fully coupled problem, given the secondary contribution of feedback effects on the responses. In addition, even in this case, second or higher order interactions are negligible ($\sum_i S_{tot,i} = 1.001 \approx 1$).

Table 4.16: *Comparison among the PCE evaluations (both of orders 3 and 4) and the MC reference. The two PCE approximations are able to represent the statistical information with excellent accuracy.*

| | e_μ [%] | e_{σ^2} [%] | $\max e_{pdf}$ [%] |
|-------------|-------------|--------------------|--------------------|
| PCE order 3 | 0.04 | 0.86 | 0.03 |
| PCE order 4 | 0.04 | 0.44 | 0.03 |

Table 4.17: Sensitivity indices in the coupled case for effective multiplication factor. The macroscopic fission cross sections and the fission yields give the only relevant contribution to the response variance.

| | P | γ | $\Sigma_{f,5}$ | $\Sigma_{f,6}$ | ν_5 | ν_6 |
|-------------|-----------------------|-----------------------|-----------------------|-----------------------|-----------------------|-----------------------|
| S_i | 3.60×10^{-3} | 3.40×10^{-3} | 1.55×10^{-1} | 1.02×10^{-1} | 4.40×10^{-1} | 2.95×10^{-1} |
| $S_{tot,i}$ | 3.70×10^{-3} | 3.40×10^{-3} | 1.56×10^{-1} | 1.02×10^{-1} | 4.41×10^{-1} | 2.95×10^{-1} |

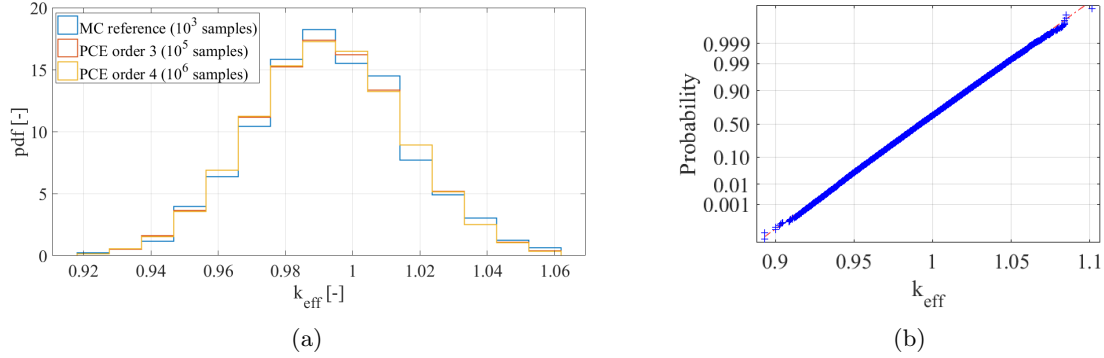


Figure 4.12: (a) Pdf representation of k_{eff} using different polynomials orders and number of samples compared with the reference MC sampling. (b) Normal probability plot for the 3rd order PCE. Blue crosses are the related to the sampling whereas the dashed line is the reference Gaussian.

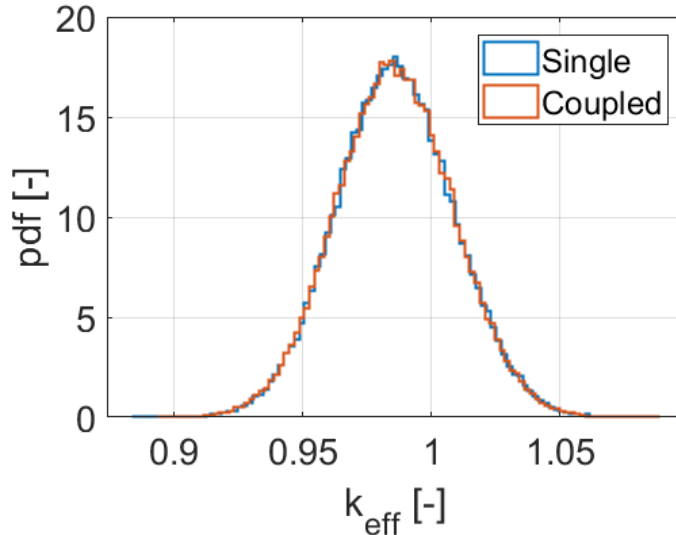


Figure 4.13: k_{eff} comparison between single-physics and coupled problem. Since the flow field obtained from the nominal steady-state coupled problem is also the one used as input for the neutronics-only calculations and it has almost no influence on the response variance, the two curves are almost superposed. This confirms feedback effects play a secondary role.

4.6 Summary

A careful and systematic analysis on steady-state simulations on CNRS benchmark showed that only a fraction of possible input parameters affect the response(s) in a non-negligible way. To overcome the problem of "curse of dimensionality", de-coupled calculations (neutronics with fixed nominal flow and temperature fields, and fluid-dynamics with fixed nominal fission power density) were performed. The thermal fluid-dynamic part showed only the heat transfer coefficient γ introduced a perturbation on the maximum temperature above 1%. The single-physics neutronics counted about 70 inputs: 6-groups fission cross sections ($\Sigma_{f,g}$), 6-groups scattering cross sections, 6-groups average number of neutrons produced per fission event (ν_g), 6-groups fission prompt spectrum, and 8-families precursors decay constants and fractions. Two different approaches were presented to treat the high dimensionality, the mean value and the class approach. The former divided inputs in classes, analyzing a single (averaged) value representative of the whole class. The latter took the same classes distinction but a PCE evaluation was performed on the whole set of inputs for each class. The parameter ranking, performed with sensitivity indices, showed that only $\Sigma_{f,5}$, $\Sigma_{f,6}$, ν_5 and ν_6 gave relevant contribution to the k_{eff} , while others were considered negligible.

During coupled steady-state simulations, γ and the reactor power P were added to the set of inputs. The number of model evaluations needed by the PCE code was 97. For what concerns the results, the polynomial order/quadrature grid level study is carried out as a preliminary test to check the correctness of the polynomial approximation. At the same time, results were compared with a reference MC, obtained with 10^3 random samples. The agreement between order 3 and 4 polynomial and the MC reference was excellent for both responses. Choosing the order 3 polynomial approximation because of the reduced number of model evaluations and agreement with the mC reference, the maximum relative error was 0.2% on the responses, lower than 0.2% on the pdf mean, and 1.0% on the pdf variance. The maximum temperature is mainly sensitive to P and γ , while the k_{eff} is affected mostly by neutronics parameters. It is worth highlighting that the reference model needed around 1500 h to generate the 10^3 responses, while the sampling on the PCE approximation required a few seconds for 10^6 samples.

Chapter 5

Steady-state Simulations of the Molten Salt Fast Reactor

According to the preliminary design, illustrated in Figure 1.2, a consistent computational domain is chosen. Being each sector indistinguishable from others (e.g. it has the same components, geometry) and assuming a symmetry along the azimuthal angle, the domain can be reduced to one sixteenth, as reported in Figure 5.1. The same geometry was successfully analyzed by [18].

In contrast to the CNRS benchmark, the actual MSFR design contains several components, constituted by other materials. Therefore, even in a simplified model, the primary loop, upper and lower reflectors, pump and heat exchanger (HX) need to be included along with the salt, having different thermodynamic and neutronic properties. The heat exchanger is sized to transfer $187.5 \text{ MW}_{\text{th}}$ (one sixteenth of the nominal 3 GW_{th}). This heat sink is modeled according to the formula $P_{\text{out}} = \gamma(T_{\text{ave,HX}} - T_{\text{sec}})$, where γ is the heat transfer coefficient (uniform in the domain), $T_{\text{ave,HX}}$ is the average temperature in the heat exchanger and T_{sec} is the temperature of the secondary loop. The pump is sized to provide the nominal flowrate ($1211.26 \text{ kg s}^{-1}$, which is $1/16^{\text{th}}$ of the value found in [3]).

From the neutronics point of view, density feedback together with Doppler effects are taken into account. Analogously to the CNRS benchmark, 6 energy groups and 8 precursors families are assumed to be sufficient to treat those dependencies. Then, the S_2 discrete ordinates approximation is chosen for the angular discretization. The thermal-hydraulic problem is approached using the Boussinesq approximation to model buoyancy forces, assuming incompressible flow. Turbulence is studied with the $k - \epsilon$ model, already implemented in `DGFlows`. The spacial approximation both for the neutronics and thermal fluid-dynamics is preformed by using around 53000 volumes, taking into account variation in materials, reported in Figure 5.2. The mesh was generated with the open source program `Gmsh`.

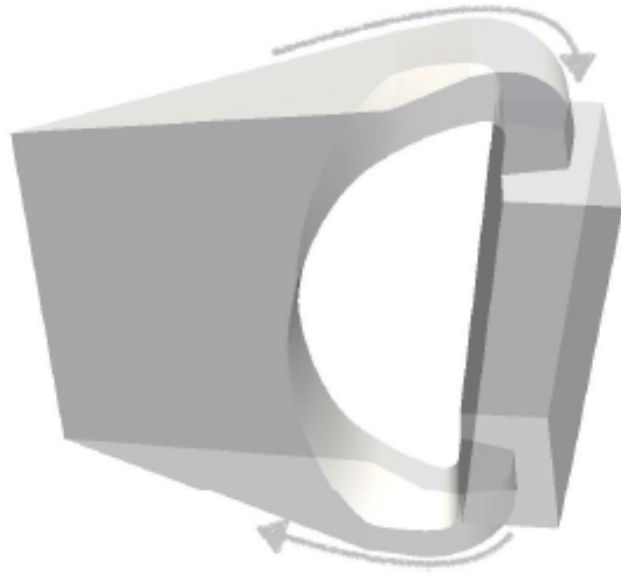


Figure 5.1: *Computational domain MSFR [18]. Thanks to the system symmetry, it can be reduced to one sixteenth of the whole domain.*

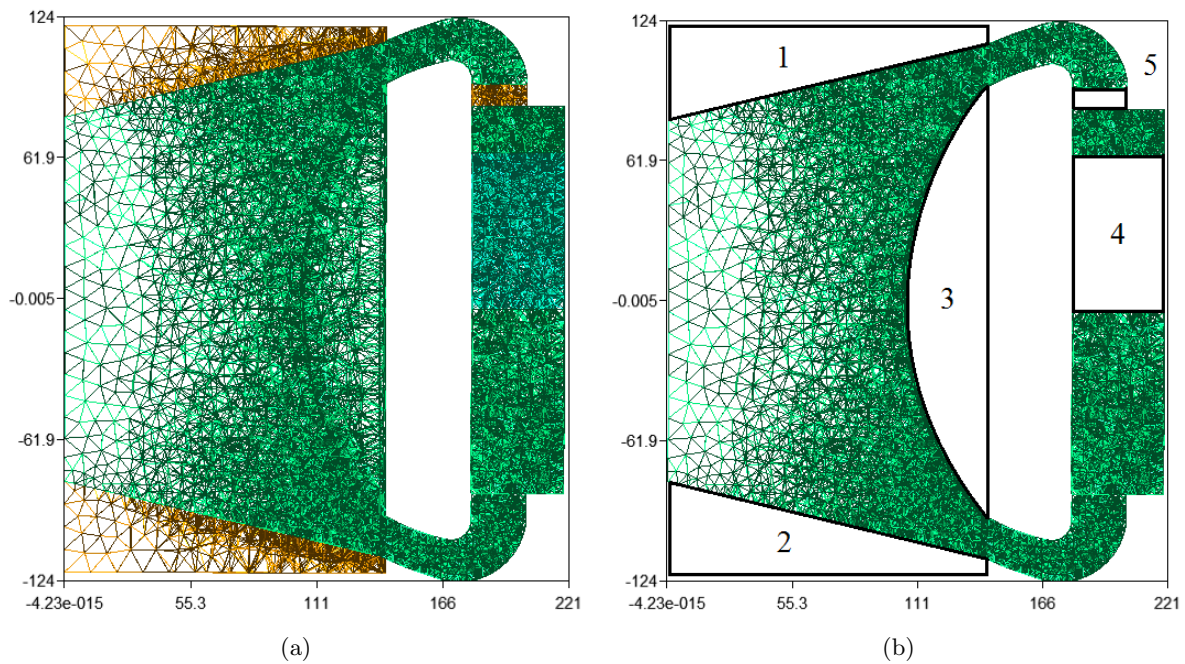


Figure 5.2: (a) *Space domain discretization adopted for both PHANTOM- S_N and DGFlows, generated with Gmsh. It includes 53000 volumes. Different materials are represented with different colors.* (b) *Representation of the core discretization. Other components are numbered for clarity. Upper and lower reflectors (1-2), blanket (3), heat exchanger (4) and pump (5).*

5.1 Preliminary approach to the problem

The CNRS benchmark was a test case containing the most relevant features of the MSFR. Thus, the analysis on the MSFR preliminary design is carried out trying to take advantage from the CNRS benchmark as much as possible. Strong coupling between neutronics and thermal fluid-dynamics along with fast spectrum and transport of precursors are the main characteristics of both systems. On the other hand, a more complex (3D) geometry, together with forced flow in presence of turbulent phenomena, represent additional complications on top of previously mentioned mechanisms.

The computational efforts to solve larger set of equations, which include, among others, closures for turbulence models, is much greater, even starting from steady-state solutions, as described in Chapter 4. Thus, performing a study to validate the PCE model with a reference MC sampling is simply unfeasible and results obtained in Chapter 4 are extrapolated for this case. In fact, Chapters 4.3, 4.4 and 4.5 showed that the number of model evaluations for order 4 PCE with level 4 quadrature rises up to 533, clearly too many for an analysis on such a complex system. However, level 3 quadrature can integrate exactly polynomials up to order $2n_{lev} - 1$, which corresponds, considering 5 points for level 3 quadratures, to order 4. On the other hand, performing a MC simulation with at least 10^3 samples is beyond the computational power available. Consequently, any kind of polynomial approximation is obtained, it is supposed to be in agreement with a reference MC evaluation.

The maximum (T_{max}) and minimum (T_{min}) temperature, together with the effective multiplication factor (k_{eff}) are the studied responses, analogously to the CNRS benchmark. In addition, the average reactor temperature (T_{ave}) and the whole temperature field are analyzed as well.

Being impossible to perform an extensive parameter study, the choice of inputs and their statistical information is related to the results of the CNRS benchmark. Concerning the neutronics part, 0-th order scattering matrix, as well as the prompt neutron emission χ , had negligible effects on the k_{eff} and thus they are excluded from the analysis. Likewise, the thermal expansion coefficient and the salt kinematic viscosity are neglected due to their irrelevance on the maximum temperature, while the lid velocity was a parameter specifically defined for the only CNRS benchmark. On the other hand, the reactor power (P) and the heat transfer coefficient (γ) were directly related to the energy balance and in turn with the whole temperature field, whereas the macroscopic fission cross sections on the k_{eff} . Despite the neutron fission yield ν_g had the strongest contribution to the k_{eff} it is not analyzed because no statistical information are available. In fact libraries and publications focus only on their mean value without even mentioning possible uncertainties. Consequently, these quantities are assumed to be exact. The whole set of inputs is reported in Table 5.1. The delayed neutron fraction and decay constants are added to the list because they may have relevant changes with respect to the CNRS benchmark due to the presence of forced flow and turbulent phenomena.

Again, inputs statistical information depends on the distinction between *material properties* and *controllable parameters*, already explained in Chapter 4.1. The inputs mean value is set as the one of the relative parameter in nominal conditions. The variance is taken from libraries and/or material data when it is possible. On the contrary, for those parameters which do not have a precise value, their variance is assumed 5 % for normally distributed inputs and 20 % for uniformly distributed inputs. The reason is twofold. First, it is related to the impossibility to recover accurate enough data. Especially extrapolation may lead to inconsistent or meaningless results. Secondly, it allows performing a parameter ranking with same inputs variability, as done

in the CNRS benchmark, emphasizing which of them contribute the most to the response(s) variance.

Analogously to what described in Chapter 4.1, the complete problem is the final step after studies on single-physics/de-coupled cases. Neutronics and thermal fluid-dynamics are studied separately, especially to reduce the parameter space. Results are combined to properly study the coupled problem, minimizing the input quantity to reduce the number of model evaluations. In particular, the neutronics study should be able to reduce the parameter space very effectively. Being computational expensive and much less effective in the perspective of a parameter space reduction, the thermal fluid-dynamic analysis is no performed. According to Chapter 4.4, the *class approach* revealed to be the proper way to address the high dimensionality.

In Table 5.2 values computed in nominal conditions are reported for whole set of single-value responses (i.e. maximum, minimum, and average temperature along with the effective multiplication factor). Differently from Table 4.2, they are computed only in the coupled case. Neutronics-only calculations are based on the coupled code with nominal thermal fluid-dynamic parameters, analogously to what described in Chapter 4.1.

Table 5.1: Complete set of input parameters for both thermal fluid-dynamics and neutronics for the MSFR. Symbols are introduced with their respective meanings.

| Thermal fluid-dynamics | | Neutronics | |
|------------------------|---|----------------|---|
| <i>Symbol</i> | <i>Meaning</i> | <i>Symbol</i> | <i>Meaning</i> |
| c_p | Fuel salt specific heat at constant pressure | β_i | i-th family delayed neutron fraction (8 families) |
| k | Fuel salt thermal conductivity | λ_i | i-th family decay constant (8 families) |
| γ | Heat exchanger volumetric heat transfer coefficient | $\Sigma_{f,g}$ | g-th group macroscopic fission cross section (6 groups) |
| P | Reactor power | | |

Table 5.2: Reference values in nominal condition for non-stochastic case. They refers to the nominal steady state on the MSFR in the coupled case. Responses are maximum (T_{max}), minimum (T_{min}) and average (T_{ave}) temperature along with the effective multiplication factor (k_{eff}).

| T_{max} [K] | T_{min} [K] | T_{ave} [K] | k_{eff} [-] |
|---------------|---------------|---------------|---------------|
| 1082 | 924 | 966 | 1.00998 |

5.2 Single-physics case: neutronics-only problem

Analogously to Chapter 4.4, the neutronics-only case is studied starting from the coupled steady-state solution. The coupling strategy is explained in Chapter 3.2. The first evident difference with the CNRS benchmark is the neutron spectrum, which strongly affects the set of relevant parameters. According to what discussed in Chapter 5.1, the list of inputs mean values is reported in Table 5.3. Being all material properties, each input distribution is normal. In this preliminary step, inputs are compared with same variance, 5% consistently with previous steps, to select the ones with strongest effects.

Using the *class approach*, the number of model evaluations was 161 for β and λ class (8 families), whereas 97 for the Σ_f class (6 groups). Due to high request of memory, the number of submissions to the HPC were limited. The set of external coupling scripts were modified. Further information are found in Appendix A. The first step of the results analysis consists of a comparison between variances of each class, reported in Table 5.4. First, the macroscopic fission cross section variance is at least three order of magnitude higher than the other classes. Thus, no inputs belonging to β and λ classes are taken into account for further studies. Secondly, these values are very similar to the one in the CNRS benchmark case (Table 4.10). It seems that, despite the problem complexity increased, the overall parameter ranking does not lead to very different results. In fact, the main changes in the problem, regards the fluid-dynamic, with the introduction of forced flow and turbulence. However, we saw in Chapter 4 that the neutronics and thermal fluid-dynamics have limited interactions on the neutronics behavior in spite of the coupling, thus, retrieving same orders of magnitudes for same classes. Finally, the presence of forced flow increases the sensitivity to the neutrons precursors on k_{eff} , being standard deviations 2/3 times higher, but still orders of magnitude lower than Σ_f class.

Inside the Σ_f class, a limited number of energy groups may be relevant. Sensitivity indices were computed to explore this aspect and they are reported in Table 5.5. Due to the harder spectrum, groups with higher energy are subjected to more fission reactions. Consequently, sensitivity indices for those groups are higher with respect to the CNRS benchmark case. In fact, groups 2, 3, 4 and 5 are taken for further analysis, having similar sensitivity indices, despite Σ_f mean values were different. In addition, considering these groups, more than 90% of the class variance is taken into account, ensuring an appropriate representation of statistical information.

Table 5.3: *List of MSFR neutronics-only parameters with their mean values.*

| Symbol | Value | Symbol | Value | Symbol | Value |
|--------------|------------------------|---------------------|------------------------|-------------------------|------------------------|
| $\beta_1[-]$ | 1.230×10^{-4} | $\lambda_1[s^{-1}]$ | 1.247×10^{-2} | $\Sigma_{f,1}[cm^{-1}]$ | 4.446×10^{-3} |
| $\beta_2[-]$ | 7.145×10^{-4} | $\lambda_2[s^{-1}]$ | 2.829×10^{-2} | $\Sigma_{f,2}[cm^{-1}]$ | 2.517×10^{-3} |
| $\beta_3[-]$ | 3.596×10^{-4} | $\lambda_3[s^{-1}]$ | 4.252×10^{-2} | $\Sigma_{f,3}[cm^{-1}]$ | 1.805×10^{-3} |
| $\beta_4[-]$ | 7.941×10^{-4} | $\lambda_4[s^{-1}]$ | 1.330×10^{-1} | $\Sigma_{f,4}[cm^{-1}]$ | 2.618×10^{-3} |
| $\beta_5[-]$ | 1.474×10^{-3} | $\lambda_5[s^{-1}]$ | 1.925×10^{-1} | $\Sigma_{f,5}[cm^{-1}]$ | 5.200×10^{-3} |
| $\beta_6[-]$ | 5.145×10^{-4} | $\lambda_6[s^{-1}]$ | 6.665×10^{-1} | $\Sigma_{f,6}[cm^{-1}]$ | 1.395×10^{-2} |
| $\beta_7[-]$ | 4.655×10^{-4} | $\lambda_7[s^{-1}]$ | 1.635 | | |
| $\beta_8[-]$ | 1.511×10^{-4} | $\lambda_8[s^{-1}]$ | 3.555 | | |

Table 5.4: *Variance comparison between input classes in the neutronics-only case. Σ_f has a variance at least five orders of magnitude higher with respect to other classes. Even for the MSFR, in steady-state simulations β and λ classes have practically no influence on the effective multiplication factor.*

| | Σ_f class | β class | λ class |
|----------|-----------------------|-----------------------|------------------------|
| Variance | 2.22×10^{-4} | 4.42×10^{-9} | 6.08×10^{-11} |

Table 5.5: *Sensitivity indices for Σ_f class reported for each energy group. With the same logic of the CNRS benchmark, four energy groups give relevant effects on the effective multiplication factor (2-5). They are taken for further analysis.*

| | Group 1 | Group 2 | Group 3 | Group 4 | Group 5 | Group 6 |
|-------------|-----------------------|-----------------------|-----------------------|-----------------------|-----------------------|-----------------------|
| S_i | 2.21×10^{-2} | 9.09×10^{-2} | 2.57×10^{-1} | 2.48×10^{-1} | 3.33×10^{-1} | 4.91×10^{-2} |
| $S_{tot,i}$ | 2.21×10^{-2} | 9.09×10^{-2} | 2.57×10^{-1} | 2.48×10^{-1} | 3.33×10^{-1} | 4.91×10^{-2} |

5.3 Multi-physics case: coupled neutronics and thermal fluid-dynamics problem

Differently from the analysis in Chapter 4, the thermal fluid-dynamic only case is not performed because the set of inputs (4 in total) it is already small enough and a PCE analysis involving tens of simulations is no more justified, due to higher computational cost. Thus, we moved directly to the coupled study. Analogously to Chapter 4, the coupling between neutronics and thermal fluid-dynamics triggers feedback effects. In this case, both density and Doppler feedback effects are taken into account.

Despite it is conceptually similar to the CNRS benchmark and the overall set of involved phenomena is the same, the complexity introduced with the geometry, turbulence models and the presence of different materials increased considerably the computational time for the solution of the mass, momentum, energy and transport equations. In addition, the thermal fluid-dynamic code cannot solve the steady-state problem by itself. In fact, introducing a perturbation on the inputs and starting from the nominal steady-state solution, it studies the transient it provokes, which ends with the new steady-state solution. Hence, the first step of this analysis has the scope of simplifying the calculation procedure, considering that it is applied to the PCE meta-model.

The set of inputs derives from Table 5.1, having discarded the ones which are supposed to be irrelevant thanks to single-physics (neutronics-only) analysis. Mean values are, as usual, coincident with the nominal ones. Distributions are set as normal for all quantities except for P and γ . The variance on the macroscopic fission cross section can be found with a good accuracy by solving a transport equation, using a proper code. However, the implementation cannot be done in an adequate time. Finding analogous studies in literature was a second option. However, variances need to be calculated considering almost the same energy groups for the same nuclides. Unfortunately, the combination of a peculiar fuel salt composition (with ^{235}U , Pu and not well specified Minor Actinides) and values for energy groups that do not fit the models (e.g. [29]) prevent to choose reasonable values for the variance. Thus, the default standard deviation is assigned to each input, except for the salt thermal conductivity k . From [8] its value is $(1.7 \pm 0.4) \text{ W}/(\text{mK})$, where $\pm 0.4 \text{ W}/(\text{mK})$ can be interpreted as a standard deviation (i.e. the relative standard deviation is about 23%). Table 5.6 summarizes the set of inputs for the coupled thermal fluid-dynamics and neutronics case.

5.3.1 Strategy for the computational time reduction

As mentioned, the coupling is achieved by iterating the neutronics and the thermal fluid-dynamic code. Some seconds (or more often fractions of second) of the system evolution are analyzed by the thermal fluid-dynamic code. After the flow and temperature field are computed, the neutronics code updates the neutron distribution, as well as the power distribution produced by fissions, since the fission power is fixed. Once the neutron flux is obtained, and the k_{eff} is computed, the thermal fluid-dynamic code is started again to simulate the salt flow with different neutronics inputs. The process goes on until a satisfactory convergence is reached. Since we want obtain a steady-state solution, the starting point of the pseudo-transient is the steady-state solution with nominal values. As the PCE model introduces more or less small perturbations, the convergence to the new steady-state solution starting from the nominal one should be enhanced. Unfortunately, the number of iteration needed to obtain the steady-state solution with an appropriate accuracy is not known, as well as the total computational time. Especially the computational time of the neutronics code seems to be affected by the variation of cross sections and system temperature. In fact, a high number of iteration of the power method are needed to compute the neutron flux (and k_{eff}). To estimate the computational time and

the number of iterations, a preliminary simulation is performed assuming the widest variation of inputs which maximizing the maximum temperature and minimize the effective multiplication factor. Considering the PCE model with Smolyak sparse grid using level 3 cubature rules, the maximum variation of these 8 inputs can be estimated. Conservatively, assuming to have all maximum possible inputs variation at the same time, a test simulation is run. The set of perturbed inputs is showed in Table 5.7, reporting percentage variation with respect their mean value.

The parameters we monitor to ensure the conclusion of the transient are the maximum, minimum and average temperature, the power balance and the maximum temperature derivative in the whole system. Turbulence quantities may prevent the algorithm to converge, thus the time step is limited to 2 ms.

Parameters that appear in the energy conservation equation have an impact on the temperature field, but they indirectly affect the flow field, by enhancing or decreasing the mixing and/or the natural convection. Thus, varying only energy-related parameters can have an effect on the flow field, which varies from the nominal steady-state scenario to the new "perturbed" one. However, in Chapter 4.3.1, the buoyancy effect (natural convection) is related to the thermal expansion coefficient β_{exp} . Despite the CNRS benchmark has not any device to generate forced convection, the enhanced buoyancy had a negligible effect on the maximum temperature with respect to more temperature-related parameters, such as γ or P . This is even more realistic in the MSFR, where the salt moves thanks to the forced circulation. In other words, we can expect that the flow field does not vary sensibly during the pseudo-transient and, thus, it is approximately equal to the one of the nominal steady-state solution. In this way, the thermal fluid-dynamic code has to solve only the energy equation, hence being much faster.

The main task is to quantify this approximation. We run two simulations: the first one, from now on called *WithFlow*, solves the complete flow field, as well as other equations (i.e. energy conservation, neutron transport...), whereas the second one (*NoFlow*) assumes the flow field equal to the one in nominal steady-state solution, solving only the energy equation for the thermal fluid-dynamic part. Figures 5.3, 5.4, 5.5 and 5.6 compare the pseudo-transient in both cases showing (respectively) the evolution of the maximum temperature time derivative in the system, the maximum, minimum and average temperature, the power balance, and the effective multiplication factor.

Due to high computational efforts, the *WithFlow* is stopped after simulating 10.8s. The total computational time was more than 88h, parallelizing *DGFloWS* on 20 processors. On the other hand, the *NoFlow* simulation took less than 62h to simulate 18.6s.

Analyzing the plots, it is evident that for each quantity we chose, the evolution for both *NoFlow* and *WithFlow* are practically superposed, except for the maximum temperature. However, the maximum temperature assumes conservative values since it is overestimated. Especially studying Figure 5.6, the k_{eff} reaches the steady-state solution after about 20 iterations, which corresponds to approximately 12s. Corresponding to that time, all other quantities have already reached the steady-state solution. In addition, Figure 5.3 shows that the maximum temperature variation deriving from simulating another second of transient is below 0.1 K (at 12s), completely negligible considering temperature variations due to the presence of stochastic inputs. Taking 12s as a good compromise, Table 5.8 reports errors on both the *NoFlow/WithFlow* approximation and the "steady-state" approximation. For the generic quantity Q, we defined the errors $e_{NF/WF}$ as the error related to the *NoFlow/WithFlow* approximation and e_{NF} as the error related to the approximation of the *NoFlow* simulation to 12s. They are computed as

$$e_{NF/WF} = \frac{|Q_{NF}(10.8s) - Q_{WF}(10.8s)|}{Q_{WF}(10.8s)} \quad \text{and} \quad e_{NF} = \frac{|Q_{NF}(12s) - Q_{NF}(18.6s)|}{Q_{NF}(18.6s)} \quad . \quad (5.1)$$

Table 5.6: List of relevant-only parameters for the MSFR. Distributions, mean values and standard deviations are specified.

| Symbol | Units | Distribution | Mean | RSD |
|----------------|----------------------|--------------|------------------------|-----|
| c_p | J/(kgK) | normal | 1594 | 5% |
| k | W/(mK) | normal | 1.7 | 23% |
| γ | W/(m ³ K) | uniform | 1.995×10^7 | 20% |
| Power | W | uniform | 1.875×10^8 | 20% |
| $\Sigma_{f,2}$ | cm ⁻¹ | normal | 2.517×10^{-3} | 5% |
| $\Sigma_{f,3}$ | cm ⁻¹ | normal | 1.805×10^{-3} | 5% |
| $\Sigma_{f,4}$ | cm ⁻¹ | normal | 2.618×10^{-3} | 5% |
| $\Sigma_{f,5}$ | cm ⁻¹ | normal | 5.200×10^{-3} | 5% |

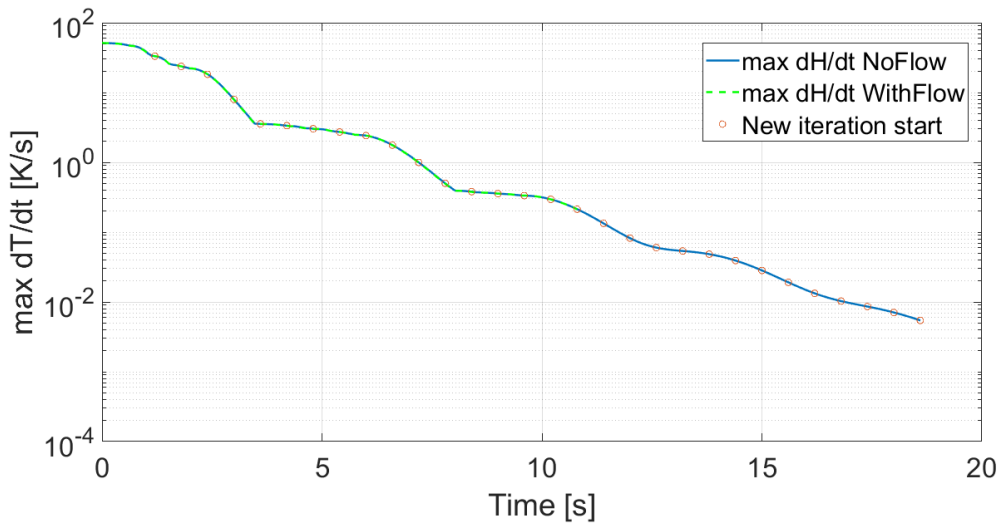


Figure 5.3: Maximum temperature time derivative during the pseudo-transient. If multiplied by the dt , it indicates the temperature variation in that time interval. Choosing a threshold, the required number of simulation time can be chosen.

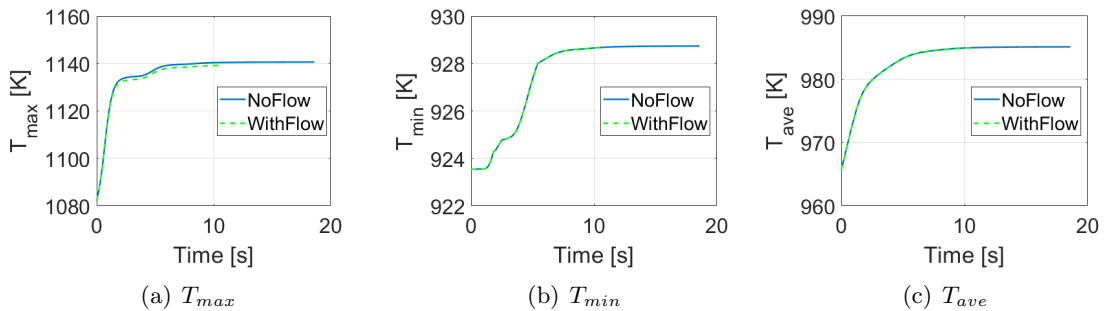


Figure 5.4: (a) T_{max} evolution during the pseudo-transient. It shows when the steady state for this response is reached. In addition, for this temperature the NoFlow approximation appears to be conservative. (b) T_{min} evolution during the pseudo-transient. It shows that after 10s the temperature transient ended. (c) T_{ave} evolution during the pseudo-transient. After an initial transient (up to 10s), the average temperature reaches steady-state condition.

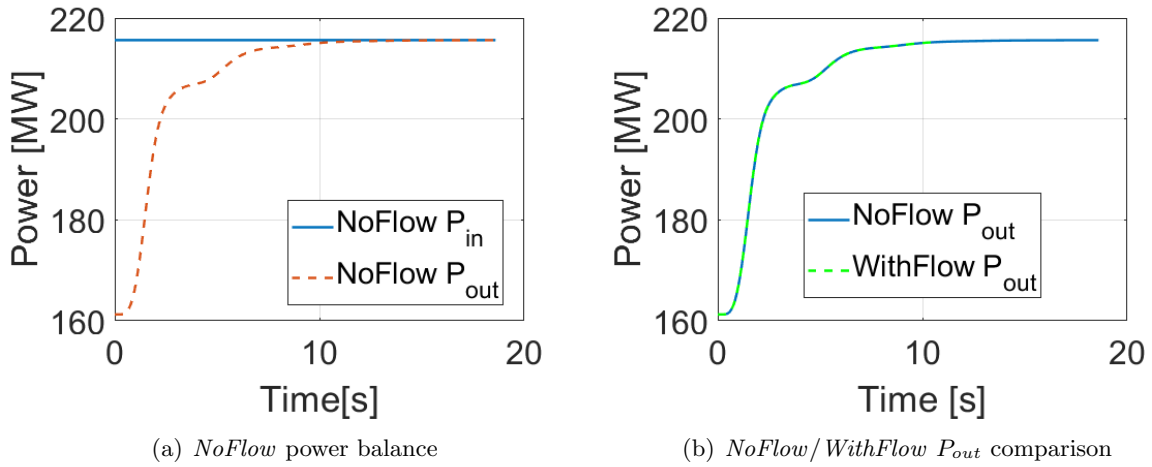


Figure 5.5: (a) *Evolution of the power balance during the pseudo-transient. The input power is the one produced by fissions and it is set to 115% of the nominal value, whereas the output power, transferred in th HX increases progressively. The transient ends after 11s* (b) *Output power evolution comparison between NoFlow and WithFlow. Both transients are superposed, and no evident differences appears*

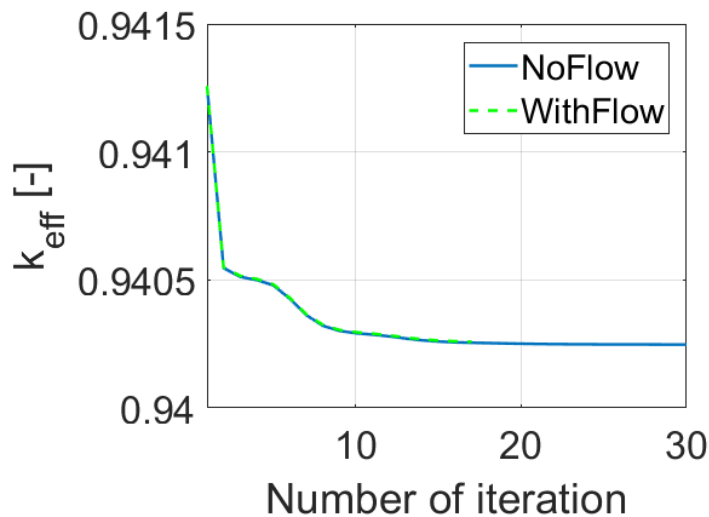


Figure 5.6: *Effective multiplication factor comparison between NoFlow and WithFlow simulation. They are superposed for the whole transient, showing no evident errors caused by the approximation. k_{eff} is evaluated at the beginning of each iteration. After 20 iterations (corresponding to 12s) it assumes a constant value.*

Table 5.7: *Perturbed inputs for the computational time reduction test case. They are adopted both in the Withflow and NoFlow case. They are chosen to maximize the maximum temperature and minimize the effective multiplication coefficient.*

| | c_p | k | γ | P | $\Sigma_{f,2}$ | $\Sigma_{f,3}$ | $\Sigma_{f,4}$ | $\Sigma_{f,5}$ |
|------------------------|-------|-----|----------|-----|----------------|----------------|----------------|----------------|
| Relative variation [%] | 86 | 86 | 86 | 115 | 91 | 91 | 86 | 86 |

where the comparison with the *WithFlow* takes 10.8s as best estimation of the steady-state solution.

From Table 5.8, the maximum error on the transient truncation belongs to the power and it is 0.1%, negligible with respect to the relative power increase (15%). Then, as evident, the highest error on the *NoFlow* approximation is corresponds to the maximum temperature, again order 10^{-3} , thus acceptable.

Despite the computational cost is reduced of 37 h between *NoFlow* and *WithFlow*, it is not enough to complete 161 simulations in a sufficiently short time. It is fundamental to allow a parallelization of simulations, hence reducing the number of processors needed per simulation. These computational times are achieved by using the maximum number of processors to speedup the thermal fluid-dynamic code, but in this way it is possible to run only one simulation at a time. Especially in the first seconds of the transient, the neutronics code, which runs on single core, takes several hours to compute the new neutron distribution and the k_{eff} . It is, in fact, the calculation bottleneck, during the first iterations, as shown in Table 5.9. However, **DGFLows** computational time is much lower since it exploits 20 processors (the speedup is linear if the processors' number is higher than 2, i.e. doubling the number of processors halves the computational time). Because the biggest variations appear until 6s, according to Figures 5.4 and 5.5, updating the temperature field every 0.6s is redundant since small temperature differences generate minimal feedback effects. Thus, a way to reduce the computational time is to use longer time steps, while performing a very long first iteration with the thermal fluid-dynamic code in order to dump the temperature (and power) transient.

Finally, the coupling is performed using 5 iterations, with the first one simulating the first 4s. The magnitude of the time step is increased to 5ms, not being limited by turbulent quantities, and the number of time steps is chosen such that at the end of the 5th iteration 12s are simulated.

Table 5.8: *Table with error estimators introduced with the NoFlow/WithFlow approximation and the presence of the pseudo-transient. The maximum error on the transient truncation belongs to the power and it is 0.1%, negligible with respect to the relative power increase (15%). Then, as evident, the highest error on the NoFlow approximation is corresponds to the maximum temperature, again order 10^{-3} , thus acceptable.*

| | $e_{NF,end}$ | $e_{NF/WF}$ |
|-----------|----------------------|----------------------|
| T_{max} | 1.0×10^{-4} | 1.1×10^{-3} |
| T_{min} | 3.5×10^{-5} | 3.9×10^{-6} |
| T_{avg} | 7.4×10^{-5} | 3.3×10^{-5} |
| P_{out} | 1.0×10^{-3} | 6.2×10^{-6} |
| k_{eff} | 4.7×10^{-6} | 4.2×10^{-6} |

Table 5.9: *Computational time comparison between DGFloWS and PHANTOM-S_N in the NoFlow simulation running with DGFloWS parallelized on 20 processors. In the first iterations, PHANTOM-S_N represents the calculation bottleneck.*

| Iteration number | 1 | 2 | 3 | 4 | 5 | 7 | 10 | 13 | 18 |
|----------------------------|----------|----------|----------|----------|----------|----------|-----------|-----------|-----------|
| PHANTOM-S _N (h) | 15.0 | 11.1 | 3.40 | 1.73 | 1.00 | 1.00 | 0.84 | 0.90 | 0.65 |
| DGFloWS (h) | 0.30 | 0.13 | 0.13 | 0.13 | 0.13 | 0.13 | 0.13 | 0.13 | 0.13 |

Check on the submission performance. Actually, the previous analysis is very conservative. The set of inputs is perturbed simultaneously with the sharpest variation. This condition never happens in the generation of abscissas in the PCE code, having only some of them (and more often only one or two) varying at the same time. Consequently, the computational time needed to complete the pseudo-transient is lower or it reaches the steady state before simulating 12 s. Especially in cases in which only the cross sections are modified, the temperature field is affected only by feedback effects, which have a secondary role in the physics of the problem. As evident from Figure 5.3, we assumed no relevant contribution to the temperature if the maximum derivative is below $1 \times 10^{-1} \text{ K s}^{-1}$. After having performed 2 iterations, a check is introduced at the end of the third one to see if the residuals are below that threshold and if there were significant variations of k_{eff} between the second and the third iteration, setting a threshold of 1 pcm. It is expected that simulations in which only neutronics-related values are varied can be stopped after 3 iterations, since only feedback effects have to be applied during the calculation of the new temperature field. As simulations ended, it was noticed that the thermal conductivity had almost no effects on the temperature field, without generating any sort of transient. Analyzing the set of perturbed inputs produced by the PCE code, 56 sets over 161 see only variations in the fission cross sections and in the thermal conductivity, and performing 5 iterations is potentially useless. Generally, each iteration after the second one takes approximately 1.5 h, which implies a 3 h saving per simulation (stopping the codes at the third one when needed), for a total of 168 h for 56 simulations. Unfortunately, this control was not automatized and only a half of those simulations (27) were stopped. Finally, the total computational time for the 161 simulations was about 14 days.

5.3.2 Results: single-value temperatures

Differently from Chapter 4.5.2, a comparison with the reference MC sampling was not possible, due to the much higher computational efforts. However, using level 3 gauss quadrature rules and knowing that the corresponding number of nodes is 5 ($n_3 = 5$), it is possible to integrate exactly polynomials up to order $2n_3 - 1 = 9$, which implies that it is possible to approximate the response using polynomials up to order 4 (being the integrand the product of the response and the basis, which have both maximum order 4).

For what concerns responses, the maximum, minimum and average temperature are analyzed, along with the whole temperature field. However, the temperature field is approached differently in the next Section.

Maximum temperature. Figure 5.7 represents the maximum temperature pdfs, comparing order 3 and 4 PCE approximations with 10^5 samples each. Despite order 3 polynomials were proven to be sufficient to approximate the solution in the CNRS benchmark case, the order 4 polynomial seems to be the best compromise in this case. Analyzing expansion coefficients, fourth order terms derive from interaction among thermal-hydraulic and neutronics parameters

and, thus, they can be associated to feedback effects. Taking fourth order polynomials, the mean value is 1083 K (very near to the nominal coupled steady-state) with a variance of 478 K², almost one eighth with respect to the CNRS benchmark coupled case. Its shape is far from a normal distribution, as evident from Figure 5.7(b), not only at tails but also in the central region. In the interval [1050 K; 1100 K] the pdf is nearly uniformly distributed.

The maximum temperature appears on the symmetry axis in proximity to the upper reflector. It is much less sensitive to a variation of inputs, especially from the energy-related ones (e.g. power and heat transfer coefficient), as evident in Table 5.10 where sensitivity indices are reported. This may be caused by the radical changes in the domain geometry and features. Differently from the CNRS benchmark, heat is transferred to a secondary system only in a small region of the domain (i.e. the heat exchanger), which is very far from the point in which the maximum temperature appears. In fact, γ total sensitivity index is only 0.05, even lower than c_p . Vice versa, the reactor power P is the term with the highest contribution, with a total sensitivity index of 0.85. It confirms what found in the analogous case of the CNRS benchmark (Table 4.14). The maximum temperature was very sensitive to P , and now it is much more evident. In addition, sensitivity indices confirm neutronics parameters give no contributions to the maximum temperature, despite high fourth order expansion coefficients. It worth to notice that the thermal conductivity, the last thermodynamic parameter, has a sensitivity index of the same order of magnitude of neutronics parameters. Finally, it can be showed that $\sum_i S_{tot,i} = 1.028 \approx 1$.

Table 5.10: *Sensitivity indices for the maximum temperature in the MSFR domain. P and γ have strongest influence on the response, while other thermodynamic properties and neutronics parameters can be neglected. Being located near the reflectors, it is much more sensitive to the power rather than the heat transfer coefficient. Second or higher order interactions can be neglected.*

| | P | γ | c_p | k | $\Sigma_{f,2}$ | $\Sigma_{f,3}$ | $\Sigma_{f,4}$ | $\Sigma_{f,5}$ |
|-----------|-----------------------|-----------------------|-----------------------|-----------------------|-----------------------|-----------------------|-----------------------|-----------------------|
| S_i | 8.38×10^{-1} | 4.23×10^{-2} | 9.72×10^{-2} | 1.76×10^{-9} | 1.99×10^{-9} | 1.81×10^{-7} | 1.26×10^{-6} | 2.32×10^{-6} |
| S_{tot} | 8.54×10^{-1} | 4.72×10^{-2} | 1.05×10^{-1} | 4.53×10^{-3} |

Minimum temperature. The minimum temperature statistical behavior can be interesting, because the salt can solidify below 858 K, as indicated in Chapter 1.1.2. The reactor is sized to have a minimum temperature sufficiently higher with respect to this limit. In fact, the minimum temperature the primary system can reach is the minimum temperature of the secondary loop, which is 908 K, thus making the solidification impossible even in case of stochastic data, while ensuring at least a temperature difference of 15 K between primary and secondary side (in nominal conditions the minimum temperature of the primary system is 650 °C). However, The statistical analysis on the minimum temperature can be relevant also to study the performances of HX (e.g. guarantee 15 K as minimum temperature difference with a probability higher than 99 %).

Figure 5.8 reports the minimum temperature pdfs, comparing order 3 and 4 PCE approximations with 10⁵ samples each. Comments made for the maximum temperature are valid in this case too. Then, the order 4 polynomial are taken as best compromise. Its mean value is 924 K (equal to the nominal value in the non-stochastic case), while the variance is 26 K². Since the lowest temperature possible is set by boundary conditions, this reflects on the mean value and variance, and consequently on the pdf shape. In fact, below 920 K the pdf sharply goes to zero. Figure 5.8(b) shows the pdf shape is nearly normal in the central region, but it is far from a normal distribution especially at tails.

Considering the heat exchanger constraint mentioned previously, the probability of having a minimum temperature difference of 15 K is 53.2 %, while, fixing the minimum probability to 99 %, the temperature difference is 8.4 K, which may be too low depending on the kind of HX and on the operational mode.

Sensitivity indices are reported in Table 5.11. As mentioned, the minimum temperature is found in the HX, far from the region in which the vast majority of fission reactions happens and where the temperature decrease is determined by the heat transfer coefficient. Thus, it is meaningful to see that γ total sensitivity index is by far the highest (above 0.8), whereas the power one, which is still relevant, plays a secondary role, along with the c_p . Analogously to Table 5.10, all other parameters have negligible effects with respect to γ , but in this case they are of the order of $10^{-2}J$. In this case, $\sum_i S_{tot,i} = 1.179$, which cannot be approximated to 1. The strongest second order contribution comes from the interaction between thermal-hydraulic parameters and neutronics one, confirming relevant effects of feedback.

Table 5.11: *Sensitivity indices for the minimum temperature in the MSFR domain. P and γ have strongest influence on the response, whereas other thermodynamic properties and neutronics parameters first order interactions can be neglected. However, total sensitivity indices show clear importance of second or higher order interactions. Being located in the heat exchanger, the minimum temperature is much more sensitive to the heat transfer coefficient rather than the reactor power.*

| | P | γ | c_p | k | $\Sigma_{f,2}$ | $\Sigma_{f,3}$ | $\Sigma_{f,4}$ | $\Sigma_{f,5}$ |
|-----------|-----------------------|-----------------------|-----------------------|-----------------------|-----------------------|-----------------------|-----------------------|-----------------------|
| S_i | 1.27×10^{-1} | 6.86×10^{-1} | 3.89×10^{-2} | 2.16×10^{-8} | 2.16×10^{-8} | 2.18×10^{-8} | 2.15×10^{-8} | 2.23×10^{-8} |
| S_{tot} | 2.19×10^{-1} | 7.24×10^{-1} | 7.68×10^{-2} | 3.18×10^{-2} |

Average temperature. Figure 5.9 shows the average temperature pdfs, comparing order 3 and 4 PCE approximations with 10^5 samples each. Using the same logic of maximum and minimum temperatures, order 4 polynomials are considered as best approximation. The mean value is 966 K with a variance of 73 K^2 . The pdf shape is nearly normal in the central region, but evident discrepancies appear near the tails.

Sensitivity indices, reported in Table 5.12, are more interesting to analyze. As usual, fission cross sections and thermal conductivity have negligible effects on the average temperature. On the other hand, the sum of reactor power and the heat transfer coefficient first order sensitivity indices is higher than 0.91. However, the power has twice the effect on the average temperature with respect to γ , because the region in which it is significantly perturbed by the heat transfer coefficient is limited to the heat exchanger. Despite the salt specific heat has a total sensitivity index in between the relevant (i.e. P and γ) and irrelevant parameters (i.e. $\Sigma_{f,2-5}$ and k), its contribution is negligible with respect to the power and the heat transfer coefficient. In fact, changing c_p does not change considerably the mean temperature.

Finally, $\sum_i S_{tot,i} = 1.078$, which can be arguably approximated to 1.

5.3.3 Results: temperature field

Data regarding the temperature field are available as averaged temperatures on the volumes center of mass, as well as their coordinates. Solid components, such as reflectors and blanket, have their own temperature field, but it is set by default (uniform 900 K) because the neutronics code needs a temperature to define the cross sections, while heat conduction in the solid is not taken into account. Thus, these components are excluded from the analysis.

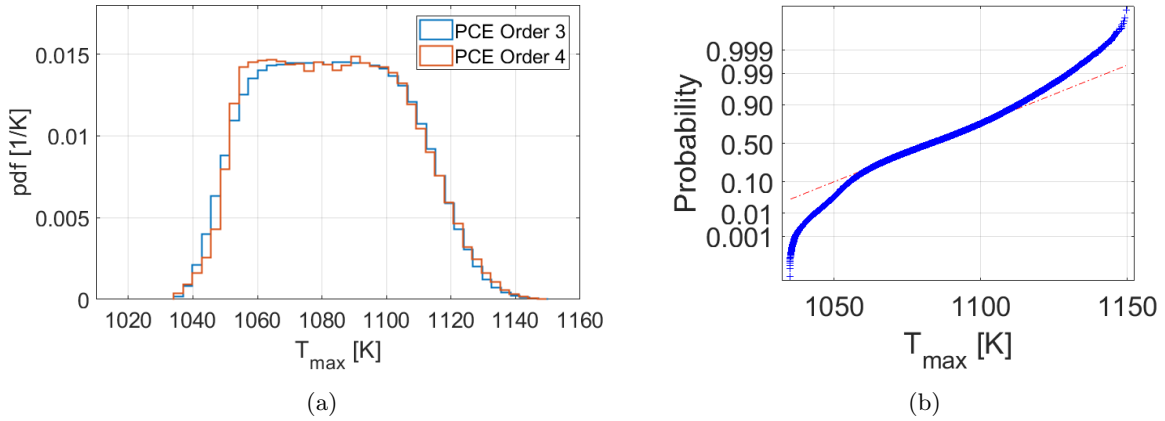


Figure 5.7: (a) *Maximum temperature pdfs, comparing order 3 and 4 PCE approximations with 10^5 samples each. Despite order 3 polynomials were proven to be sufficient to approximate the solution is the CNRS benchmark case, order 4 polynomial seem to be the best compromise in this case.* (b) *Normal probability plot on the fourth order polynomial PCE approximation. Its shape is far from a normal distribution not only at tails but also in the central region.*

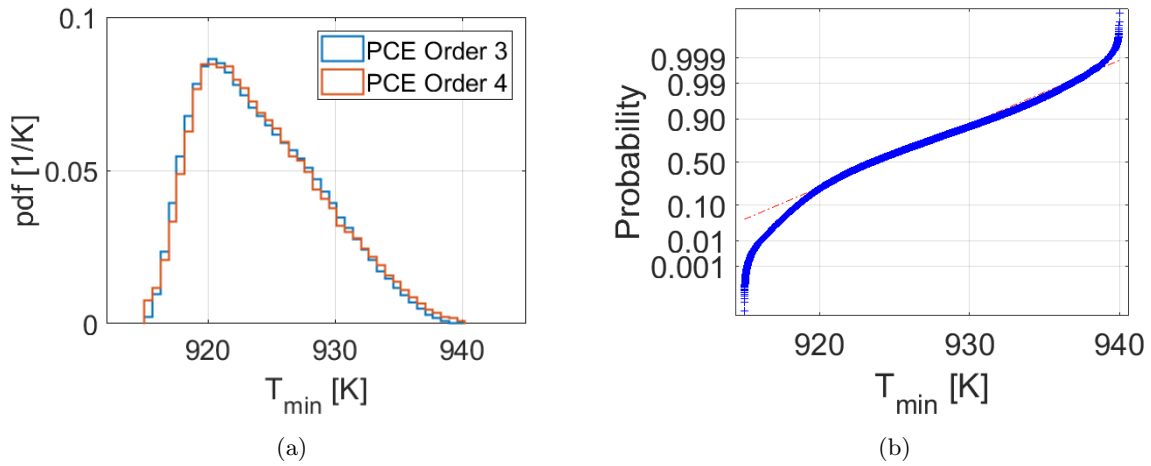


Figure 5.8: (a) *Minimum temperature pdfs, comparing order 3 and 4 PCE approximations with 10^5 samples each. Despite order 3 polynomials were proven to be sufficient to approximate the solution is the CNRS benchmark case, order 4 polynomial seem to be the best compromise in this case.* (b) *Normal probability plot on the fourth order polynomial PCE approximation. The curve follows a normal distribution in the central region whereas discrepancies appear at tails.*

Table 5.12: *Sensitivity indices for the average temperature in the MSFR domain. P and γ have strongest influence on the response, while other thermodynamic properties and neutronics parameters first order interactions can be neglected. However, total sensitivity indices show clear importance of second or higher order interactions. Its sensitivity to the power and the heat transfer coefficient is in between the maximum and minimum temperature.*

| | P | γ | c_p | k | $\Sigma_{f,2}$ | $\Sigma_{f,3}$ | $\Sigma_{f,4}$ | $\Sigma_{f,5}$ |
|-----------|-----------------------|-----------------------|-----------------------|-----------------------|-----------------------|-----------------------|-----------------------|-----------------------|
| S_i | 6.15×10^{-1} | 3.08×10^{-1} | 1.11×10^{-2} | 7.39×10^{-9} | 1.98×10^{-8} | 5.16×10^{-8} | 3.45×10^{-8} | 5.68×10^{-9} |
| S_{tot} | 6.56×10^{-1} | 3.25×10^{-1} | 2.49×10^{-2} | 1.15×10^{-2} |

The PCE code created an approximation for each averaged value (53000 elements), along with the calculation of the sensitivity indices. The temperature field analysis is performed differently from the single values responses. For this kind of applications, knowing the temperature field is particularly important to ensure salt chemical stability, satisfactory structural material properties, effectiveness of heat exchange between primary and secondary loop. Having assumed stochastic inputs, the whole temperature field is not exactly determined, but it is subjected to oscillations in each node. It may be relevant to quantify the probability such that the temperature is lower than a threshold in each volume. In alternative, volumes which have a temperature lower than a threshold, with a prescribed probability, may be highlighted. This last case is taken into consideration.

As an example, the previous procedure is applied adopting a probability of 0.95 and 650 °C or 750 °C as threshold temperatures. They are inlet and outlet temperatures in the HX (following [23]). This probabilistic analysis is performed to discover possible variation from the nominal design condition, pointing out whether and where there are discrepancies.

Figure 5.10 shows volumes belonging to the salt, HX and the pump, assuming 750 °C. Considering this temperature, Figure 5.10(a) reports the probability in each volume of having a temperature below this value. Despite in the majority part of the domain it is impossible that the temperature is higher than the threshold (i.e. the probability to be above is 1), there are wide regions, near the upper reflector in which the probability is far below 95 % or even 0. This is reasonable because, even considering non-stochastic inputs in the same areas, the temperature is higher than 750 °C since the maximum temperature in the domain is not found at the HX inlet. To be more clear, Figure 5.10(b) distinguishes regions in which the probability is higher (blue) and lower (red) than 95 %. As known in the non-stochastic case, the pump and the upper reflector are subjected to temperatures higher than 750 °C. On the other hand, analyzing the inlet of the HX may be interesting. Figure 5.11 reports multiple sections of the HX at different heights. Even 5 cm after, there is a wide portion in which the probability is below 95 %, which becomes negligible 5 cm downstream. This implies that at least the first 10 cm are subjected to temperature higher or equal to 750 °C with high probability, which was not predicted by non-stochastic simulations. Thus, stronger high temperature protection is needed for this component.

Analogously, Figure 5.12 shows volumes belonging to the salt, HX and the pump, assuming 650 °C. Considering this temperature, Figure 5.10(a) reports the probability in each volume to have a temperature above this value. There is a significant difference with the other threshold since non-stochastic simulations do not accept a temperature lower than 650 °C (923 K) in the whole domain. During the analysis on the minimum temperature, Figure 5.8(a) showed that there was a non-negligible probability to have a minimum temperature below 923 K. This aspect may be relevant, knowing that a margin from the eutectic point (858 K) is needed. Assuming that 650 °C was chosen to ensure a tolerable temperature difference, there is an area

in which there is a high probability it is not verified. Figure 5.12(b) reports regions in which the probability to have a temperature above 650 °C is higher (red) or lower (blue) than 95 %. The region below the HX outlet is interested by low temperature. Analogously to the previous analysis, multiple HX sections are reported in Figure 5.13 in proximity of the HX outlet. In fact, 9 cm above the outlet there is an area subjected to low temperature, which interests almost the whole surface at the outlet.

5.3.4 Results: effective multiplication factor

The effective multiplication factor is the only response for the neutronics analysis. The pdfs obtained with third and fourth order polynomials approximations and 10^5 samples, along with the normal probability plot relative to the fourth order is reported in Figure 5.14. Differently from the maximum, minimum and average temperatures, the pdf does not vary evidently if the polynomial order increases. In fact, The pdf shape is a nearly perfect normal distribution, confirming the neutronics code is linear with negligible feedback effects on the response. However, the normal probability plot, relative to fourth order polynomial, shows deviations from normality at tails probably due to small contributions of feedback effects, which was never found before. The mean value is 1.00977, near to the nominal 1.00998, with a variance of 2.070×10^{-4} . It is lower than the de-coupled case (2.220×10^{-4}) highlighting that density/Doppler feedback has a positive effect on the system, reducing the variance (i.e. thanks to feedback, where the fission reactions increase the temperature increases, reducing the density, which reduces the probability of having fissions). Thus, analyzing the variance in de-coupled simulations is not only faster, but also slightly conservative. On the other hand, differently from the temperatures, the variance computed in MSFR is higher than the CNRS benchmark at least in de-coupled simulations (1.96×10^{-4}). This fact should encourage the research to quantify more precisely the uncertainties related to the fission cross sections. Confirming what found for the CNRS benchmark, thermal fluid-dynamic parameters have negligible effects on the k_{eff} , as showed from the sensitivity indices in Table 5.13. In fact, despite P and γ had a strong effect on temperatures, here they are completely negligible with respect to fission cross sections, underlining the fact that feedback effects have secondary consequences with respect to more neutronics-related parameters. Finally, $\sum_i S_{tot,i} = 1.002$, which ensures ensure small contribution of second or higher order interactions.

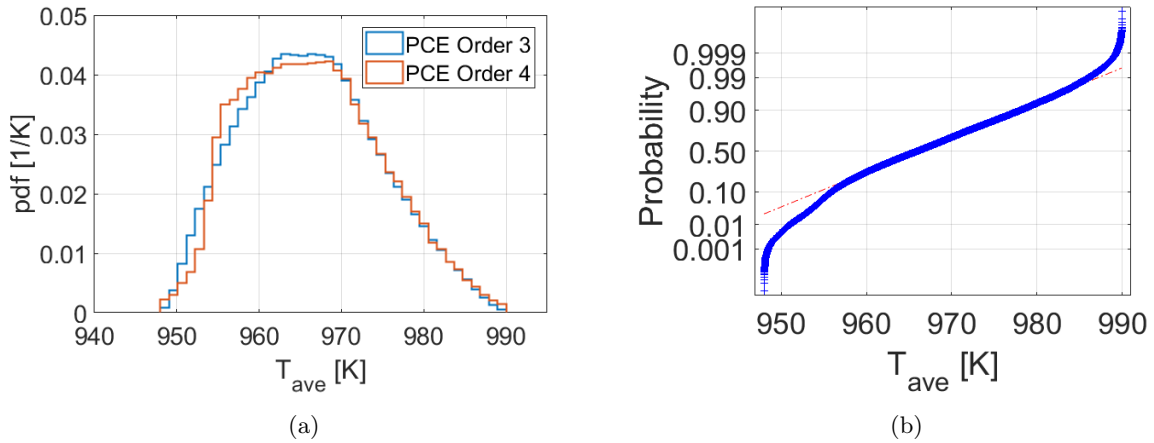


Figure 5.9: (a) Average temperature pdfs, comparing order 3 and 4 PCE approximations with 10^5 samples each. Despite order 3 polynomials were proven to be sufficient to approximate the solution in the CNRS benchmark case, order 4 polynomial seem to be the best compromise in this case. (b) Normal probability plot on the fourth order polynomial PCE approximation. The curve follows a normal distribution in the central region whereas discrepancies appear at tails.

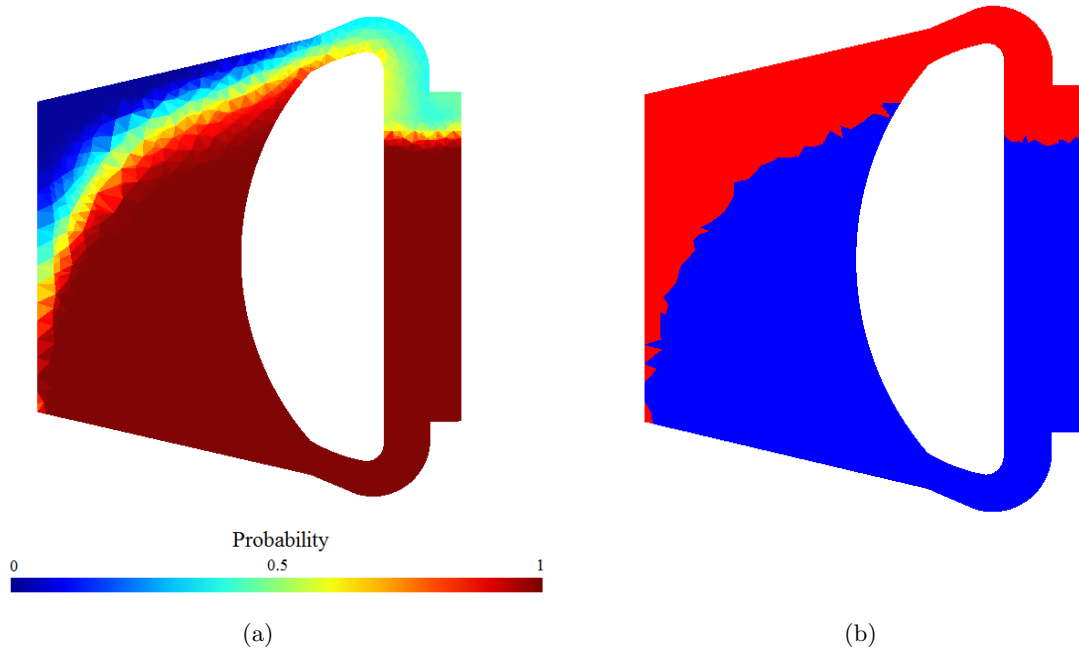


Figure 5.10: (a) Lateral view of the core and HX domain. It reports probability in each volume of finding a temperature lower than 750°C. Despite in the majority part of the domain it is impossible that the temperature is higher than this threshold, there are wide regions, near the upper reflector in which the probability is very low or even 0. (b) Distinction between regions in which the probability is higher (blue) and lower (red) than 95%.

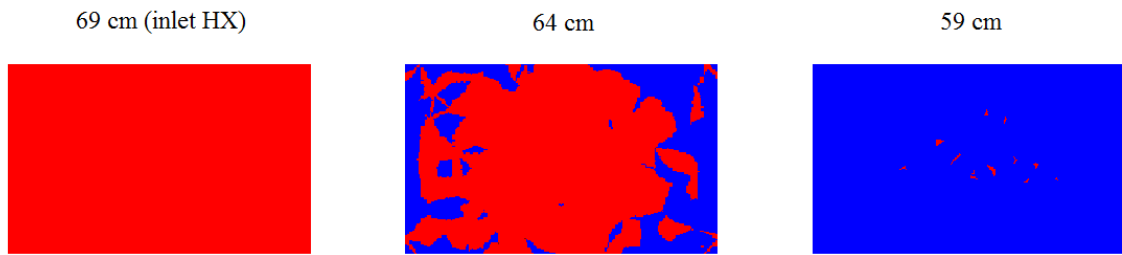


Figure 5.11: *Multiple views of the HX. Fixing 750°C as threshold temperature, blue polygons represent volumes in which the probability is below this threshold 95%, while blue ones above it. As energy is progressively transferred to the secondary loop, the salt cools down increasing the probability to have a temperature below the threshold. Despite these volumes are far from external boundaries, it is clear that even inside the HX there is a high number of surfaces for the energy transfer between primary and secondary loop. In addition, first 10 cm are subjected to temperature higher or equal to 750°C with high probability.*

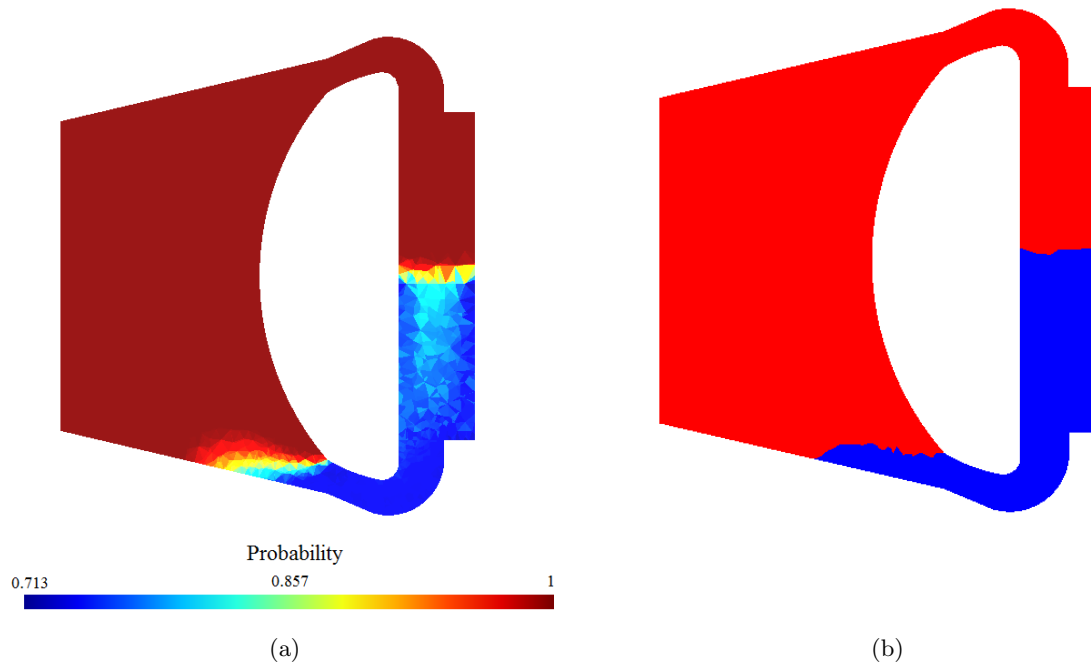


Figure 5.12: (a) *Lateral view of the core and HX domain. It reports probability in each volume of finding a temperature lower than 650°C . Even if it was not predicted by non-stochastic analysis since they fixed , 650°C as minimum temperature, there is an area (bottom part of the reactor) in which the probability is well below 1. (b) *Distinction between regions in which the probability is higher (red) and lower (blue) than 95%.**

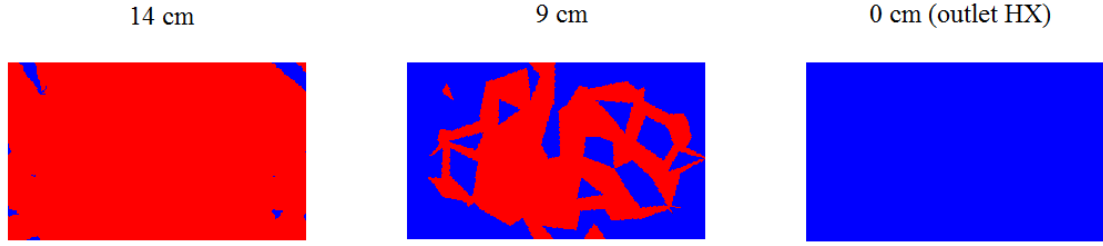


Figure 5.13: Multiple views of the HX. Fixing 650°C as threshold temperature, red polygons represent volumes in which the probability is above this threshold with 95%, while blue ones below it. As energy is progressively transferred to the secondary loop, the salt cools down increasing the probability to have a temperature below the threshold. Despite 650°C was set as minimum temperature in non-stochastic calculations, in the bottom part of the HX there is a high probability it is below this threshold. In fact, last 10 cm are subjected to temperature lower or equal to 650°C with high probability.

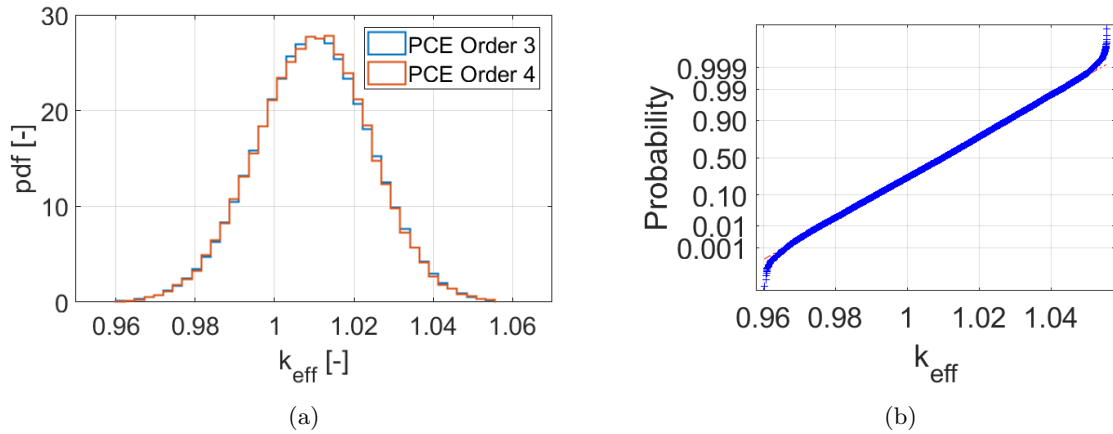


Figure 5.14: (a) k_{eff} pdfs obtained with third and fourth order polynomials approximations and 10^5 samples. Differently from the maximum, minimum and average temperatures, the pdf does not vary evidently if the polynomial order increases. (b) Normal probability plot on the fourth order polynomial approximation. Due to model linearity and negligible feedback effects, the response is almost perfectly normally distributed, except at tails.

Table 5.13: Sensitivity indices for the effective multiplication factor. Fission cross sections have the strongest contribution on the response variance, whereas other thermal fluid-dynamic related parameter have negligible influence. Second or higher order interactions can be neglected.

| | P | γ | c_p | k | $\Sigma_{f,2}$ | $\Sigma_{f,3}$ | $\Sigma_{f,4}$ | $\Sigma_{f,5}$ |
|-----------|-----------------------|-----------------------|-----------------------|------------------------|-----------------------|-----------------------|-----------------------|-----------------------|
| S_i | 6.03×10^{-4} | 1.73×10^{-4} | 2.62×10^{-5} | 7.42×10^{-11} | 9.76×10^{-2} | 2.75×10^{-1} | 2.66×10^{-1} | 3.58×10^{-1} |
| S_{tot} | 1.67×10^{-3} | 1.06×10^{-3} | 5.24×10^{-4} | 5.16×10^{-4} | 9.81×10^{-2} | 2.76×10^{-1} | 2.67×10^{-1} | 3.58×10^{-1} |

5.4 Summary

Based on the results on the CNRS benchmark, an analogous analysis is performed on the MSFR. After having defined the computational domain, along with its mesh, the reactor model was built with the thermal fluid-dynamic and neutronics code, considering new phenomena previously excluded (e.g. turbulence, 3D geometry). Maximum, minimum and average temperature, as well as the whole temperature field were chosen as relevant responses for the thermal fluid-dynamic part, whereas the effective multiplication factor was chosen for the neutronics one.

Single-physics calculations were performed on the neutronics part only since it may allow presumably a much more wide parameter reduction through the class approach. In fact, only 4 macroscopic fission cross sections energy groups (out of 6) were relevant according to the analysis. On the other hand, the β and λ class (16 parameters total) were completely excluded since they introduce a variance on k_{eff} at least five orders of magnitude lower than the Σ_f class. The parameter ranking was not performed on the thermal fluid-dynamic only case, since the computational time for each set of calculations is unsustainable compared to the effectiveness of parameter space reduction. The whole set of inputs to perturb in the coupled case was 8. Before approaching the coupled problem, a strategy for the computational time reduction had to be defined. Considering the set of perturbed parameters, it was assumed that variation in the flow field from the nominal steady-state to the generic perturbed simulation was negligible. Thus, a test case was run in advance to ensure that this hypothesis is correct, setting up a simulation with the maximum perturbed inputs. The simulation in which the momentum equations were solved (*WithFlow*) was compared to the approximated one (*NoFlow*), showing errors below 10^{-3} . This test case was also used to determine other relevant calculation parameters, such as the time step and the number of DGFloWS/PHANTOM- S_N iterations, as well as a conservative estimate of the computational time for each simulation. In the most perturbed case, the computational time was reduced to 38h, running the simulation on a HPC using 2 processors, with a 5ms time step and 5 codes iterations. Having 8 inputs, *OpenGPC* needed 161 model evaluations to build the PCE approximation with order 3 polynomials and a (Smolyak) sparse grid. The total computational time was approximately 14 days.

Responses were examined building their pdf and normal probability plots, while sensitivity indices were adopted to perform the sensitivity analysis. Due to the high computational time, a MC evaluation was not possible. On the other hand, third and fourth order polynomials were compared, showing that third order polynomials are no more sufficient to properly represent the responses, in contrast to the CNRS benchmark. In fact, fourth order polynomials seem to be the best choice in this case. Because of strong relevance of uniformly distributed inputs, the maximum, minimum and average temperature were far from being normally distributed. Mean values were very near to their nominal values, while the variance was between 2 and 8 times lower than corresponding CNRS benchmark cases, due to significant changes in the geometry. In fact, the power total sensitivity indices was higher than 0.85, whereas γ is irrelevant since it has an effect only in the HX region, which is limited. On the contrary, the minimum temperature, found in the HX, was very sensitive to γ , while P had a much lower contribution. The average temperature was in a condition in between these two values, showing c_p had a negligible contribution along with other parameters excluding P and γ . The thermal conductivity had almost no effects on the thermal-fluid dynamic parameters, even it had the highest relative standard deviation, because of the predominance of turbulent phenomena. In addition, sensitivity indices showed strong second or higher order contributions, especially for the minimum temperature, because of relevant feedback effects.

The temperature field was approached differently. Temperature values, averaged in each volume, were used to build the PCE approximation for the whole field (53000 volumes). Then, performing a random sampling, probability values such that the temperature was above 650 °C or below 750 °C were computed and represented graphically on the whole domain. Despite higher than 750 °C temperatures are foreseen in the reactor, first 10 cm of the HX were subjected to higher temperature above the 5% tolerance. On the other hand, slightly before the HX outlet, the reactor was interested by low temperature even if it was not determined by non-stochastic simulations (i.e. the minimum temperature was set to 650 °C). Thus, this region may face too short margin from solidification, which can be potentially dangerous during transient scenarios, or, more probably, it can be subjected with non-negligible probability to low temperature differences which guarantee satisfactory performances of the HX.

Finally, the effective multiplication factor was examined. Differently from the maximum, minimum and average temperature, no relevant changes appear among different order approximations. Because of the model linearity and secondary effects of feedback, the pdf was almost perfectly normally distributed, except at tails, with a mean value of 1.00976, near to the nominal one. The coupling with thermal fluid-dynamics code, thanks to the introduction of feedback effects, reduces the variance on the k_{eff} . However it is higher than the one computed in the CNRS benchmark case. Thermal fluid-dynamic parameters had negligible influence.

Chapter 6

Conclusions

In this thesis, a novel Uncertainty Quantification (UQ) method, the Polynomial Chaos Expansion (PCE), was applied to the new generation IV reactor concept, the Molten Salt Fast Reactor (MSFR), developed by EU in the context of the Horizon2020 SAMOFAR project. The UQ was paired with variance-based sensitivity analysis, using sensitivity indices. The reactor model was made with an in-house developed, multi-physics codes, `DGFlows` and `PHANTOM-SN`. `OpenGPC`, equipped with Smolyak sparse grids, was adopted for the PCE construction. These tools were exploited on two problems, the CNRS benchmark and the MSFR. The former was a test case to understand the capabilities of both multi-physics codes and PCE code, testing it in case of high inputs dimensionality. The latter was approached based on the experience of the test case and represented the actual subject of this work. The maximum temperature (T_{max}) and the effective multiplication factor (k_{eff}) were the analyzed responses for the CNRS benchmark, whereas the minimum temperature (T_{min}) along with the average temperature (T_{ave}) and the temperature field were added during the MSFR study.

The first application was a test case developed at CNRS/LPSC/Grenoble, and known as the CNRS benchmark, which contains the main features of the MSFR, such as the precursors motion, strong coupling between thermal hydraulics and neutronics, as well as fast neutron spectrum. Single-physics and de-coupled simulations (neutronics with fixed nominal flow and temperature fields, and fluid-dynamics with fixed nominal fission power density) were run in advance to limit the number of parameters, assuming that only a fraction of possible inputs affect the response(s) in a non-negligible way. It was fundamental since the PCE needed a higher number of model evaluations if the parameter space increases. The thermal fluid-dynamic part showed that only the heat transfer coefficient γ introduced a perturbation on the maximum temperature above 1%. Two different approaches (the *mean value* and the *class approach*) were introduced to perform the parameter ranking on the single-physics neutronics calculations, which counted about 70 inputs. The former approach divided inputs in classes, analyzing a single (averaged) value representative of the whole class. The latter took the same classes distinction but a PCE evaluation was performed on the whole set of inputs for each class. Uncertainty quantification, combined with sensitivity analysis, performed with (Sobol's) sensitivity indices, found that only $\Sigma_{f,5}$, $\Sigma_{f,6}$ ν_5 and ν_6 gave relevant contribution to the k_{eff} , while others were considered negligible. Steady-state multi-physics simulations on the CNRS benchmark involved relevant-only thermal fluid-dynamic and neutronics parameters as well as the reactor power. The number of needed model evaluations code was 97. Results were compared order 3 with (level 3 quadrature rule) and order 4 (level 4 quadrature rule) PCE approximation with the reference MC sampling (obtained considering the same parameter space and 10^3 samples) and they showed excellent agreement, while highlighting minimal differences between order 3

and 4 polynomials for both responses, thus indicating third order polynomials were a good compromise between efficiency (i.e. low number of model evaluations) and accuracy. Maximum temperature was mainly sensitive to thermal fluid-dynamic related parameters, while it had almost no contribution from fission cross sections and fission yields. Its pdf had evident deviation from the normal distribution at tails, due to non-linearity in γ and strong contribution of uniformly distributed inputs. On the other hand, neutronics-related parameters were of primarily importance on the effective multiplication factor statistics, while it was insensitive to thermal fluid-dynamics parameters. Due to secondary effects of feedback and the relevance of normally-distributed only parameters, the response pdf is almost a perfect gaussian. It is worth highlighting that the reference model needed around 1500 h to generate the 10^3 responses, while the sampling on the PCE approximation required a few seconds for 10^6 samples.

Having established that the PCE method could be successfully applied to a simplified molten salt reactor system, the analysis could be extended to the actual topic of this work, the MSFR. New phenomena and features, such as turbulence and 3D geometry, were added for a complete description of the system. The computational domain was chosen on the basis of the system symmetry and several materials/components were distinguished with different material properties. Maximum, minimum and average temperature, as well as the whole temperature field were chosen as relevant responses for the thermal fluid-dynamic part, whereas the effective multiplication factor was chosen for the neutronics one. Single-physics calculations were performed on the neutronics part only since it may allow presumably a much more wide parameter reduction through the class approach. In fact, only 4 macroscopic fission cross sections energy groups (out of 6) were relevant according to the analysis. On the other hand, the β and λ class (16 parameters total) were completely excluded since they introduce a variance on k_{eff} at least five orders of magnitude lower than the Σ_f class. The parameter ranking was not performed on the thermal fluid-dynamic only case, since the computational time for each set of calculations was unsustainable compared to the effectiveness of parameter space reduction. The whole set of parameters was composed by 8 inputs, including thermal fluid-dynamic ones (i.e. power, heat transfer coefficient, salt specific heat and salt thermal conductivity), requesting 161 model evaluations, according to the PCE code (adopting order 3 polynomials and a sparse grid). Despite the low number of simulations, they were too computational expensive to be performed in acceptable amount of time. Considering the set of perturbed parameters, it was assumed that variation in the flow field from the nominal steady state to the generic perturbed simulation was negligible. Thus, a test case was run in advance to ensure that this hypothesis is correct, setting up a simulation with the maximum perturbed inputs. The simulation in which the momentum equations were solved (*WithFlow*) was compared to the approximated one (*NoFlow*), showing errors below 10^{-3} . This test case was also used to determine other relevant calculation parameters, such as the time step and the number of `DGFlows/PHANTOM-SN` iterations. In the most perturbed case, the computational time was reduced to 38 h, running the simulation on a HPC using 2 processors, with a 5 ms time step and 5 codes iterations. With these settings, the total computational time was approximately 14 days.

Comparison with the MC reference was not possible due to the high computational time. However, computing the approximation with several polynomial orders showed that fourth order polynomials are more appropriate to represent the results, in contrast with the CNRS benchmark, where third order was sufficient. Maximum, minimum and average temperature had mean values near their nominal one, while their variances were between 2 and 8 times lower than the CNRS benchmark case. Their distributions were far from normal due to the high relevance of uniformly distributed parameters. Sensitivity indices proved neutronics inputs had significant effects, being related to fourth order terms. In addition, the salt thermal conduc-

tivity had negligible contributions, even it had the highest relative standard deviation. Power and the heat transfer coefficient were the most relevant inputs, but their contributions widely varied depending on the response. The power had a total sensitivity index higher than 0.85 on maximum temperature, whereas γ is irrelevant since it has an effect only in the HX region, which is limited. On the contrary, the minimum temperature, found in the HX, is very sensitive to γ , while P has a much lower contribution. The average temperature is in a condition in between these two values. The specific heat sensibly contributed to the variance only in the maximum temperature case, in which it was even stronger than the heat transfer coefficient.

The temperature field was approached differently. The PCE approximation was built for each volume. Then, performing a random sampling, probability values such that the temperature was above 650 °C or below 750 °C (outlet and inlet temperature on the HX) were computed and represented graphically on the whole domain. First 10 cm of the HX were subjected to temperature higher than 750 °C. In addition, slightly before the HX outlet, the reactor was interested by temperature below 650 °C with non-negligible probability even if it was not determined by non-stochastic simulations, being exposed to solidification and scarce performances.

Finally, the effective multiplication factor was examined. The mean value was near to the nominal one, and its variance reduces with respect to the de-coupled case, thanks to the presence of feedback effects, but it was higher than the CNRS benchmark coupled simulations. Because of the model linearity and secondary effects of feedback, the pdf is almost perfectly normally distributed. Thermal fluid-dynamic parameters had negligible influence, as found in the CNRS benchmark case.

In conclusion, PCE method was successfully applied to the MSFR, both on a ad-hoc test case and on the actual design. The CNRS benchmark has proven to be representative of the MSFR behavior even from the sensitivity analysis point of view. Thermal hydraulic-related responses were mainly affected by the power and heat transfer coefficient, while weakly by thermodynamic properties. On the other hand, the effective multiplication factor was strongly perturbed by fission cross sections and fission yields, while it was insensitive to any other input. Order 3 polynomials approximations seemed adequate for the case, being the response slightly non-linear only in rare instances, whereas fourth order polynomials for the MSFR, since it had stronger feedback effects. The temperature field was analyzed, representing results in an alternative way, giving suggestions on weaknesses of components from a probabilistic point of view.

Despite a 23 % relative standard deviation was assigned to the thermal conductivity, the variance introduced to each response was negligible, thus spending resources for an improvement in its statistic information is not only irrelevant, but also ineffective in reducing the system uncertainties. On the other hand, the specific heat had a relevant impact on the maximum temperature which is a fundamental parameter that has to be considered carefully during the design process. Power, heat transfer coefficient, and fission cross sections had a dominant role in the response variance determination, needing a deeper and more realistic analysis. In particular, fission cross sections introduced big oscillations on the effective multiplication factor (± 2500 pcm), even higher than the CNRS benchmark test case, which is not tolerable for such applications. The power and the heat transfer coefficient were assumed uniformly distributed with a default standard deviation in absence of additional information. The next step of steady-state analysis may consist of introducing better approximation of their statistical behavior or even studying them as epistemic variables with other methods. Further studies are thus recommended, expanding the space of parameters, especially the thermal fluid-dynamic one. Salt density and flowrate/pressure jump in the pumps were not assessed in this study for lack of time, but they have presumably deep impacts on responses while needing at the same time stronger

computational efforts. However, performing more detailed analysis should require a deeper knowledge about the MSFR design (e.g. maximum/minimum power excursion, performances of control systems, additional features of heat exchangers) and more detailed information about the statistical properties of inputs, especially variances. Among all, fission cross sections seem to be of primary importance from this point of view. This study suggested to focus on groups 3,4 and 5 especially (i.e. between 0.7 keV and 0.5 MeV), which approximately corresponds to the resonance region, being almost 85 % of the variance concentrated here.

Transients, especially accidental ones, were not treated, but they are fundamental for the whole design process. Detailed analyses on those aspects are, thus, strongly recommended.

Bibliography

- [1] International Energy Agency, editor. *Key world energy statistics 2018*, 2018.
- [2] M. Allibert, M. Aufiero, M. Brovchenko, S. Delpech, V. Ghetta, D. Heuer, A. Laureau, and E. Merle-Lucotte. Molten salt fast reactors. In Igor L. Pioro, editor, *Handbook of Generation IV Nuclear Reactors*, pages 157–188. Woodhead Publishing, Sawston, England, 2016.
- [3] M. Allibert, D. Gérardin, D. Heuer, E. Huffer, A. Laureau, E. Merle, S. Beils, A. Cammi, B. Carlucci, S. Delpech, A. Gerber, E. Girardi, J. Krepel, D. Lathouwers, D. Lecarpentier, S. Lorenzi, L. Luzzi, M. Ricotti, and V. Tiberi, editors. *Description of initial reference design and identification of safety aspects*. SAMOFAR European Project D1.1, 2017.
- [4] K. F. Alvin, S. M. Deland, B. M. Rutherford, and K. V. Diegert, editors. *Estimation of Total Uncertainty in Modeling and Simulation*. Sandia Report, Sandia National Laboratories, Albuquerque, New Mexico, April 2000.
- [5] World Nuclear Association, editor. *World Nuclear Association Official Website*. <https://world-nuclear.org/information-library/current-and-future-generation/molten-salt-reactors.aspx>.
- [6] M. Aufiero, M. Brovchenko, A. Cammi, I. Clifford, O. Geoffroy, D. Heuer, A. Laureau, M. Losa, L. Luzzi, E. Merle-Lucotte, M.E. Ricotti, and H. Rouchd. Calculating the effective delayed neutron fraction in the molten salt fast reactor: Analytical, deterministic and monte carlo approaches. *Annals of Nuclear Energy*, 65(1):78–90, 2014.
- [7] O. Beneš and R. J. M. Konings. Thermodynamic properties and phase diagrams of fluoride salts for nuclear applications. *Journal of Fluorine Chemistry*, 130(1):22–29, 2009.
- [8] O. Beneš, M. Salanne, M. Levesque, and R. J. M. Konings, editors. *Physico-Chemical properties of the MSFR fuel salt*. EVOL Deliverable D3.2, 2013.
- [9] P. A. Cavallo and N. Sinha. Error quantification for computational aerodynamics using an error transport equation. *Journal of Aircraft*, 44(6):1954–1963, 2007.
- [10] B. Cockburn, G. Karniadakis, and C. W. Shu. *Discontinuous Galerkin methods: theory, computation and application*. Science and business media. Springer, Dordrecht, 2012.
- [11] F. D’Auria, C. Camargo, and O. Mazzantini. The best estimate plus uncertainty (bepu) approach in licensing of current nuclear reactors. *Nuclear Engineering and Design*, 248:317–328, 2012.
- [12] S. Delpech, E. Merle-Lucotte, D. Heuer, M. Allibert, V. Ghetta, C. Le-Brun, X. Doligez, and G. Picard. Reactor physic and reprocessing scheme for innovative molten salt reactor system. *Journal of Fluorine Chemistry*, 130(1):11–17, 2009.

- [13] J. H. Ferziger and P. Milovan. *Computational Methods for Fluid Dynamics*. Springer, Dordrecht, 3rd edition, 2002.
- [14] Generation IV International Forum, editor. *Generation IV International Forum Official Website*. https://www.gen-4.org/gif/jcms/c_9502/generation-iv-goals.
- [15] P. N. Haubenreich and J. R. Engel. Experience with the molten-salt reactor experiment. *Nuclear Applications and Technologies*, 8(2):118–136, 1970.
- [16] T. Jamasb, W. Nuttall, and M. Pollitt. *Future electricity technologies and systems*. Woodhead Publishing, Sawston, England, 2006.
- [17] D. Lathouwers, M. Tiberga, A. Cammi, E. Cervi, S. Lorenzi, D. Oliveira, M. Aufiero, A. Laureau, and P. Rubiolo, editors. *Verification and Validation studies*. SAMOFAR European Project D4.3, 2018.
- [18] A. Laureau, editor. *Développement de modèles neutroniques pour le couplage thermohydraulique du MSFR et le calcul de paramètres cinétiques effectifs*. Ph.D Thesis. Physique Nucléaire Expérimentale. Université Grenoble Alpes, 2015.
- [19] A. Laureau, M. Aufiero, P. R. Rubiolo, E. Merle-Lucotte, and D. Heuer. Coupled neutronics and thermal-hydraulics transient calculations based on a fission matrix approach: Application to the molten salt fast reactor. In *Mathematics and Computations, Supercomputing in Nuclear Applications and Monte Carlo International Conference, (M and C+SNA+MC 2015)*, pages 3064–3075, Nashville, USA, 2015.
- [20] O. P. Le Maître and O. M. Knio. *Spectral Methods for Uncertainty Quantification: With Applications to Computational Fluid Dynamics*. Scientific Computation. Springer, Dordrecht, 2010.
- [21] D. LeBlanc. Molten salt reactors: A new beginning for an old idea. *Nuclear Engineering and Design*, 240(6):1644–1656, 2010.
- [22] G. Locatelli, M. Mancini, and N. Todeschini. Generation iv nuclear reactors: Current status and future prospects. *Energy Policy*, 61:1503–1520, 2013.
- [23] L. Mathieu, D. Heuer, E. Merle, R. Brissot, C. Brun, E. Liatard, J. M. Loiseaux, O. Meplan, A. Nuttin, and D. Lecarpentier. Possible configurations for the thorium molten salt reactor and advantages of the fast non-moderated version. *Nuclear science and engineering*, 161:78–89, 2009.
- [24] E. Merle, editor. *Concept of Molten Salt Fast Reactor*. Molten Salt Reactor Workshop, MSFR Presentation. PSI, France, January 2017.
- [25] K. L. Murty and I. Charit. Structural materials for gen-iv nuclear reactors: Challenges and opportunities. *Journal of Nuclear Materials*, 383(1-2):189–195, 2008.
- [26] W. Oberkampf, J. Helton, and K. Sentz, editors. *Mathematical representation of uncertainty*. Non-Deterministic Approaches Forum. Seattle, WA, 16-19 April 2001.
- [27] Z. Perkó, L. Gilli, D. Lathouwers, and J. L. Kloosterman. Grid and basis adaptive polynomial chaos techniques for sensitivity and uncertainty analysis. *Journal of Computational Physics*, 260:54–84, 2014.

- [28] Z. Perkó, D. Lathouwers, J. L. Kloosterman, and T. Van Der Hagen. Large scale applicability of a Fully Adaptive Non-Intrusive Spectral Projection technique: Sensitivity and uncertainty analysis of a transient. *Annals of Nuclear Energy*, 71:272–292, 2014.
- [29] D. Rochman, M. Herman, P. Oblozinsky, and S. F. Mughabghab, editors. *Preliminary Cross Section and n -bar Covariances*. Report for WPEC Subgroup 26. Energy Sciences and Technology Department, National Nuclear Data Center, Brookhaven National Laboratory, 2007.
- [30] C. J. Roy and W. L. Oberkampf. A comprehensive framework for verification, validation, and uncertainty quantification in scientific computing. *Computer Methods in Applied Mechanics and Engineering*, 200(25-28):2131–2144, 2011.
- [31] A. Saltelli, T. Andres, M. Ratto, F. Campolongo, J. Cariboni, D. Gatelli, M. Saisana, and S. Tarantola. *Global Sensitivity Analysis*. Wiley, Hoboken, 2008.
- [32] A. Saltelli, P. Annoni, I. Azzini, F. Campolongo, M. Ratto, and S. Tarantola. Variance-based sensitivity analysis of model output. design and estimator for the total sensitivity index. *Computer Physics Communications*, 181(2):259–270, 2010.
- [33] S. Sankaran and A. L. Marsden. A stochastic collocation method for uncertainty quantification and propagation in cardiovascular simulations. *Journal of Biomechanical Engineering*, 133(3):1–12, 2011.
- [34] R. G. Sargent. Verification and validation of simulation models. *Journal of Simulation*, 7(1):12–24, 2013.
- [35] J. Serp, M. Allibert, O. Benejs, S. Delpech, O. Feynberg, V. Ghetta, D. Heuer, D. Holcomb, V. Ignatiev, J. L. Kloostermang, L. Luzzi, E. Merle-Lucotte, R. Uhlíř, J. and Yoshioka, and D. Zhimin. The molten salt reactor (MSR) in generation IV: Overview and perspectives. *Progress in Nuclear Energy*, 77:308–319, 2014.
- [36] T. I. P. Shih and B. R. Williams. Development and evaluation of an a posteriori method for estimating and correcting grid-induced errors in solutions of the navier-stokes equations. In *47th AIAA Aerospace Sciences Meeting including the New Horizons Forum and Aerospace Exposition*, pages 1–22, Orlando, USA, January 2009.
- [37] B. Sudret. Global sensitivity analysis using polynomial chaos expansions. *Reliability Engineering & System Safety*, 93(7):964–979, 2008.
- [38] M. Tiberga, D. Lathouwers, and J. L. Kloosterman. A discontinuous galerkin fem multi-physics solver for the molten salt fast reactor. In *International Conference on Mathematics and Computational Methods applied to Nuclear Science and Engineering (M&C 2019)*, Portland, OR, USA, August 25–29 2019.
- [39] N. Wiener. The homogeneous chaos. *American Journal of Mathematics*, 60(4):897–936, 1938.
- [40] G. E. Wilson. Historical insights in the development of best estimate plus uncertainty safety analysis. *Annals of Nuclear Energy*, 52:2–9, 2013.
- [41] D. Xiu and G. E. Karniadakis. The wiener-askety polynomial chaos for stochastic differential equations. *Society for Industrial and Applied Mathematics*, 13(3):635–659, 2002.

Acknowledgments

This thesis was written at TU Delft university, in the RID (Reactor Instituut Delft). First, I would like to thank prof. Sandra Dulla who put me in contact with the NERA group and for the continuous interest she had on the work, despite she was far from the "operating center". Under the supervision of prof. Danny Lathouwers, I was able to easily understand the fundamental tools thanks to Ph.D Marco Tibergha and Dr. Zoltàn Pérkò, who helped me with the thermal-hydraulic/neutronics codes and the PCE code respectively. Especially from Marco, I could learn a lot not only about PHANTOM- S_N and DGFloWS, but also about the writing procedure of scientific papers, as well as many other things. All of them were patient and guided me on the correct pathway, even with small hints, with frequent and constructive meeting, which ensured the good success of the work. Moreover, I was able to join to the SAMOFAR final meeting (held in Delft The Veste Theater) which was very instructive since recapped in a multi-disciplinary way what done in last years on the MSFR technology.

This international collaboration was extremely advantageous, surely for me and for other members of the team, since it culminated with the writing of a conference paper. In addition, there should be enough material for an article paper, which is a further proof of the fruitful cooperation.

I hope I can have the possibility to work on new/updated projects with these people, even if I will not probably work in the academic environment, and I would like to take this opportunity to thank them one more time.

Appendix A

Details on communication scripts

The submission process using nested submissions is not straightforward due to the absence of *qsub* and *qstat* functions on slave nodes. Thus, the correlations between Python scripts and the cluster may be strong. Here it is presented a detailed description of Python scripts to clarify their mechanism and interactions.

The following list is organized distinguishing two main processes, the job submission and the acquisition of outputs.

- **Submission process.**

- *PrepareSubmission*. The script is called by the MATLAB® code, after it saves the structure in which all relevant information are present (*SampleStructure*). The script takes the abscissas, already re-scaled with their mean value and standard deviation, as well as the set of variable names and the set of indices corresponding to the calculations to perform. Then, since there can be folders with results of previous calculations, it deletes all the calculations folders. Subsequently it creates a number of folders with unique names equal to the number of calculations it has to submit lately. It creates a list containing the number of the *i*-th calculation, the vector of the variables names subjected to the UQ study, the vector of perturbed abscissas. For each line of the list it sends the *i*-th line as an input for the *SubmitCalculation* script. Inside this loop, a check on the number of submitted calculations is present. Since it can be interesting and useful for the reader, it is reported here:

```
Nsimul =int(subprocess.check_output("ssh -o StrictHostKeyChecking=no -o
UserKnownHostsFile=/dev/null -o LogLevel=QUIET Proper HPC 'qstat -u User-
name — grep R -c' ", shell=True))
```

Where *Username* has to be substituted with the personal username account, while *Proper HPC* is the address of the HPC. The command *'qstat -u Username — grep R -c'* counts the number of jobs belonging to that *Username*. Since it contains a *qstat* command and it is run on a slave node, the line *ssh -o StrictHostKeyChecking=no -o UserKnownHostsFile=/dev/null -o LogLevel=QUIET Proper HPC* should be added to come back temporarily on the master node. It is important that each command performed on the master node is written in the same line. Two or more commands on the master node cannot be performed in this way. Then the command *subprocess.check_output* takes the output, which normally is only displayed (*string* type). Finally it is converted in integer.

This value is compared with a customer set maximum number of parallel submissions. If the submissions number is lower than this threshold, the script calls *SubmitCalculation*.

- *SubmitCalculation*. It receives the i -th submission line. It is a list type object containing the input matrix line, the index of that line, the variables names and a proper index corresponding to that submission line. This last parameter is necessary to synchronize the submission line with its folder. As mentioned, calculation folders are created in advanced. However, by using an optional function in the PCE code, some preliminary model evaluations are performed to select responses with values above a given threshold. Some of this evaluations can be in common (i.e. they have the same inputs) with the actual set of submissions. Since the response(s) were already evaluated, the code does not submit that job, jumping that folder. The index takes into account this fact, avoiding overwriting folders which still contain the outcomes of the simulations.

The following script sections contains the whose set of nominal values belonging to the widest set of variables. For example, in Chapter 4.1 we defined the 70 different inputs for both neutronics and thermal fluid-dynamics. Using the class approach only a fraction on them were subjected to uncertainty quantification. The script has the nominal values of all those variables. Thanks to the vector of variables names, the script recognizes which variables are subjected to the UQ study, assigning to the others their nominal value. Then, it collects the complete set of variables and it starts to modify the inputs. In this way the input files may be modified with the same value, since that parameter still has its nominal value. This procedure was adopted to generalize the script, without considering a modification every time the set of inputs plugged in the PCE model were changed.

Afterwards, each input file containing a potentially random variable is modified. The modification process involves: a) opening that file in reading mode and a new one in writing mode. Then, it scrolls the whole file copying each line in the new one except for the one that contains the input, which is substituted with the updated value. Finally, both files are closed and the new one is transferred to the calculation folder. The submission to the cluster is performed with a command similar to the one to obtain the number of simulations. In fact, we are still working on processors, thus, not having the *qsub* command. Since we need to retrieve the jobID, this time it is not possible to write all commands in one line and an additional script (*SubmissionAux*) is called instead of writing it in a single line.

- *SubmissionAux*. It communicates with *SubmitCalculation*, which runs on a processor, through .txt files, since *SubmissionAux* runs on the master node. It needs the index to select the correct folder and start the proper submission procedure. Then, once the submission is done, it writes a .txt file containing the jobID, read afterwards by *SubmitCalculation*.

- **Response acquisition.**

- *RequestStatusUpdate*. It checks for each valid calculation index (the same described in the *SubmitCalculation*) if the simulation associated to its jobID is still running. As explained, not having the *qstat* function on the processor, sequence analogous to the one to submit the i -th calculation. To this purpose, another script (*StatusAux*, which is not examined) works in a similar way to the *SubmissionAux*: it is run on the master node and it takes the jobID as input via .txt file, it checks the calculation

status and write it on another .txt file to make it accessible to *RequestStatusUpdate*. If the calculation is no more on the cluster (i.e. it ended), performing the command *qstat* gives a status different from zero. If this condition is satisfied, the script checks if the output files were generate. Generally they are two, one for the neutronics and the second for the thermal fluid-dynamic code. It merges all the outputs, which is fundamental since the PCE code needs a vector with the whole set of responses, updating the *SampleStructure* in the responses and status entries, changing it from *Submitted* to *Fetchd*.

– *StatusAux*.

Figure A.1 visualizes the communication process.

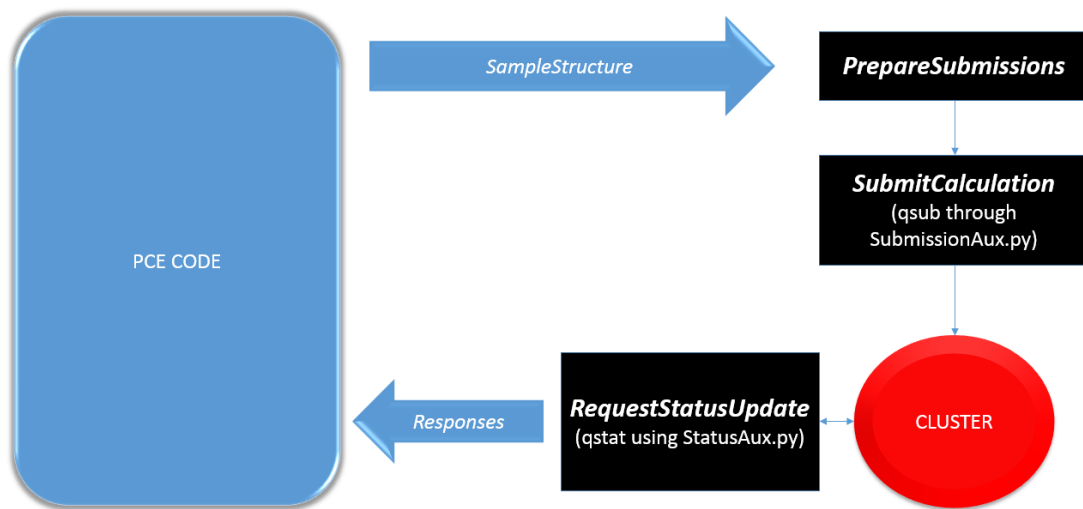


Figure A.1: *Visualization of the communication process*

Appendix B

Boussinesq approximation

The Boussinesq approximation consists of assuming constant density in each term of the equations except for the body force term. This term is responsible for the presence of a buoyancy force. The buoyancy force (per unit volume) can be expressed as

$$F_b = \mathbf{g} (\rho - \rho_0) \quad ,$$

where ρ_0 is the density in some reference conditions (pressure and temperature in general). With the Boussinesq approximation, the density is expressed with a Taylor expansion, as a function of temperature, up to the first order

$$\rho = \rho_0 - \rho_0 \beta_{exp} \Delta T \quad .$$

The buoyancy term can be re-written as

$$F_b = -\mathbf{g} \beta_{exp} \Delta T \quad \text{where} \quad \beta_{exp} = \frac{1}{\rho_{ref}} \left(\frac{d\rho}{dT} \right)_{ref} \quad .$$

β_{exp} can be determined by experiments and it is, in general a function of temperature. In this analysis it was assumed constant with temperature.

Finally, the momentum source term in Eq. (3.2) can be expressed as

$$S_u = \rho g \beta_{exp} (T - T_{ref})$$